(4)

AD-A231 928

Technical Document 1983
November 1990

Characterizing and Improving the Performance of the MVDR Processor

M. Reuter

NAVAL OCEAN SYSTEMS CENTER
San Diego, California 92152-5000

J. D. FONTANA, CAPT, USN
Commander

H. R. TALKINGTON, Acting
Technical Director

ADMINISTRATIVE INFORMATION

This work was performed by the Naval Ocean Systems Center, San Diego, CA 92152-5000, under program element 0602314N. The work was performed for the Office of Naval Technology, Arlington, VA 22217, by the Signal Processing Technology Branch, Code 733, Naval Ocean Systems Center.

Released by
D. K. Barbour, Head
Signal Processing Technology
Branch

Under authority of
J. A. Roese, Head
Signal and Information
Processing Division

FS

CONTENTS

CONTENTS (Continued)

FIGURES

CONTENTS (Continued)

FIGURES (Continued)

CONTENTS (Continued)

FIGURES (Continued)

TABLES

1.0 Introduction

We will confine ourselves to the analysis of *frequency domain narrowband* array processing. Specifically, we will analyze two well known methods, the conventional or Bartlett processor and the minimum variance distortionless response (MVDR) processor (Johnson, 1982). We will assume all noise and source signals are temporally wide sense stationary, ergodic random processes.

1.1 Notation

Lower case bold letters represent vectors. Upper case bold letters are matrices. A vertical vector is denoted $\mathbf{x}$, $\mathbf{x}^H$ its complex conjugate or Hermitian transpose, and $\mathbf{x}^T$ its transpose.

1.2 Array Processing

Generally stated, our array processing problem consists of spatially sampling a signal-plus-noise field and localizing an acoustic source which produces a spatially correlated signal of some frequency f_o. The output y of the array processor is

$$y = \mathbf{a}^H \mathbf{x} , \tag{1.1}$$

where $\mathbf{a}$ is the complex weight vector and $\mathbf{x}$ is the frequency-domain data vector. We calculate the i^{th} element of $\mathbf{x}$ by sampling the Fourier transform of length 2T of the output of the i^{th} sensor $x_i(t)$ at the frequency of interest, i.e., $x_i(f_o) = \int_{-T}^{T} x_i(t)\, e^{-j2\pi f_o t} dt$. The output power of the processor or the variance of the process y is then defined as

$$P_{out} = \lim_{T \to \infty} \frac{1}{2T} E\{| y |^2\} = \lim_{T \to \infty} \frac{1}{2T} \mathbf{a}^H E\{\mathbf{x}\mathbf{x}^H\}\mathbf{a} = \mathbf{a}^H \mathbf{R}\, \mathbf{a} \tag{1.2}$$

where E{ } denotes the expectation operator. We define $\mathbf{R}$ as the cross-spectral density matrix (CSDM). The weight vector $\mathbf{a}$ will be a function of the signal that we presume is propagating across the array. If indeed there is such a signal vector in $\mathbf{R}$, the array processor will coherently add the signal components observed at each of the sensors while hopefully incoherently adding the noise components. Peak(s) in P_{out} will identify or localize the acoustic source(s).

We must note that in practice we can not compute the ensemble average in equation (1.2). So we use the ergodicity assumption to estimate $\mathbf{R}$ by dividing the time series data into L segments and computing

$$\hat{R} = \frac{1}{L}\sum_{l=1}^{L} x_l(f_o)x_l^H(f_o)\ , \tag{1.3}$$

where $x_{ml}(f_o)$ is the Fourier transform of the l^{th} segment of time series data observed at sensor m sampled at the frequency f_o and normalized by its length.

1.2.1 Plane-wave signal model

We will use plane-wave signals in our analysis and simulations. That is, in a signal-plus-noise environment a plane-wave signal s(t,z) propagates with velocity c in the direction -**k**, where -**k** is a unit vector normal to the plane of the wavefront. The time series output of the m^{th} sensor is then

$$x_m(t) = s(t + \frac{z_m^T k}{c}) + n_m(t), \tag{1.4}$$

where z_m is the coordinate vector of the m^{th} sensor with respect to some origin and $n_m(t)$ is the noise process at the sensor. In general $n_m(t)$ might contain temporal and spatial white noise (receiver noise) and also spatially correlated components from other acoustic sources (interferers). The Fourier transform of a sample function of the process $x_m(t)$ is then

$$x_m(f) = s(f)\ e^{-j\frac{2\pi f}{c}(z_m^T k)} + n_m(f)\ . \tag{1.5}$$

If s(t,z) is a narrowband process, the Fourier transform will be

$$x_m(f_o) = s(f_o)\ e^{-j\frac{2\pi f_o}{c}(z_m^T k)} + n_m(f_o) \tag{1.6}$$

where we have sampled the noise spectrum at frequency f_o. Including the f_o^{th} frequency component of all the sensors in vector form we get

$$x = s(f_o)s + n \tag{1.7}$$

where **s** represents the phase-shift components of the plane wave signal and **n** represents the noise. The *signal vector* will be shown as **s**.

The cross spectral density matrix of this signal-plus-noise environment will be

$$R = E\{xx^H\} = E\{|\ s(f_o)\ |^2 ss^H + nn^H + sn^H + ns^H\}\ . \tag{1.8}$$

If the noise is spatially white (contains no interferers) and is temporally uncorrelated with the signal, then

$$R = \sigma_s^2 ss^H + \sigma_n^2 I \,, \tag{1.9}$$

where we have normalized the signal and noise spectrums so that σ_s^2 and σ_n^2 represent the signal and noise powers respectively at each sensor.

We note that we have assumed plane-wave models for convenience only. The analysis presented here is applicable to the more general matched-field case.

1.2.2 Conventional processor

The simplest and most commonly used array processing algorithm is the conventional processor. The weight vector is simply the ideal signal vector that we predict is propagating in the "direction of look." We will call this weight vector the steering vector e, i.e., a = e in this processor. If we use the one-signal model from equation (1.9) and steer towards the signal (e = s),

$$P_{CONV} = e^H R\, e = M^2 \sigma_s^2 + M\, \sigma_n^2 \tag{1.10}$$

where M is the number of sensors. We will normalize P_{CONV} by $\frac{1}{M^2}$ so

$$P_{CONV} = \frac{1}{M^2}\, e^H R\, e = \sigma_s^2 + \frac{\sigma_n^2}{M} \,. \tag{1.11}$$

The conventional processor can produce good results for large aperture arrays that are spatially sampled at the Nyquist rate. In fact for some minimum interelement spacing, as $M \rightarrow \infty$ the conventional processor's beamwidth and sidelobes become zero ($| e^H s |^2 \rightarrow 0$ where s is a signal vector and $e \neq s$). However there can be serious beamwidth and sidelobe problems for finite-sized arrays that are not "packed." In this case performance might be degraded severely. As as result, array processing techniques have been developed that are not as sensitive to these factors. We will discuss the most common one.

1.2.3 Minimum variance distortionless response processor

The MVDR (Owsley, 1985) method determines the weight vector a that minimizes the output power or variance $P = a^H R\, a$ subject to the single boresight constraint $a^H e = 1$. That is the processor allows a signal modeled by e to pass through the array unattenuated while nulling out signals not modeled by e. Thus the MVDR processor *adapts* itself to the noise environment. The well known solution to this constrained minimization problem achieved by using the method of Lagrange multipliers is (Johnson, 1982 and Hudson, 1981)

$$a = \frac{R^{-1} e}{e^H R^{-1} e} \,. \tag{1.12}$$

Using equation (1.2) the output power then is

$$P_{MVDR} = \frac{1}{e^H R^{-1} e} . \tag{1.13}$$

Using the one-signal model of equation (1.9) we can calculate R^{-1} in closed form using the matrix inversion lemma (Johnson, 1982, Hudson, 1981, and Steinhardt and Van Veen, 1989) as

$$R^{-1} = \frac{1}{\sigma_n^2}\left[I - \frac{\sigma_s^2}{M\sigma_s^2 + \sigma_n^2} ss^H \right] . \tag{1.14}$$

Then the output power of the processor for $e = s$ will be

$$P_{MVDR} = \sigma_s^2 + \frac{\sigma_n^2}{M} . \tag{1.15}$$

So, for this special signal-plus-noise environment, the output power of the MVDR processor when steered at the signal is equal to the normalized P_{CONV} of equation (1.10), i.e., no adaptivity takes place.

1.2.3.1 Adaptivity

We will illustrate the adaptive properties of the MVDR processor by comparing the output powers of the MVDR and conventional processors using the signal-plus-noise model of equation (1.9) when steered *away* from the signal ($e \neq s$). We also gain insight into adaptivity by examining the effect the conventional beampattern has on the MVDR processor.

The output powers of the conventional and MVDR processors using the matrix of equation (1.9) when steered away from the signal are

$$P_{CONV} = \frac{\sigma_s^2}{M^2} | e^H s |^2 + \frac{\sigma_n^2}{M} , \tag{1.16}$$

and

$$P_{MVDR} = \sigma_s^2 | a^H s |^2 + \sigma_n^2 | a |^2 \tag{1.17}$$

where **a** is calculated from equation (1.12). Now using equations (1.12), (1.14), and (1.17) we get

$$P_{MVDR} = \frac{\sigma_n^2}{M - \frac{\sigma_s^2}{M\sigma_s^2 + \sigma_n^2} | e^H s |^2} . \tag{1.18}$$

Note that $| e^H s |^2$ is equal to the conventional beampattern value at **s** when steered at **e**. Now the

signal s can be interpreted as an interfering signal and the MVDR processor will suppress the output power due to this interferer. The question arises of how well does the MVDR processor null out the interferer as compared to the conventional processor? We will answer this question initially by examining the ratio $\frac{P_{MVDR}}{P_{CONV}}$. That is, our measure of performance will be the ratio of output powers of the MVDR and conventional processors. The better the MVDR processor performs over the conventional, the smaller this ratio. The upper bound on this ratio is one, i.e., under certain conditions the MVDR performance equals the conventional.

Now using equations (1.16) and (1.18) we get the performance ratio relation

$$P_{RAT} = \frac{M^2\sigma_n^2(M\sigma_s^2 + \sigma_n^2)}{(M\sigma_n^2 + \sigma_s^2|\, e^H s\,|^2)(M\sigma_n^2 + \sigma_s^2(M^2 - |\, e^H s\,|^2))}\,, \tag{1.19}$$

where $P_{RAT} = 1$ for $e = s$, and $P_{RAT} < 1$ for $e \neq s$. Analysis of this equation will show that for a given σ_s^2, σ_n^2 and M, if $|\, e^H s\,|^2 \ll M^2$ (the signal falls on or near a null in the conventional beampattern) the performance of the MVDR processor will be similar to the conventional ($P_{RAT} \approx 1$). However the MVDR processor might perform much better than the conventional ($P_{RAT} \ll 1$) for some $0 < |\, e^H s\,|^2 < M^2$. Note however that as $|\, e^H s\,|^2 \rightarrow M^2$, $P_{RAT} \rightarrow 1$. See Lapic, Lockwood, and Gingras (1988) for a more complete analysis of the effects of the conventional beampattern on MVDR performance. Moreover, for $|\, e^H s\,|^2 < M^2$, the higher the signal power σ_s^2, the better the MVDR performance over the conventional. Also, the lower the white noise power, the better the MVDR performance.

1.2.3.2 Simulation

A simple example will illustrate these conditions. We will compute the performance ratio of equation (1.19) by processing a 20-element horizontal random array that is receiving a 30-hz plane wave with bearing 180° from the y-axis at 0° declination angle in spatially white noise. The diameter of the array is six wavelengths or 975 feet assuming sound velocity of 4875 feet/second. Table 1.1 displays the ratio of equation (1.19) for various signal and noise powers when we steer at the signal and away from the signal for the cases when the signal falls on a null of the conventional beampattern and when it falls on a sidelobe. The beampattern values are given in the table. We can see that these numbers agree with the previous statements. Note also for this special signal-plus-noise environment, that when we steer at the signal ($e = s$) P_{RAT}=1.

Table 1.1. Conventional and MVDR processor performance ratio (P_{RAT}) for various signal and noise powers when steered at signal (180°), when steered in direction where signal falls on beampattern null (57°), and when steered in direction where signal falls on sidelobe (43°) for a 20-element horizontal random array.

Signal and noise powers	e = s $\| e^H s \|^2$ = 26.02 dB	s on null $\| e^H s \|^2$ = -17.45 dB	s on sidelobe $\| e^H s \|^2$ = 18.69 dB
σ_n^2 = 0 dB, σ_s^2 = 0 dB	0 dB	~0 dB	- 5.87 dB
σ_n^2 = 0 dB, σ_s^2 = 10 dB	0 dB	- 0.04 dB	- 14.91 dB
σ_n^2 = 0 dB, σ_s^2 = -10 dB	0 dB	~0 dB	- 0.79 dB
σ_n^2 = 20 dB, σ_s^2 = 0 dB	0 dB	~0 dB	- 0.02 dB
σ_n^2 = -20 dB, σ_s^2 = 0 dB	0 dB	- 0.38 dB	- 24.80 dB

2.0 Characterizing MVDR Performance

The array designer only can control the performance of the conventional processor via the array geometry since the designer generally has no control over the signal and noise environment. While array element "shading" is used in conventional processing, this method suppresses *all* of the sidelobes at the expense of more severe tolerances on the array parameters. However the MVDR processor offers additional flexibility due to its ability to adapt to the noise environment and decrease only *selected* sidelobes. More severe array parameter tolerances also are required for MVDR processing (see mismatch example of table 2.1). One of the significant costs of this adaptivity is the need to have a full rank CSDM R. Naturally the $O(M^3)$ numerical operations needed to invert R can also lead to a significant computational burden.

In the previous section we illustrated that while the array geometry influences MVDR performance, the spatially correlated and uncorrelated noise environment also plays a significant role. In this section we will use parameters that have proven illuminating in describing the adaptive nature of the MVDR processor. We use these parameters to characterize MVDR performance under various environmental conditions so that we will be able to identify and characterize situations where MVDR performance is degraded.

2.1 Mismatch

Environmental mismatch is an example of a situation in which MVDR performance, under certain circumstances, can be severely degraded. This degradation occurs when the signal we attempt to steer towards is not correctly modeled by e. We then are faced with the classic problem of mismatch in adaptive array processing (Cox, 1973). There can be many factors which contribute to mismatch. Our knowledge of the acoustic environment might be inaccurate to the extent that the underlying model we use for the signal is incorrect. For instance, the wavefront of the signal might be curved rather than the assumed plane. We might have imprecise knowledge of the array geometry or sensor positions in situations where calibration is impossible. The signal might be correlated with noise or other signals. A faulty estimate of R from equation (1.3) could lead to this condition. In any case, the MVDR processor can be very sensitive to this mismatch.

To illustrate MVDR performance degradation due to mismatch and the conditions under which it is most severe we will use the example given in the previous chapter. We use the same 20-element random circular array except now we will not have precise knowledge of the sensor positions. Using equation (1.5), the m^{th} element of the steering vector e when steered at s is now

$$e_m = e^{-j\frac{2\pi f_o}{c}(z_m + \epsilon)^T k} \tag{2.1}$$

where z_m is the actual sensor position vector and ϵ is the error vector associated with our sensor position assumption. The magnitude of ϵ is a random variable uniformly distributed between 0 and $0.1\lambda_o$ and the phase is a random variable uniformly distributed between 0 and 2π. Table 2.1 contains the performance ratio of equation (1.19) calculated under these conditions for the cases described in the previous section.

Table 2.1. Conventional and MVDR processor performance ratio (P_{RAT}) for various signal and noise powers when steered at signal (180^o), when steered in direction where signal falls on beampattern null (57^o), and when steered in direction where signal falls on sidelobe (43^o) for a 20-element horizontal random array with *sensor position estimate errors.*

Signal and noise powers	$e = s + \epsilon$ $\lvert e^H s \rvert^2 = 25.82$ dB	s on null $\lvert e^H s \rvert^2 = -3.89$ dB	s on sidelobe $\lvert e^H s \rvert^2 = 18.43$ dB
$\sigma_n^2 = 0$ dB, $\sigma_s^2 = 0$ dB	- 2.60 dB	- 0.08 dB	- 5.73 dB
$\sigma_n^2 = 0$ dB, $\sigma_s^2 = 10$ dB	- 9.81 dB	- 0.80 dB	- 14.72 dB
$\sigma_n^2 = 0$ dB, $\sigma_s^2 = -10$ dB	- 0.24 dB	~0 dB	- 0.76 dB
$\sigma_n^2 = 20$ dB, $\sigma_s^2 = 0$ dB	~0 dB	~0 dB	- 0.02 dB
$\sigma_n^2 = -20$ dB, $\sigma_s^2 = 0$ dB	- 19.40 dB	- 4.82 dB	- 24.60 dB

The null and sidelobe values are given in the table. Note that due to the sensor position errors these values have changed somewhat from those of paragraph 1.2.3.2 and table 1.1. Most importantly the mainlobe response has decreased to $\lvert e^H s \rvert^2 = 25.82$ dB. We can see that the values in the last two columns of table 2.1 are similar to those of table 1.1. However column one demonstrates that when we have mismatch, the MVDR processor treats the signal as an interferer even though we are actually attempting to steer towards it. In this case, a small P_{RAT} is evidence of the deleterious effects of mismatch. Note also that mismatch becomes more of a problem at higher signal-to-noise ratios (σ_s^2/σ_n^2).

2.2 Characteristics of the MVDR Processor - Single Interferer Case

To begin our analysis of the characteristics of the MVDR processor let us first assume the CSDM R of equation (1.2) has the form

$$R = \sigma_n^2 I + \sigma_s^2 ss^H + \sigma_t^2 tt^H , \tag{2.2}$$

where σ_n^2 is the power of the spatially uncorrelated (white) process, σ_s^2 is the power of a signal represented by vector s and σ_t^2 is the power of an interferer with vector t. The output power of the MVDR processor is

$$P_{MVDR} = a^H R\, a \tag{2.3}$$

where a is given by equation (1.12). Using R above we have

$$P_{MVDR} = \sigma_n^2 |a|^2 + \sigma_s^2 |a^H s|^2 + \sigma_t^2 |a^H t|^2 , \tag{2.4}$$

where $|\,.\,|^2$ denotes magnitude squared.

We see that the MVDR output power consists of three components in this case: output powers due to white noise ($\sigma_n^2|a|^2$) which is dependent of the magnitude squared of the weight vector, the signal ($\sigma_s^2|a^H s|^2$), and the interferer ($\sigma_t^2|a^H t|^2$). The MVDR processor attempts to minimize these three terms. The importance of white noise power, interferer power, and the spatial distribution of the interferer to MVDR performance becomes apparent when we steer at the signal s. Naturally in this case, the constraint $a^H s = 1$ requires the processor to minimize only $\sigma_n^2|a|^2$ and $\sigma_t^2|a^H t|^2$, i.e.,

$$P_{MVDR} = \sigma_n^2 |a|^2 + \sigma_s^2 + \sigma_t^2 |a^H t|^2 . \tag{2.5}$$

Using the results presented in appendix A (equation A.5) for $Q = \sigma_t^2 tt^H$ we get the MVDR weight vector

$$a = \frac{(\sigma_n^2 I + \sigma_t^2 tt^H)^{-1} e}{e^H (\sigma_n^2 I + \sigma_t^2 tt^H)^{-1}} . \tag{2.6}$$

Then using the matrix inversion lemma we get

$$a = \frac{e - \dfrac{t^H e}{M + \alpha^2} t}{M - \dfrac{|e^H t|^2}{M + \alpha^2}} \tag{2.7}$$

where $\alpha^2 = \sigma_n^2/\sigma_t^2$. Since the output power P_{MVDR} of equation (2.5) is dependent on $|a^H t|^2$ and $|a|^2$, we compute them as

$$|a^H t|^2 = \frac{\left[\frac{\alpha^2}{M+\alpha^2}\right]^2 |e^H t|^2}{\left[M - \frac{|e^H t|^2}{M+\alpha^2}\right]^2} \tag{2.8}$$

$$|a|^2 = \frac{M + \frac{1}{M+\alpha^2}\left[\frac{M}{M+\alpha^2} - 2\right]|e^H t|^2}{\left[M - \frac{|e^H t|^2}{M+\alpha^2}\right]^2} . \tag{2.9}$$

2.2.1 Adaptive nulling

We initially are interested in how well and under what conditions the MVDR processor nulls out the interferer term $|a^H t|^2$. Appendix B (equations B.1 - B.5) contains an analysis which shows that $|a^H t|^2$ is an increasing function of α^2. So for a given $|e^H t|^2$ ($0 < |e^H t|^2 < M^2$), as α^2 becomes smaller (white noise power σ_n^2 decreases or the interferer power σ_t^2 increases) the null $|a^H t|^2$ becomes deeper. We might, in this case, expect P_{RAT} of equation (1.19) to become very small. That is MVDR performance might become far superior to conventional performance. Conversely, as α^2 increases (white noise power increases or the interferer power decreases) the null $|a^H t|^2$ becomes more shallow. In fact, as $\alpha^2 \rightarrow \infty$, $|a^H t|^2 \rightarrow |e^H t|^2/M^2$. In this case we would get the normalized conventional processor "nulling" performance. P_{RAT} would then be close to unity.

It is also interesting to investigate the effect $|e^H t|^2$ (the value of the conventional beampattern at t when steered at e) has on MVDR nulling. In appendix B (equations B.6 - B.9) we show that $|a^H t|^2$ is an increasing function of $|e^H t|^2$. So for a given α^2 as $|e^H t|^2$ increases from zero to M^2, $|a^H t|^2$ approaches the normalized conventional beampattern at t ($|e^H t|^2/M^2$). That is very little adaptive nulling takes place. In fact, if $|e^H t|^2 = M^2$ we have effectively steered at t.

To sum up we make the following observations: if we steer at s and $\sigma_n^2/\sigma_t^2 \ll 1$ the MVDR processor emphasizes the nulling $|a^H t|^2$ of the signal. Likewise, if $\sigma_n^2/\sigma_t^2 \gg 1$, the MVDR processor emphasizes the minimization of the magnitude squared of the weight vector at the expense of interferer nulling. In this latter case the adaptive nulling properties of the MVDR processor might be degraded severely.

2.2.2 Magnitude squared of the weight vector

The magnitude squared of the weight vector **a** has proven to be a useful parameter for characterizing and gauging the adaptive nature of the MVDR processor (Hudson, 1981). As pointed out above, $|\ \mathbf{a}\ |^2$ can play a critical role in MVDR performance so it certainly deserves further examination. We follow the nulling analysis from above to determine the effect noise power and spatial distribution of the interferer have on $|\ \mathbf{a}\ |^2$. As shown in appendix B (equations B.10 - B.14), $|\ \mathbf{a}\ |^2$ is a decreasing function of α^2 for $0 < \alpha^2 < \infty$ for some $|\ \mathbf{e}^H\mathbf{t}\ |^2$ $(0 \leq |\ \mathbf{e}^H\mathbf{t}\ |^2 < M^2)$. In other words, while the MVDR processor puts an increasingly deeper null in the direction of **t** ($|\ \mathbf{a}^H\mathbf{t}\ |^2$) as $\alpha^2 \rightarrow 0$, the magnitude of the weight vector *increases*. Conversely, while MVDR performance approaches conventional performance (no adaptivity) as $\alpha^2 \rightarrow \infty$, the magnitude of the weight vector *decreases*. In fact $|\ \mathbf{a}\ |^2 = 1/M$ in the latter case.

$|\ \mathbf{a}\ |^2$ behaves in an interesting way with respect to $|\ \mathbf{e}^H\mathbf{t}\ |^2$. In appendix B (equations B.15 - B.17) we show that $|\ \mathbf{a}\ |^2$ is maximum for

$$|\ \mathbf{e}^H\mathbf{t}\ |^2_{MAX} = \frac{M^2(M + \alpha^2)}{M + 2\alpha^2}\ . \tag{2.10}$$

That is $|\ \mathbf{a}\ |^2$ is an increasing function of $|\ \mathbf{e}^H\mathbf{t}\ |^2$ for $|\ \mathbf{e}^H\mathbf{t}\ |^2 < \frac{M^2(M + \alpha^2)}{M + 2\alpha^2}$ and a decreasing function of $|\ \mathbf{e}^H\mathbf{t}\ |^2$ for $|\ \mathbf{e}^H\mathbf{t}\ |^2 > \frac{M^2(M + \alpha^2)}{M + 2\alpha^2}$. We see that as $\alpha^2 \rightarrow 0$, $|\ \mathbf{e}^H\mathbf{t}\ |^2_{MAX} \rightarrow M^2$. That is for high interferer powers, we can consider $|\ \mathbf{a}\ |^2$ generally as being an increasing function of $|\ \mathbf{e}^H\mathbf{t}\ |^2$.

We now can think of $|\ \mathbf{a}\ |^2$ as a gauge of the "effort" that the MVDR processor is putting into adaptive nulling. The magnitude of the weight vector increases as the noise environment becomes more severe (large σ_t^2 and/or large $|\ \mathbf{e}^H\mathbf{t}\ |^2$).

2.2.3 Performance improvement due to adaptivity

The value $|\ \mathbf{a}\ |^2$ alone cannot be used to measure improvement in performance over the conventional processor. As was pointed out previously, for very large $|\ \mathbf{e}^H\mathbf{t}\ |^2$ nulling might be degraded severely. The corresponding increase in $|\ \mathbf{a}\ |^2$ (resulting in greater output power due to noise) can even further degrade performance. The problem occurs because the MVDR processor attempts to minimize both noise terms in equation (2.5). The amount of emphasis the processor places on nulling as opposed to minimizing $|\ \mathbf{a}\ |^2$ is dependent on the noise powers and $|\ \mathbf{e}^H\mathbf{t}\ |^2$.

Another parameter that has proven useful in analytically characterizing the MVDR processor is the *performance improvement due to adaptivity* or PIA (Jablon, 1986). It is defined as the MVDR output signal to noise ratio over the conventional output signal to noise ratio or

$$\text{PIA} = \frac{\text{SNR}_{\text{MVDR}}}{\text{SNR}_{\text{CONV}}} . \tag{2.11}$$

The greater this ratio, the better the MVDR processor performs over the conventional. PIA = 1 signifies that no adaptivity occurs. This parameter inherently separates the MVDR output power due to white noise and interferers from the output power due to the signal unlike P_{RAT} of section 1.0.

We note that PIA is not necessarily a good measure of how *detection* is affected by mismatch. While the degradation in PIA of a particular MVDR response under conditions of mismatch might be severe, the corresponding increase in the magnitude of the weight vector will actually *contribute* to the detection of the signal. A better measure of detection degradation might be $P_{MVDR(mismatch)}/P_{MVDR(nomismatch)}$. However PIA will be a better performance measure if we desire to do interarray coherent processing. In this case, a high PIA is of critical importance. We also believe that understanding how PIA is affected by various noise environments contributes to a better understanding of how the MVDR processor works.

Using equations (2.2), (2.8), and (2.9) and that

$$\text{SNR}_{\text{CONV}} = \frac{M^2\sigma_s^2}{M\sigma_n^2 + \sigma_t^2 |\, e^H t \,|^2} \tag{2.12}$$

and

$$\text{SNR}_{\text{MVDR}} = \frac{\sigma_s^2}{\sigma_n^2 |\, a \,|^2 + \sigma_t^2 |\, a^H t \,|^2} \tag{2.13}$$

we get

$$\text{PIA} = 1 + \frac{|\, e^H t \,|^2}{\alpha^2(M + \alpha^2)} - \frac{(|\, e^H t \,|^2)^2}{M^2\alpha^2(M + \alpha^2)} . \tag{2.14}$$

As we would expect PIA is a decreasing function of α^2. This can be proven in the fashion of appendix B.

2.2.3.1 Optimal sidelobe level

Since PIA is a quadratic equation with respect to $|\, e^H t \,|^2$, we take the derivative of PIA with respect to $|\, e^H t \,|^2$ to get an $|\, e^H t \,|^2$ that optimizes PIA as

$$|\, e^H t \,|^2_{OPT} = \frac{M^2}{2} . \tag{2.15}$$

Then

$$PIA_{MAX} = 1 + \frac{M^2}{4\alpha^2(M + \alpha^2)} . \tag{2.16}$$

So for the one interferer case of equation (2.2), we get maximum MVDR performance as measured by PIA if the interferer falls on a sidelobe that has a magnitude of $M^2/2$. A sidelobe level of this magnitude results in the best balance of interferer nulling and $| a |^2$ minimization. Interestingly $| e^H t |^2_{OPT}$ is *not* a function of α^2 (noise powers).

2.3 Characteristics of the MVDR Processor - Multiple Interferer Case

It must be emphasized that the previous analysis was based upon the special one-signal case of equation (2.2). Analytical calculations, such as those above for a more general interferer matrix **Q**, are difficult due to the matrix inverse required to calculate the weight vector **a**. Such calculations however can be accomplished using the results in (Lapic, Lockwood, and Gingras 1988, and Mohnkern, 1989), i.e., by treating the interferer vectors as mutually orthogonal. That is we will assume the CSDM **R** with N interferers is represented by

$$R = \sigma_n^2 I + \sigma_s^2 s s^H + \sum_{i=1}^{N} \sigma_{ti}^2 t_i t_i^H \tag{2.17}$$

where

$$t_i^H t_j = 0 \quad \text{for } i \neq j \tag{2.18}$$

and $N < M$.

Now using the result of appendix A (equation A.5) where

$$W = \sigma_n^2 I + \sum_{i=1}^{N} \sigma_{ti}^2 t_i t_i^H , \tag{2.19}$$

W^{-1} can be represented by

$$W^{-1} = \frac{1}{\sigma_n^2}\left[I - \sum_{i=1}^{N} \frac{\sigma_{ti}^2}{\sigma_n^2 + M\sigma_{ti}^2} t_i t_i^H \right] . \tag{2.20}$$

Then as in equation (2.7) we compute the weight vector for this signal and noise environment as

$$\mathbf{a} = \frac{\mathbf{e} - \sum_{i=1}^{N} \frac{\mathbf{t}_i^H \mathbf{e}}{M + \alpha_i^2} \mathbf{t}_i}{M - \sum_{i=1}^{N} \frac{|\mathbf{e}^H \mathbf{t}_i|^2}{M + \alpha_i^2}} \tag{2.21}$$

where $\alpha_i^2 = \sigma_n^2/\sigma_{ti}^2$. Then

$$|\mathbf{a}^H \mathbf{t}_i|^2 = \frac{\left[\frac{\alpha_i^2}{M + \alpha_i^2}\right]^2 |\mathbf{e}^H \mathbf{t}_i|^2}{\left[M - \frac{|\mathbf{e}^H \mathbf{t}_i|^2}{M + \alpha_i^2}\right]^2} \quad \forall\, i \tag{2.22}$$

and

$$|\mathbf{a}|^2 = \frac{M - 2\sum_{i=1}^{N} \frac{|\mathbf{e}^H \mathbf{t}_i|^2}{M + \alpha_i^2} + M\sum_{i=1}^{N} \frac{|\mathbf{e}^H \mathbf{t}_i|^2}{(M + \alpha_i^2)^2}}{\left[M - \sum_{i=1}^{N} \frac{|\mathbf{e}^H \mathbf{t}_i|^2}{M + \alpha_i^2}\right]^2} . \tag{2.23}$$

Now we will simplify $|\mathbf{a}|^2$ above by assuming that $|\mathbf{e}^H \mathbf{t}_i|^2 = |\mathbf{e}^H \mathbf{t}|^2$ and $\sigma_{ti}^2 = \sigma_t^2$ or $\alpha_i^2 = \alpha^2$for all i. So,

$$|\mathbf{a}|^2 = \frac{M + \frac{1}{M + \alpha^2}\left[\frac{M}{M + \alpha^2} - 2\right] N |\mathbf{e}^H \mathbf{t}|^2}{\left[M - \frac{N|\mathbf{e}^H \mathbf{t}|^2}{M + \alpha^2}\right]^2} . \tag{2.24}$$

Note that since the interferers are mutually orthogonal, equation (2.22) is identical in form to equation (2.8) so the previous analysis of adaptive nulling also holds for this special multiple interferer case.

An analysis identical to that of appendix B shows that $|\mathbf{a}|^2$ in this case is an *increasing* function of N for $1 \leq N \leq M$. That is as the number of interferers increases $|\mathbf{a}|^2$ also increases for fixed α^2 and $|\mathbf{e}^H \mathbf{t}|^2$. This fact reinforces the view that we can use $|\mathbf{a}|^2$ to measure the "effort" the MVDR processor is putting into adaptive nulling. Naturally we would expect a multiple interferer environment to pose more of a challenge to nulling than a one interferer situation.

2.3.1 Performance improvement due to adaptivity

We now repeat the PIA calculations for this multiple interferer environment using the previous assumptions. Using equations (2.17), (2.22), and (2.23) and that

$$\mathrm{SNR}_{\mathrm{CONV}} = \frac{\mathrm{M}^2\sigma_s^2}{\mathrm{M}\sigma_n^2 + \mathrm{N}\sigma_t^2 |\, \mathrm{e}^{\mathrm{H}}\mathrm{t}\, |^2} \tag{2.25}$$

and

$$\mathrm{SNR}_{\mathrm{MVDR}} = \frac{\sigma_s^2}{\sigma_n^2 |\, \mathrm{a}\, |^2 + \mathrm{N}\sigma_t^2 |\, \mathrm{a}^{\mathrm{H}}\mathrm{t}\, |^2} \tag{2.26}$$

we get

$$\mathrm{PIA} = 1 + \frac{\mathrm{N} |\, \mathrm{e}^{\mathrm{H}}\mathrm{t}\, |^2}{\alpha^2(\mathrm{M} + \alpha^2)} - \frac{(\mathrm{N} |\, \mathrm{e}^{\mathrm{H}}\mathrm{t}\, |^2)^2}{\mathrm{M}^2\alpha^2(\mathrm{M} + \alpha^2)} \,. \tag{2.27}$$

2.3.1.1 Optimal sidelobe level

As before we find an $|\, \mathrm{e}^{\mathrm{H}}\mathrm{t}\, |^2$ that optimizes PIA under the multiple interferer assumption as

$$|\, \mathrm{e}^{\mathrm{H}}\mathrm{t}\, |^2_{\mathrm{OPT}} = \frac{\mathrm{M}^2}{2\mathrm{N}} \,. \tag{2.28}$$

Interestingly, $\mathrm{PIA}_{\mathrm{MAX}} = 1 + \frac{\mathrm{M}^2}{4\alpha^2(\mathrm{M} + \alpha^2)}$ as in the one interferer case. We can view this as the optimal (as measured by PIA) sidelobe level for an N-interferer environment under the assumption that the interferers are mutually orthogonal and approximately of the same power. Note that equation (2.28) is simply equation (2.15) divided by the number of interferers. That is as the number of interferers increases the average sidelobe level must decrease in order to maintain optimal (with respect to PIA) MVDR processing.

Since the PIA of equation (2.27) is also a quadratic function of N, we now find the number of interferers that optimizes PIA given a sidelobe level $|\, \mathrm{e}^{\mathrm{H}}\mathrm{t}\, |^2$ as

$$\mathrm{N}_{\mathrm{OPT}} = \frac{\mathrm{M}^2}{2|\, \mathrm{e}^{\mathrm{H}}\mathrm{t}\, |^2} \,. \tag{2.29}$$

If we use the results presented in Mohnkern (1989), where it is shown that under this interferer power assumption the ratio of number of interferers to the number of sensors that maximizes "excess array

gain" (array gain (dB) - 10logM) is 1/2, we get a corresponding optimal average sidelobe level of

$$| e^H t |^2_{OPT} = M . \tag{2.30}$$

So if the number of interferers equals half the number of sensors, we get maximum "excess array gain" *and* optimum PIA if the sidelobe condition of equation (2.30) is met.

2.4 Simulations

The parameters $| a |^2$ and PIA also have proven useful in analyzing and characterizing the effects of mismatch on MVDR performance. Based upon the previous analysis we expect the MVDR processor under conditions of mismatch to perform as if the "interferer" is falling on a very high sidelobe (mainlobe in this case) since the processor treats any signal s as an interferer if $| e^H s |^2 < M^2$.

To show this we will use the examples presented in section 2.1 for the signal and white noise power cases ($\sigma_n^2 = 0$ dB, $\sigma_s^2 = 10$ dB) and ($\sigma_n^2 = 10$ dB, $\sigma_s^2 = 0$ dB). Figure 2.1 is the MVDR array response and $| a |^2$ for the case where we have perfect knowledge of sensor positions and ($\sigma_n^2 = 0$ dB, $\sigma_s^2 = 10$ dB). Note the interesting behavior of $| a |^2$. As we steer through the 180° region the signal enters the mainlobe of the beampattern and we see the characteristic increase in $| a |^2$ since the signal is treated as an interferer. However when we steer close to s, $| a |^2$ quickly drops to the minimum level (1/M or -13.01 dB in this case). The P_{MVDR} in this direction is due primarily to the signal power σ_s^2, i.e., $P_{MVDR} \approx \sigma_s^2$, because of the $a^H s = 1$ constraint. As we steer beyond 180° $| a |^2$ first increases dramatically then drops off as the signal leaves the mainlobe. Note also the similarities between the side region of P_{MVDR} and $| a |^2$ where there is no signal. P_{MVDR} virtually mirrors $| a |^2$ so the majority of the MVDR output power in these directions is due to white noise.

Figure 2.2 contains the results for the ($\sigma_n^2 = 10$ dB, $\sigma_s^2 = 0$ dB) case. The behavior of $| a |^2$ is not nearly as dramatic as in the previous example because the MVDR performance is dominated by the white noise term σ_n^2, i.e., the MVDR processor emphasizes the minimization of $| a |^2$ as opposed to nulling. These observations are entirely consistent with the analysis above.

2.4.1 Mismatch revisited

We now include the 0.1λ sensor position uncertainties in our simulations. Table 2.2 contains $| a |^2$ and PIA for the two input SNR scenarios when we steer at 180° azimuth. The nonmismatch case is included for comparison. Here even though we are steering at 180° azimuth, $e \neq s$ and the MVDR processor views the signal as an interferer.

We note the dramatic difference between the PIA of the high SNR case and the low SNR case. Note also that the PIA for the low SNR case is not significantly less than the PIA that we obtain with perfect sensor position knowledge (PIA = 1 or 0 dB). This merely indicates that the MVDR processor

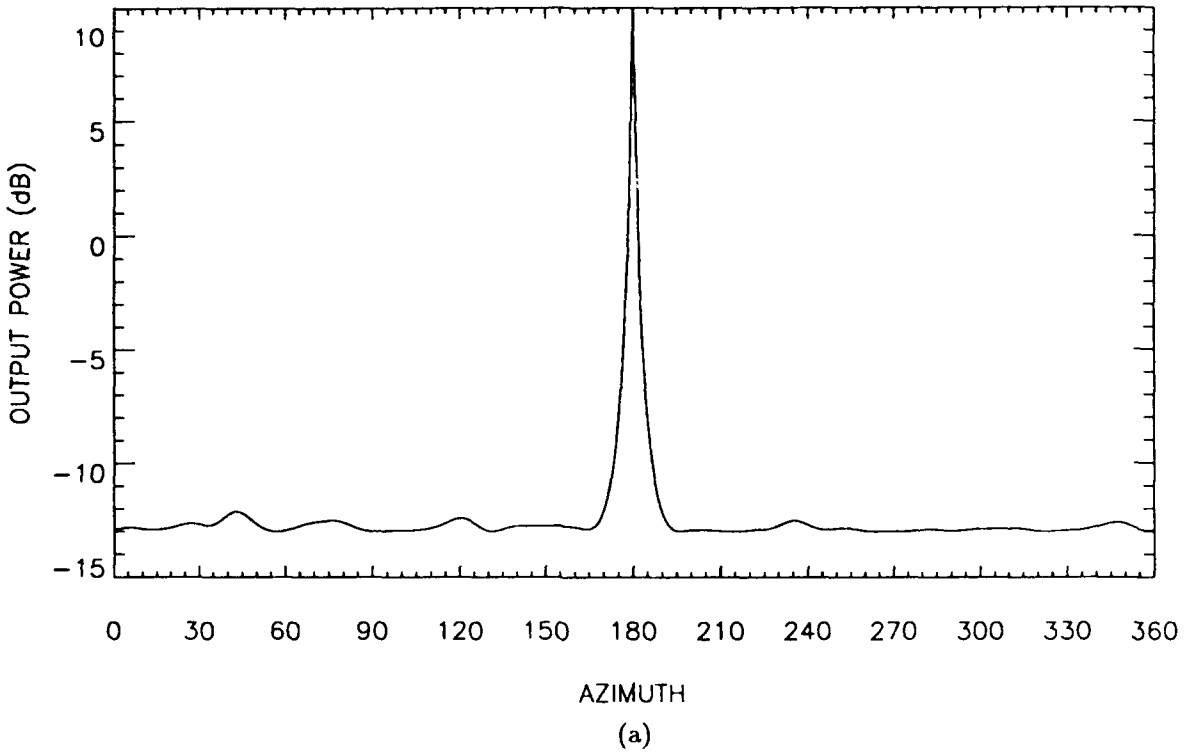

(a)

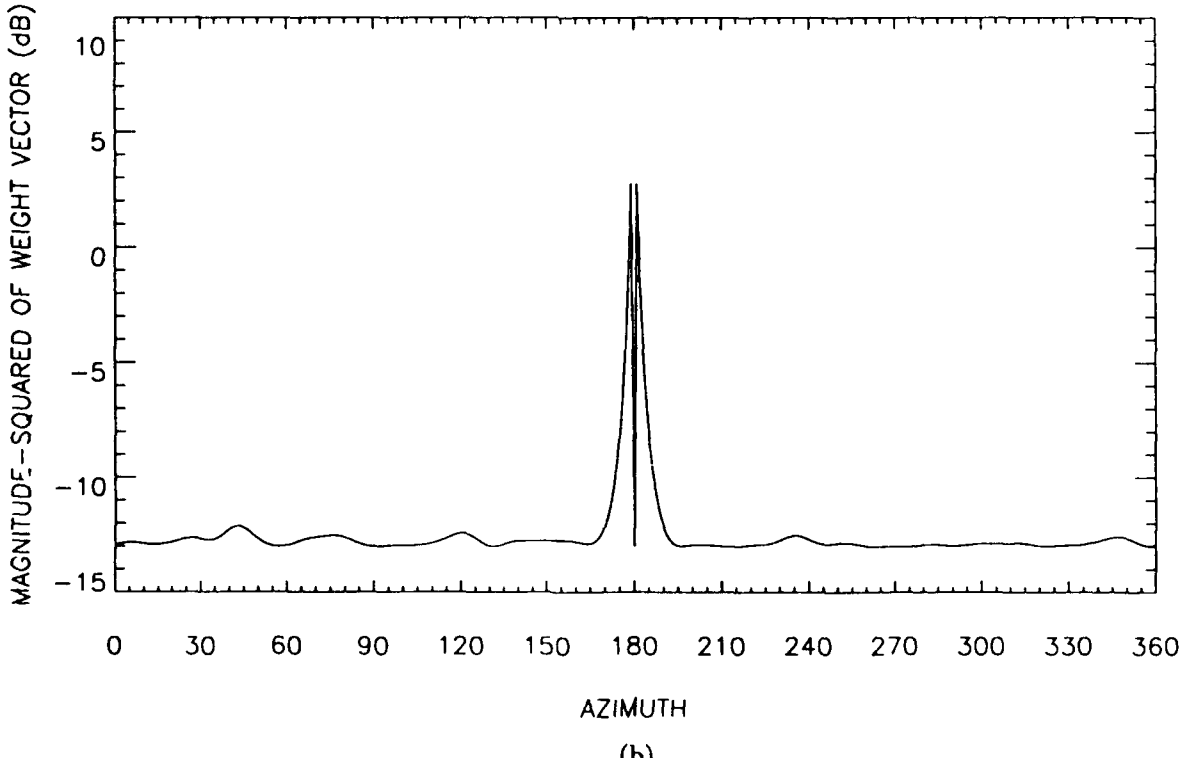

(b)

Figure 2.1. MVDR processor results for signal power $\sigma_s^2 = 10$ dB and noise power $\sigma_n^2 = 0$ dB: (a) output power, (b) corresponding magnitude squared of the weight vector $| \mathbf{a} |^2$.

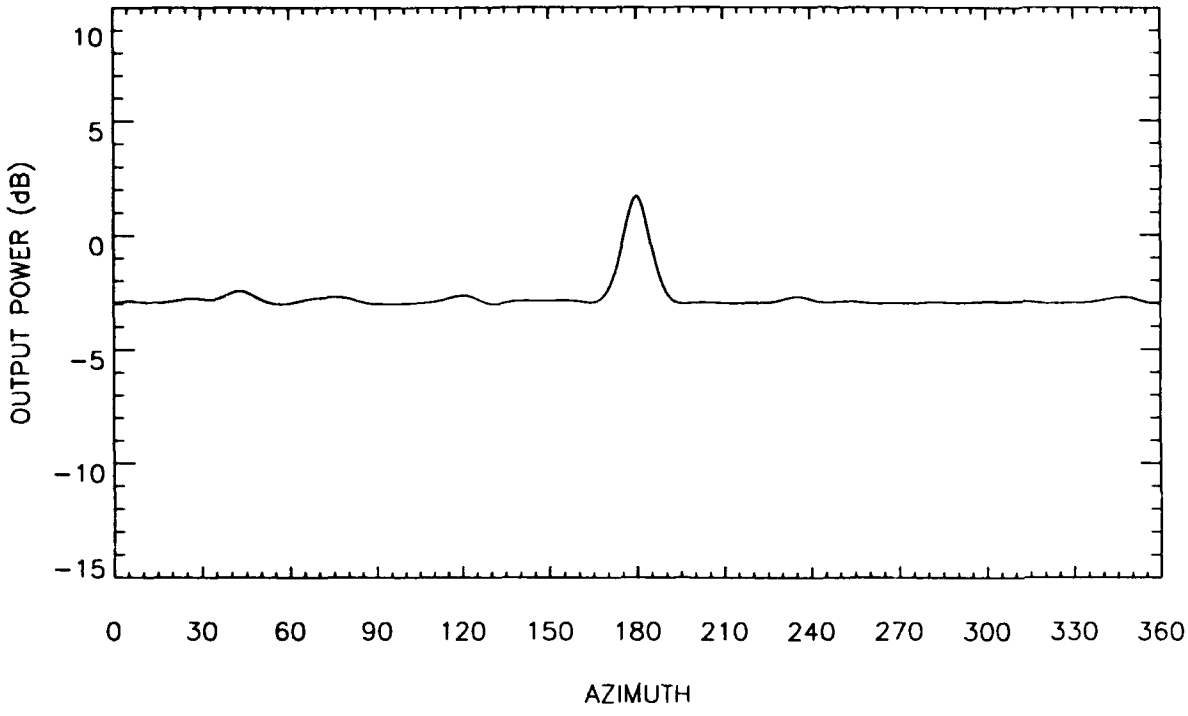

(a)

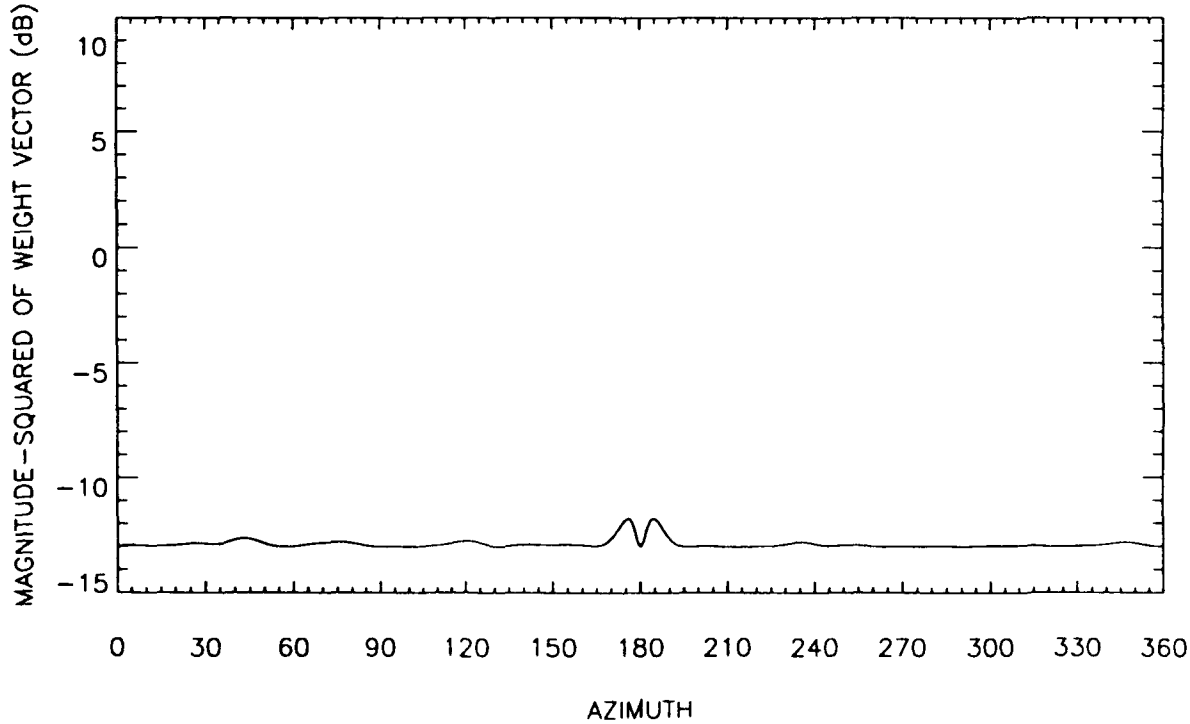

(b)

Figure 2.2. MVDR processor results for signal power $\sigma_s^2 = 0$ dB and noise power $\sigma_n^2 = 10$ dB: (a) output power, (b) corresponding magnitude squared of the weight vector $\mid \mathbf{a} \mid^2$.

Table 2.2. $|\mathbf{a}|^2$ and PIA of the MVDR processor when steered at signal with (a) no mismatch and (b) mismatch caused by 0.1λ errors in sensor position estimates.

(a)

Signal and noise powers	$\|\mathbf{a}\|^2$	PIA
$\sigma_n^2 = 0$ dB, $\sigma_s^2 = 10$ dB	-13.01 dB	0 dB
$\sigma_n^2 = 10$ dB, $\sigma_s^2 = 0$ dB	-13.01 dB	0 dB

(b)

Signal and noise powers	$\|\mathbf{a}\|^2$	PIA
$\sigma_n^2 = 0$ dB, $\sigma_s^2 = 10$ dB	-0.42 dB	-32.61 dB
$\sigma_n^2 = 10$ dB, $\sigma_s^2 = 0$ dB	-12.42 dB	-1.34 dB

does not place much emphasis on nulling the signal for the low SNR case. This fact is also exhibited by $|\mathbf{a}|^2$. Conversely great emphasis is placed on nulling the signal for the high SNR case as shown by $|\mathbf{a}|^2$.

Figures 2.3 and 2.4 are the complete array responses and $|\mathbf{a}|^2$'s for these two cases. While $|\mathbf{a}|^2$ of figure 2.1 (b) exhibits a deep notch at 180°, the notch is entirely missing from $|\mathbf{a}|^2$ of figure 2.3 (b). This signifies that P_{MVDR} in this direction is primarily due to white noise, i.e., $P_{MVDR} \approx \sigma_n^2 |\mathbf{a}|^2$. This graphically explains the corresponding PIA of table 2.2. As we expect, P_{MVDR} and $|\mathbf{a}|^2$ of the low SNR case of figure 2.4 are not significantly different from those of the corresponding nonmismatch case of figure 2.2.

Since under conditions of mismatch the MVDR processor treats the signal as an interferer we can examine equation (2.10) in the context of mismatch where $\mathbf{s} = \mathbf{t}$. We see that as $|\mathbf{e}^H\mathbf{s}|^2 \rightarrow \frac{M^2(M+\alpha^2)}{M+2\alpha^2}$ mismatch becomes more severe. However when $|\mathbf{e}^H\mathbf{s}|^2$ moves beyond $\frac{M^2(M+\alpha^2)}{M+2\alpha^2}$ and approaches M^2, MVDR performance degradation due to mismatch lessens. So we might view

$$\frac{M^2(M+\alpha^2)}{M+2\alpha^2} < |\mathbf{e}^H\mathbf{s}|^2 < M^2 \tag{2.31}$$

as a region of $|\mathbf{e}^H\mathbf{s}|^2$ where mismatch can be tolerated for this simple one-signal case. Note that for high SNR situations and/or for large M this region can be quite narrow.

2.4.2 MVDR performance with an interferer

Previously we noted the important effect an interferer has on MVDR performance. To see how an interferer affects the mismatch situation we include a relatively strong interferer (10 dB) in the above simulations. We will place the interferer at a null and a high sidelobe observed while steered at 180°. These directions will be identical to those described in section 1.0.

Table 2.3 contains the results for the case where the interferer falls on a null and table 2.4 contains the case where the interferer falls on a sidelobe. While $|\mathbf{a}|^2$ and PIA of the high SNR case of table 2.3 (interferer on null) are not markedly different from those of table 2.2 (single signal only), there is a considerable amount of improvement in PIA shown in table 2.4 (interferer on sidelobe). From our knowledge of the effect the spatial distribution of the interferer has on MVDR performance we conclude that since the MVDR processor exerts more effort nulling the interferer when it falls on a sidelobe than when it falls on a null we get improvement in MVDR performance over conventional performance. Also since $|\mathbf{a}|^2$ increases in magnitude when an interferer falls on a sidelobe, the MVDR processor places more emphasis on minimizing $|\mathbf{a}|^2$ thus sacrificing to a certain extent unwanted signal nulling.

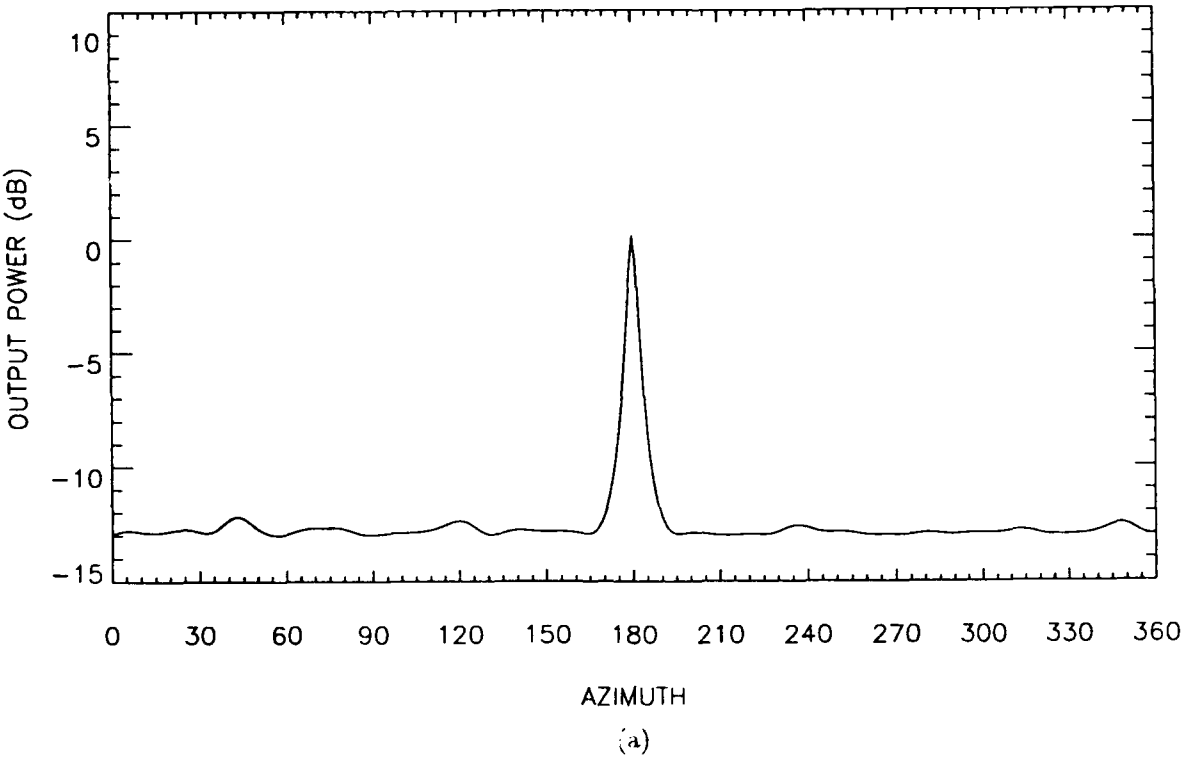

(a)

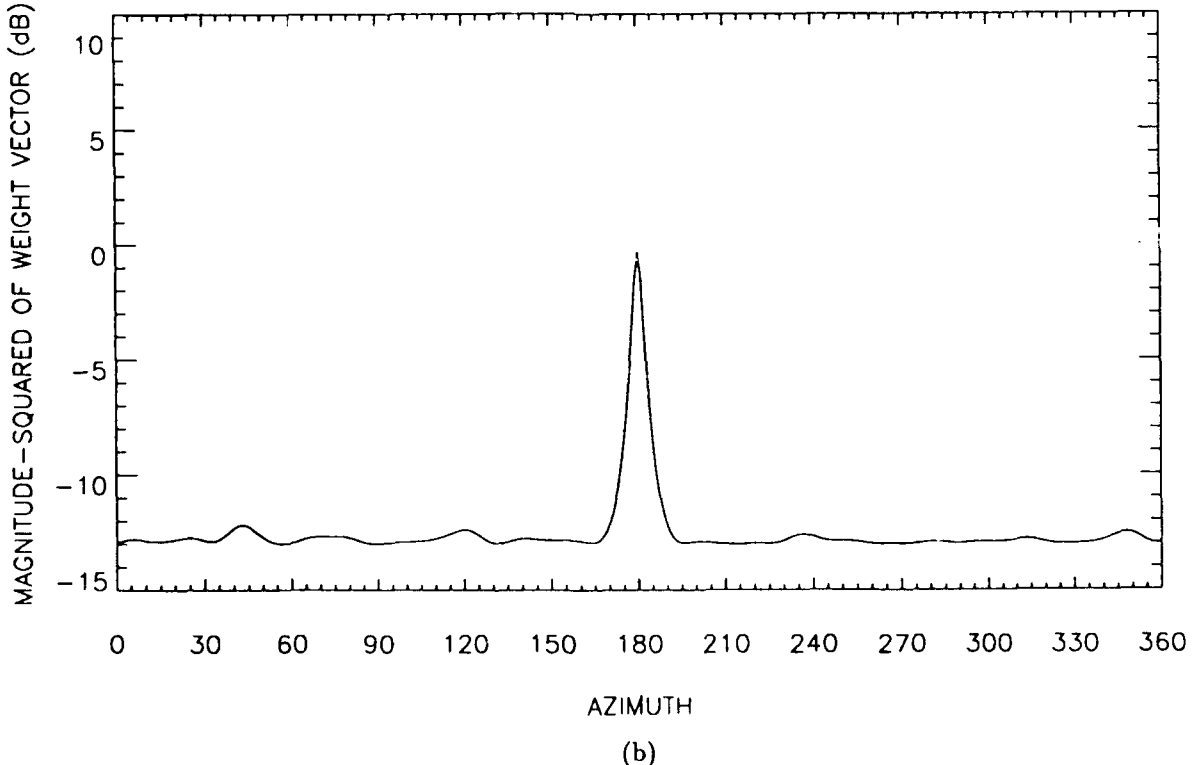

(b)

Figure 2.3. MVDR processor results for signal power $\sigma_s^2 = 10$ dB and noise power $\sigma_n^2 = 0$ dB with 0.1λ sensor position error: (a) output power, (b) corresponding magnitude squared of the weight vector $\mid \mathbf{a} \mid^2$.

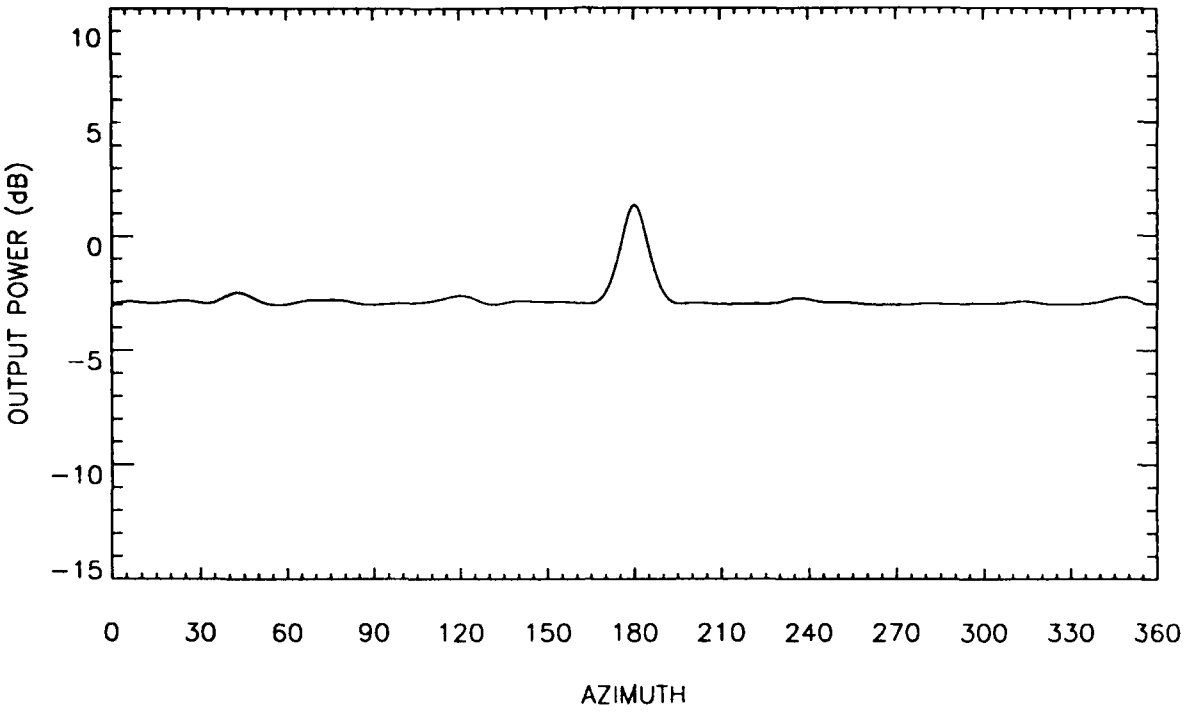

(a)

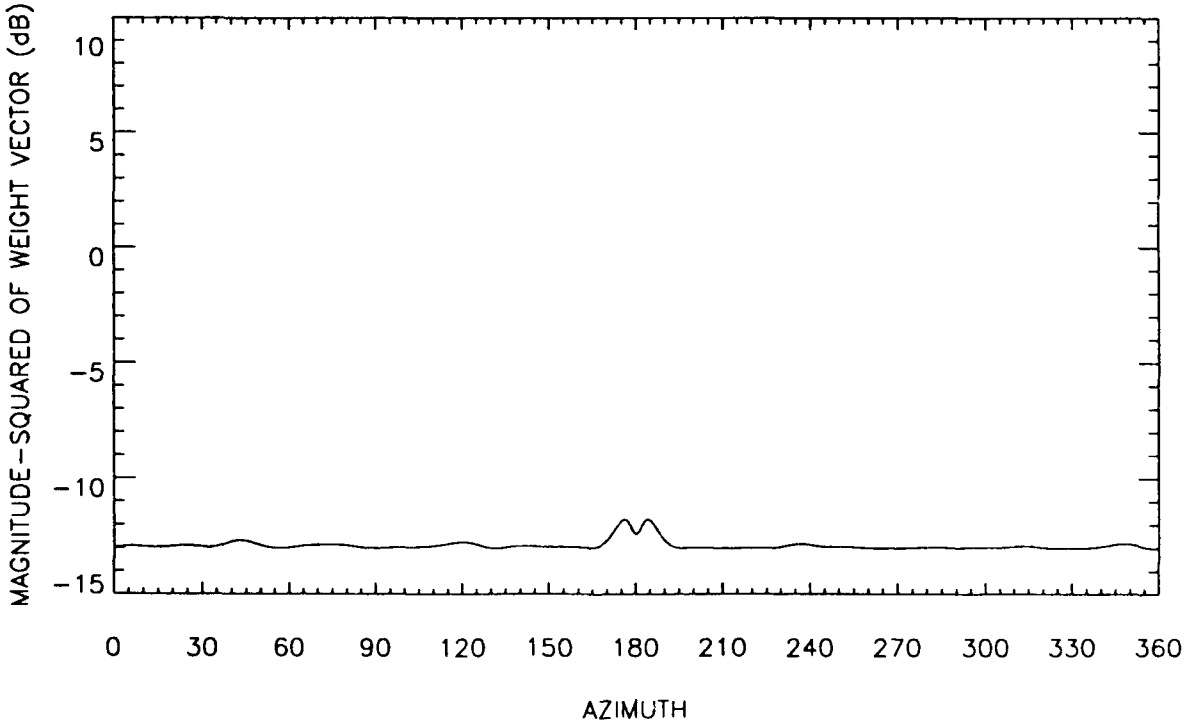

(b)

Figure 2.4. MVDR processor results for signal power $\sigma_s^2 = 0$ dB and noise power $\sigma_n^2 = 10$ dB with 0.1λ sensor position error: (a) output power, (b) corresponding magnitude squared of the weight vector $| \mathbf{a} |^2$.

Table 2.3. $|\mathbf{a}|^2$ and PIA of the MVDR processor when steered at signal with a 10 dB interferer falling on a null with (a) no mismatch and (b) mismatch caused by 0.1λ errors in sensor position estimates.

(a)

Signal and noise powers	$\|\mathbf{a}\|^2$	PIA
$\sigma_n^2 = 0$ dB, $\sigma_s^2 = 10$ dB	-13.01 dB	$\sim$ 0 dB
$\sigma_n^2 = 10$ dB, $\sigma_s^2 = 0$ dB	-13.01 dB	$\sim$ 0 dB

(b)

Signal and noise powers	$\|\mathbf{a}\|^2$	PIA
$\sigma_n^2 = 0$ dB, $\sigma_s^2 = 10$ dB	-0.35 dB	-30.75 dB
$\sigma_n^2 = 10$ dB, $\sigma_s^2 = 0$ dB	-12.42 dB	-1.10 dB

Table 2.4. $|\mathbf{a}|^2$ and PIA of the MVDR processor when steered at signal with a 10 dB interferer falling on a sidelobe with (a) no mismatch and (b) mismatch caused by 0.1λ errors in sensor position estimates.

(a)

Signal and noise powers	$\|\mathbf{a}\|^2$	PIA
$\sigma_n^2 = 0$ dB, $\sigma_s^2 = 10$ dB	-12.13 dB	14.91 dB
$\sigma_n^2 = 10$ dB, $\sigma_s^2 = 0$ dB	-12.21 dB	5.87 dB

(b)

Signal and noise powers	$\|\mathbf{a}\|^2$	PIA
$\sigma_n^2 = 0$ dB, $\sigma_s^2 = 10$ dB	-0.26 dB	-17.18 dB
$\sigma_n^2 = 10$ dB, $\sigma_s^2 = 0$ dB	-11.79 dB	4.47 dB

The low SNR case is also quite revealing. While table 2.3 illustrates no significant change in performance, table 2.4 reveals that the MVDR processor actually is performing much better than a conventional processor (PIA $>$ 0 dB) when the interferer falls on the sidelobe. We conclude that since mismatch does not cause unwanted signal nulling in this case, the MVDR processor is free to null out the interferer. Enhanced nulling is also demonstrated by the slight increase in $|\ \mathbf{a}\ |^2$ from table 2.2 to table 2.4.

These simulations reveal that the severity of mismatch as measured by PIA is a function of the spatial distribution of the interferers (and as a result array geometry) and the signal and noise (white and correlated) powers.

3.0 Improving MVDR Performance

We have demonstrated the utility of the parameters $|\ \mathbf{a}\ |^2$ and PIA in characterizing MVDR performance. We have also shown how these parameters are affected by the environment (white noise power, interferer powers, spatial distribution of interferers). In this section we will analyze algorithms that attempt to enhance MVDR performance by synthetically altering the environment.

3.1 Optimal Robust MVDR Algorithm

We now attempt to improve upon MVDR performance under conditions of mismatch. MVDR-based methods that are relatively immune to mismatch are traditionally called *robust* algorithms. The classic problem is to prevent unwanted signal nulling while preserving the adaptive nulling properties of the MVDR processor.

To begin we assume the following general form of the CSDM

$$\mathbf{R} = \sigma_n^2\,\mathbf{I} + \sigma_s^2 \mathbf{s}\mathbf{s}^H + \mathbf{Q}\,, \tag{3.1}$$

where Q is the cross spectral representation of the interferer environment and s represents the signal of interest. If we attempt to steer at s under conditions of mismatch, i.e., $\mathbf{e} \neq \mathbf{s}$, the MVDR weight vector is

$$\mathbf{a} = \frac{\mathbf{R}^{-1}\mathbf{e}}{\mathbf{e}^H\mathbf{R}^{-1}\mathbf{e}}\,. \tag{3.2}$$

Ideally we would like a to be represented as in equation (A.5), however mismatch causes the matrix inverse term in equation (3.2) to remain a function of s. We logically might assume a truly robust MVDR algorithm that completely preserves the nonmismatch nulling properties would subtract $\sigma_s^2\mathbf{s}\mathbf{s}^H$ from R thus giving the nonmismatch weight vector of equation (A.5). Since this would be impossible we attempt to add robustness to the processor in other ways.

3.1.1 Heuristic view

We have seen that as σ_n^2 increases, the sensitivity of the MVDR processor to mismatch decreases. So an intuitive robust method would synthetically increase the white noise in R by adding an ϵ^2 to the diagonal elements, i.e.,

$$\hat{\mathbf{R}} = \mathbf{R} + \epsilon^2\,\mathbf{I}\,, \tag{3.3}$$

where $0 \leq \epsilon^2 < \infty$. Then the robust weight vector is

$$\hat{a} = \frac{\hat{R}^{-1}e}{e^H\hat{R}^{-1}e} \tag{3.4}$$

with output power

$$\hat{P}_{MVDR} = \hat{a}^H R\, \hat{a}\ . \tag{3.5}$$

Note that as $\epsilon^2 \rightarrow \infty$, the white noise term dominates $\hat{R}$ of equation (3.4) and $\hat{a} \rightarrow e$. We use the calculated CSDM of equation (3.1) in the calculation of $\hat{P}_{MVDR}$ since using $\hat{R}$ would unnecessarily add white noise power to the output. Thus we must actually compute the robust weight vector $\hat{a}$ and form the quadratic of equation (3.5) as opposed to directly computing the MVDR output power as in equation (1.13).

Interestingly, adding a component to the diagonal element of the CSDM is also a method of inverting ill-conditioned matrices. So we see that while this method might enable us to invert a rank-defficient CSDM, it can also lead to a decrease in adaptivity of the MVDR processor.

We have also seen that as σ_s^2 decreases, the sensitivity of the MVDR processor also decreases. Since we cannot simply subtract σ_s^2 from R we might subtract a portion of the spatially correlated component from R , i.e.,

$$\hat{R} = \sigma_n^2 I + (1 - \zeta^2)(\sigma_s^2 ss^H + Q) \tag{3.6}$$

where $0 \leq \zeta^2 < 1$. Then

$$\hat{R} = (1 - \zeta^2)R - (1 - \zeta^2)\sigma_n^2 I + \sigma_n^2 I \tag{3.7}$$

or

$$\hat{R} = (1 - \zeta^2)\left[R + \frac{\zeta^2}{1 - \zeta^2}\sigma_n^2 I\right]. \tag{3.8}$$

Since the $(1 - \zeta^2)$ term will cancel when we form $\hat{a}$ we see that subtracting $\zeta^2(\sigma_s^2 ss^H + Q)$ from R is equivalent to adding synthetic white noise to R where

$$\epsilon^2 = \frac{\zeta^2}{1 - \zeta^2}\sigma_n^2\ . \tag{3.9}$$

3.1.2 Optimal solution

Since the magnitude of the weight vector is sensitive to the amount of white noise in R, we can use a norm bound on $\hat{\mathbf{a}}$ as another constraint on the MVDR processor (Hudson, 1981). That is we want to

$$\min(\ \hat{\mathbf{a}}^H \mathbf{R}\ \hat{\mathbf{a}})\ \text{subject to}\ \hat{\mathbf{a}}^H \mathbf{e} = 1\ \textit{and}\ |\ \hat{\mathbf{a}}\ |^2 = \delta^2\ . \tag{3.10}$$

The well known result of this optimization problem is

$$\hat{\mathbf{a}} = \frac{(\mathbf{R} + \epsilon^2 \mathbf{I})^{-1}\mathbf{e}}{\mathbf{e}^H(\mathbf{R} + \epsilon^2 \mathbf{I})^{-1}\mathbf{e}} \tag{3.11}$$

where ϵ^2 in this case is a Lagrange multiplier. So synthetically adding white noise to R *or* subtracting a portion of the correlated component from R is optimal in the sense of (3.10). Solving for ϵ^2 such that $|\ \hat{\mathbf{a}}\ |^2 = \delta^2$ unfortunately is a difficult problem.

An approach to solving $|\ \hat{\mathbf{a}}\ |^2 = \delta^2$ in terms of ϵ^2 is given in Hudson (1981). The approach uses the eigen decomposition of R (Johnson, 1982) as

$$\mathbf{R} = \sum_{i=1}^{M} \lambda_i \mathbf{v}_i \mathbf{v}_i^H \tag{3.12}$$

where $\mathbf{v}_i$ are the eigenvectors and λ_i the associated eigenvalues with $\lambda_1 \geq \lambda_2 \geq \ldots \geq \lambda_M$. Then

$$(\mathbf{R} + \epsilon^2 \mathbf{I})^{-1} = \sum_{i=1}^{M} \frac{1}{\lambda_i + \epsilon^2} \mathbf{v}_i \mathbf{v}_i^H \tag{3.13}$$

and

$$|\ \hat{\mathbf{a}}\ |^2 = \frac{\sum_{i=1}^{M} \left[\frac{1}{\lambda_i + \epsilon^2}\right]^2 |\ \mathbf{e}^H \mathbf{v}_i\ |^2}{\left[\sum_{i=1}^{M} \frac{|\ \mathbf{e}^H \mathbf{v}_i\ |^2}{\lambda_i + \epsilon^2}\right]^2} = \delta^2. \tag{3.14}$$

ϵ^2 then is found by finding the root of the equation

$$|\ \hat{\mathbf{a}}\ |^2 - \delta^2 = 0 \tag{3.15}$$

using a standard root finding technique (Kahaner, Moler, and Nash, 1989). It would seem that a considerable amount of numerical difficulties reside in this last step for large M. However positive results have been reported in Hudson (1981).

3.1.3 Simulations

To demonstrate the effect on MVDR performance of adding synthetic white noise to R we look at the mismatch simulations given in section 2.0. Specifically we analyze the mismatch-sensitive high SNR case. To begin we examine the simple one-signal case shown in table 2.2 for σ_n^2 = 0 dB and σ_s^2= 10 dB. Since in this case we want to eliminate all adaptive nulling when steered at the signal we simply let $\mathbf{a} \rightarrow \mathbf{e}$ by letting $\epsilon^2 \rightarrow \infty$. We progressively compute $\hat{\mathbf{a}}$ of equation (3.11) and $\hat{P}_{MVDR}$ of equation (3.5) for increasing values of ϵ^2 and determine the associated PIA's. Figure 3.1 contains the PIA versus ϵ^2 and $|\hat{\mathbf{a}}|^2$ versus ϵ^2. As we would expect, PIA approaches 0 dB as ϵ^2 increases. We also see how $|\hat{\mathbf{a}}|^2$ gradually approaches the minimum value of 1/M or -13.01 dB.

A slightly more interesting example is the one shown in table 2.3. Here an interferer falls on a null when we steer at 180° and we see the PIA is -30.75 dB for the (σ_n^2 = 0 dB, σ_s^2 = 10 dB) case. Figure 3.2 is the resulting plots for PIA versus ϵ^2 and $|\hat{\mathbf{a}}|^2$ versus ϵ^2. We note that these plots are similar to those of figure 3.1. This fact seems reasonable since we know that the MVDR processor is not putting "effort" into nulling this interferer. Thus the synthetic white noise only affects unwanted signal nulling as in the previous one-signal example.

We now examine the case shown in table 2.4. Here the 10 dB interferer falls on a sidelobe when we steer at 180°. Figure 3.3 clearly demonstrates the interesting effect synthetic white noise has on interferer nulling in this situation. As we add more white noise to R we see that PIA gradually rises. In fact at the ϵ^2 value of 16 dB, the PIA is markedly above 0 dB. Here we have achieved the optimal balance of unwanted signal nulling and interferer nulling by placing the correct amount of emphasis on $|\hat{\mathbf{a}}|^2$ minimization. However as we add more ϵ^2 we begin to adversely affect this balance. We see that at ϵ^2 = 34 dB we have hindered MVDR adaptive nulling to the extent that we achieve only conventional performance.

The quandary we are faced when attempting to deal with mismatch occurs when we select ϵ^2 or the corresponding normbound on $\hat{\mathbf{a}}$. Since the severity of mismatch depends upon the signal power, noise powers and the spatial distribution of the interferers we really can only guess at an appropriate ϵ^2 or $|\hat{\mathbf{a}}|^2 = \delta^2$ bound.

3.2 White Noise Constraint Robust MVDR Algorithm

As we have noted above, addition of synthetic white noise to R is the solution of the constrained optimization problem of (3.10). However it is difficult to solve for ϵ^2 in terms of the normbound constraint δ^2. Considerable amount of attention recently has been given to a technique that *approximates* (3.10) called the white noise constraint (WNC) algorithm (Cox, Zeskind, and Owen, 1987). As in the optimal solution, the WNC technique attempts to desensitize the MVDR processor to mismatch by restricting $|\hat{\mathbf{a}}|^2$ and thus constraining the output power due to white noise. We refer the reader to Cox, Zeskind, and Owen (1987) for the complete description of the method.

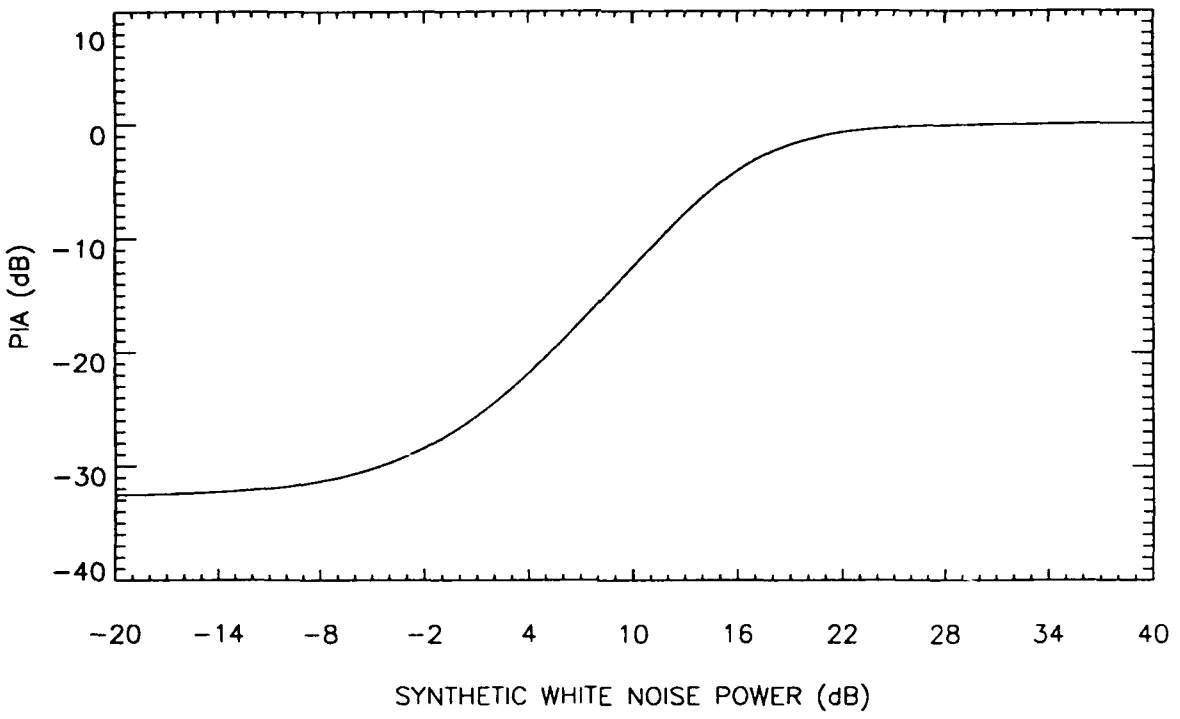

(a)

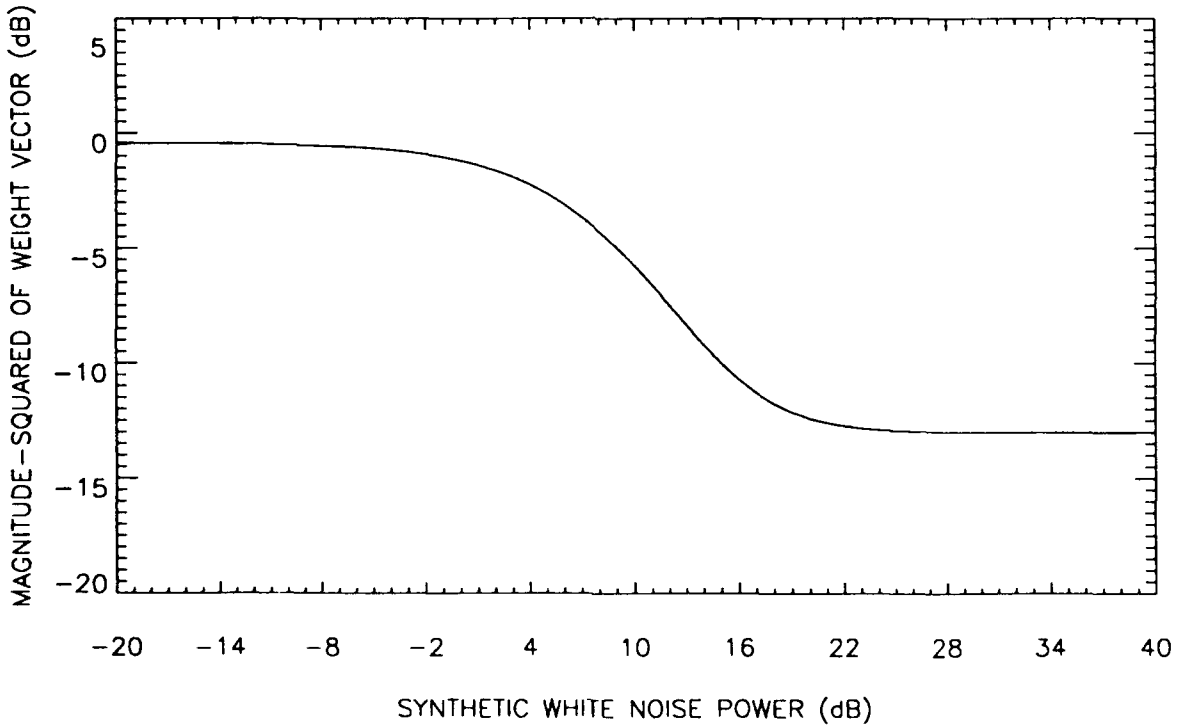

(b)

Figure 3.1. Optimal robust MVDR processor results for signal power $\sigma_s^2 = 10$ dB and noise power $\sigma_n^2 = 0$ dB: (a) PIA vs. synthetic white noise power, (b) corresponding magnitude squared of the weight vector $| \hat{a} |^2$.

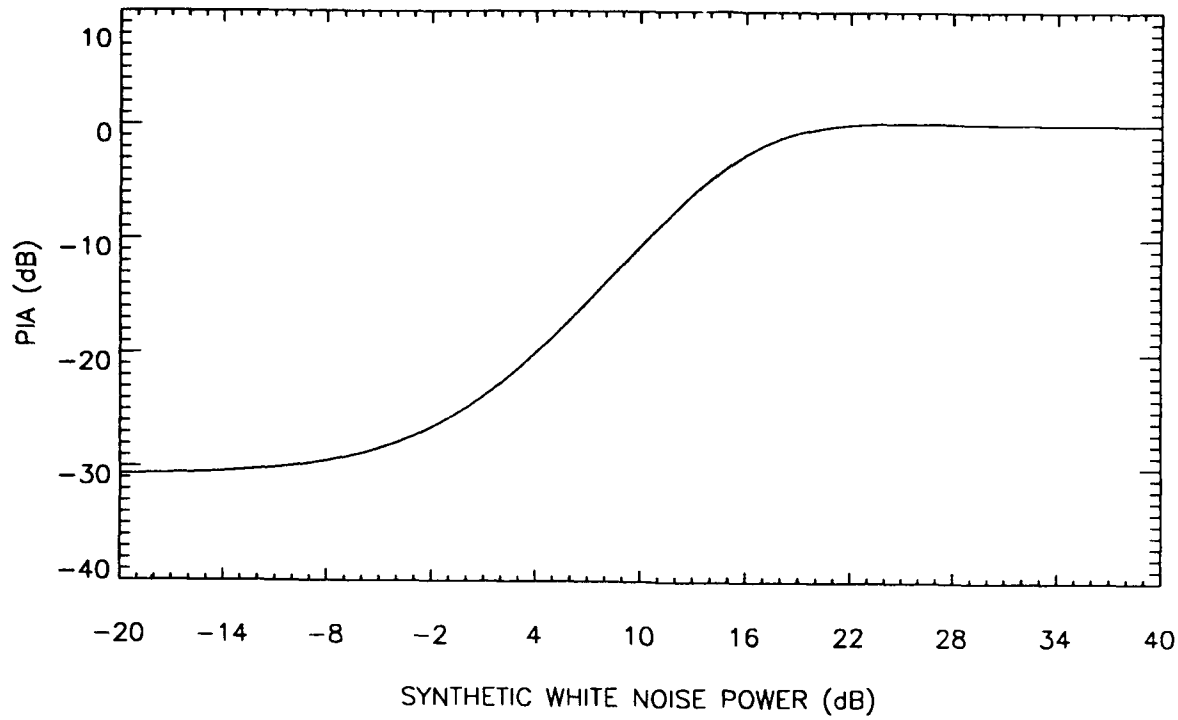

(a)

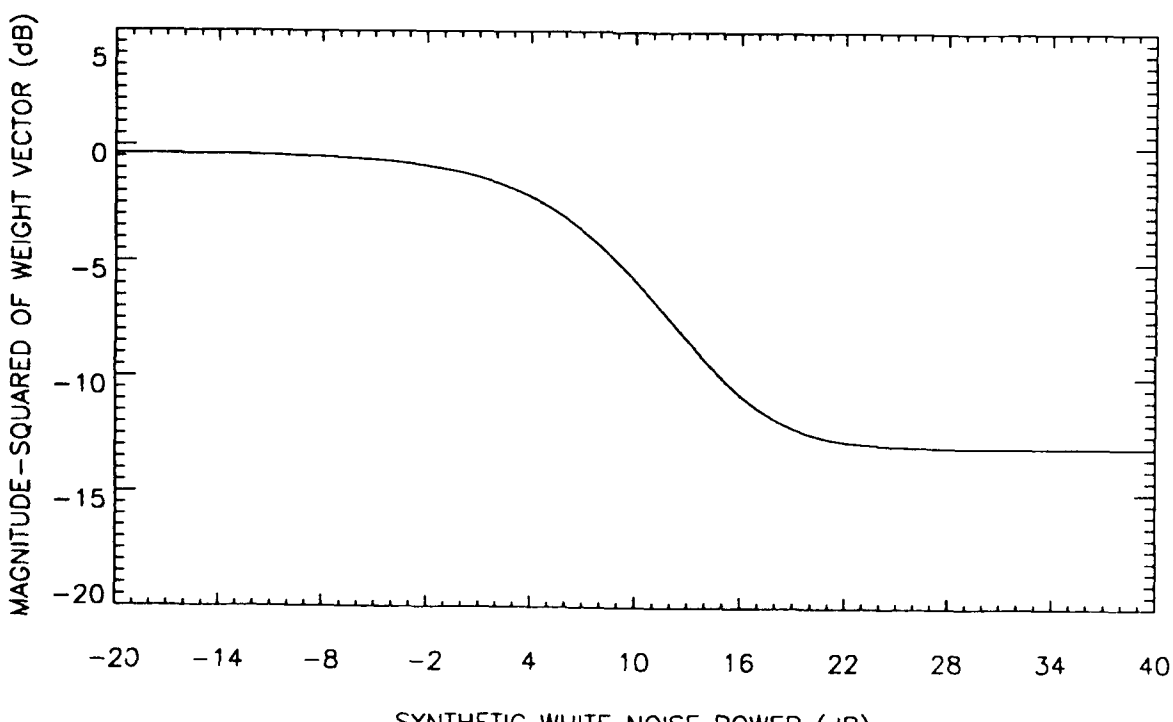

(b)

Figure 3.2. Optimal robust MVDR processor results for signal power $\sigma_s^2 = 10$ dB and noise power $\sigma_n^2 = 0$ dB with 10 dB interferer falling on null: (a) PIA vs. synthetic white noise power, (b) corresponding magnitude squared of the weight vector $|\hat{\mathbf{a}}|^2$.

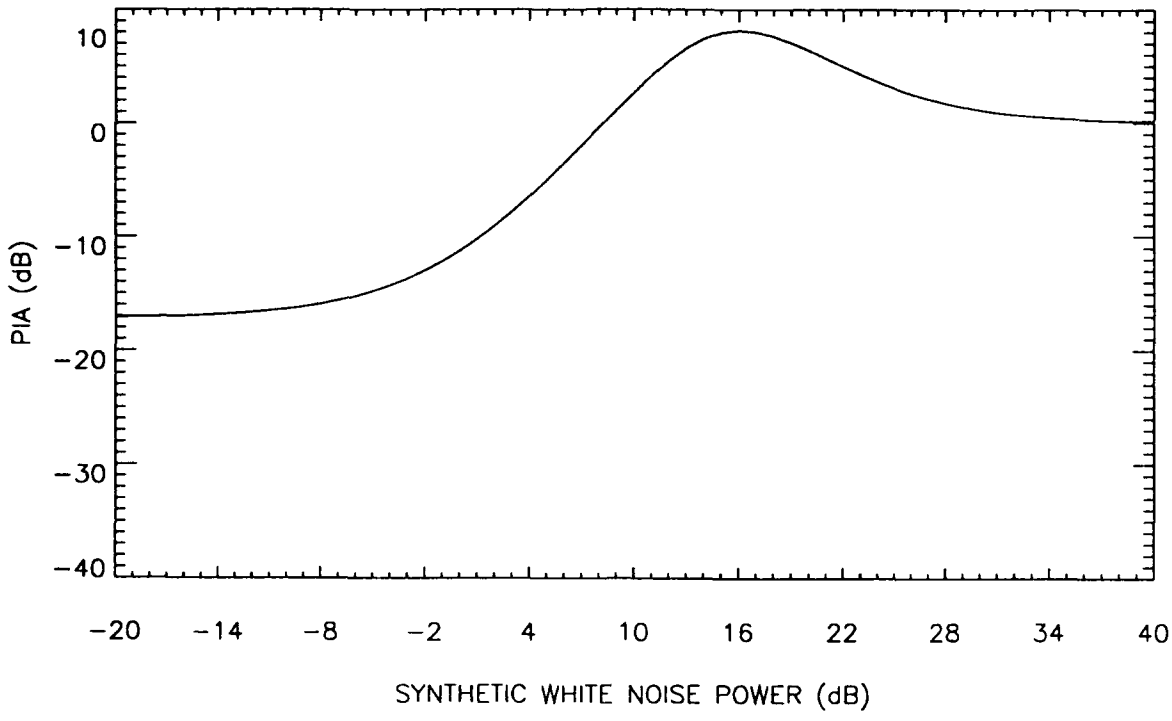

(a)

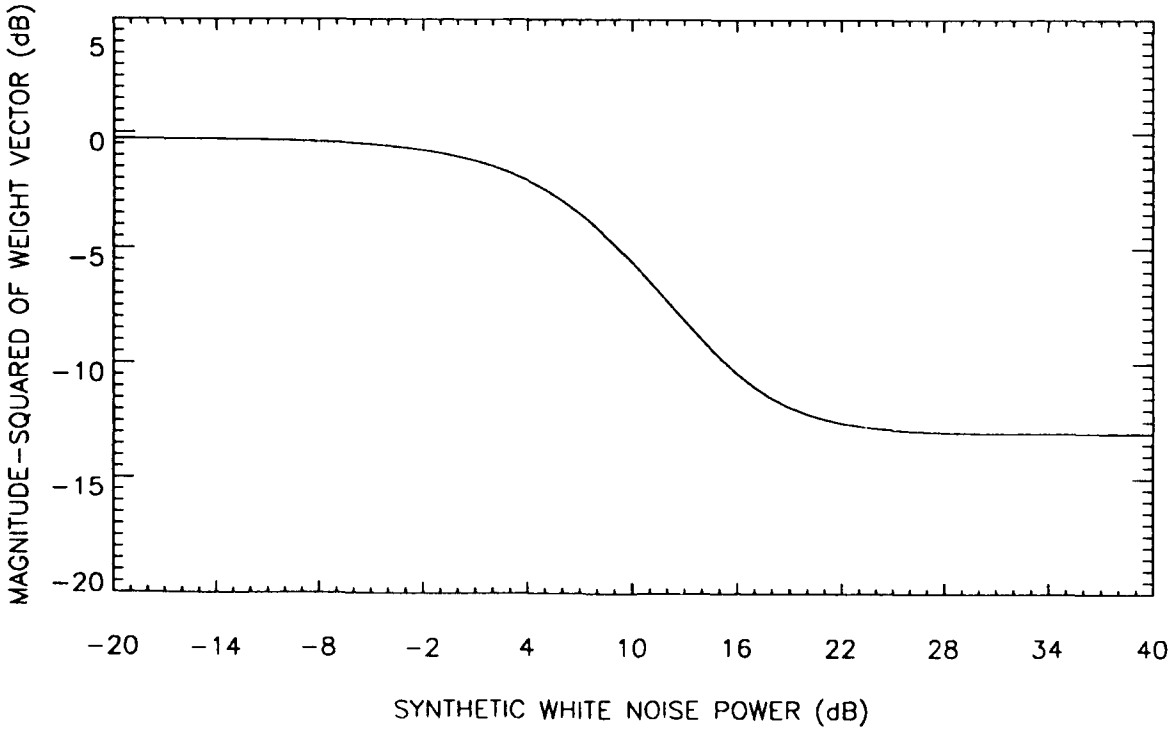

(b)

Figure 3.3. Optimal robust MVDR processor results for signal power $\sigma_s^2 = 10$ dB and noise power $\sigma_n^2 = 0$ dB with 10 dB interferer falling on sidelobe: (a) PIA vs. synthetic white noise power, (b) corresponding magnitude squared of the weight vector $| \hat{\mathbf{a}} |^2$.

The WNC weight vector is computed as

$$\hat{\mathbf{a}}_{WNC} = \frac{(\mathbf{R}^{-1} + \beta\mathbf{I})\mathbf{e}}{\mathbf{e}^H(\mathbf{R}^{-1} + \beta\mathbf{I})\mathbf{e}} \tag{3.16}$$

or

$$\hat{\mathbf{a}}_{WNC} = \frac{\mathbf{R}^{-1}\mathbf{e}}{\mathbf{e}^H\mathbf{R}^{-1}\mathbf{e} + \beta\mathbf{M}} + \frac{\beta\mathbf{e}}{\mathbf{e}^H\mathbf{R}^{-1}\mathbf{e} + \beta\mathbf{M}} \tag{3.17}$$

where β is a scaler derived from the normbound constraint and I is the identity matrix. We obtain β by solving

$$| \hat{\mathbf{a}}_{WNC} |^2 = \delta^2 . \tag{3.18}$$

We then get

$$\beta = \frac{\mathbf{e}^H\mathbf{R}^{-1}\mathbf{e}}{\mathbf{M}} \left[\sqrt{\frac{| \mathbf{a} |^2 - 1/\mathbf{M}}{\delta^2 - 1/\mathbf{M}}} - 1 \right] \tag{3.19}$$

where $| \mathbf{a} |^2$ is the magnitude or norm squared of the *unconstrained* weight vector, i.e.,

$$| \mathbf{a} |^2 = \frac{\mathbf{e}^H\mathbf{R}^{-2}\mathbf{e}}{(\mathbf{e}^H\mathbf{R}^{-1}\mathbf{e})^2} . \tag{3.20}$$

Since $| \mathbf{a} |^2 > 1/\mathrm{M}$, $\delta^2 > 1/\mathrm{M}$ and $| \mathbf{a} |^2 > \delta^2$ we see that $\beta > 0$. That is we only use the constraint if $| \mathbf{a} |^2$ exceeds the bound δ^2. Appendix C proves that $\hat{\mathbf{a}}_{WNC}$ given in equation (3.16) is equivalent to the form of the WNC weight vector given in Cox, Zeskind, and Owen (1987) for the single boresight constraint case. Now, we proceed to compute the output power of the processor as

$$\hat{\mathrm{P}}_{WNC} = \hat{\mathbf{a}}_{WNC}^H \mathbf{R}\, \hat{\mathbf{a}}_{WNC} . \tag{3.21}$$

Using equation (3.16) we get

$$\hat{\mathrm{P}}_{WNC} = \frac{\mathrm{P}_{MVDR}(2\rho + 1) + \mathrm{P}_{CONV}\rho^2}{(\rho + 1)^2} \tag{3.22}$$

where P_{MVDR} and P_{CONV} are the output powers of the unconstrained MVDR processor and the

conventional processor and

$$\rho = \sqrt{\frac{|\,\mathbf{a}\,|^2 - 1/M}{\delta^2 - 1/M}} - 1\,. \tag{3.23}$$

In other words, the output power of the WNC MVDR processor can be determined simply by scaling and summing the output powers of the unconstrained MVDR and conventional processors.

3.2.1 Rationale for the WNC algorithm

We now present a rationale for the WNC MVDR algorithm which is consistent with the analysis given at the beginning of this section. As we have shown, the method of adding robustness to the MVDR processor involves adding synthetic white noise to R or equivalently subtracting a portion of the correlated component from R. Since we want to analytically compute $\hat{\mathbf{a}}$ of equation (3.4) in order to avoid the numerical difficulties of Hudson (1981), we propose the following approach: subtract a rank-one matrix $\mathbf{d}\mathbf{d}^H$ from R of equation (3.1) to remove as much of the signal component as possible while maintaining a significant portion of the interferer component in order to ensure adequate adaptive nulling. So we compute $\hat{\mathbf{a}}_{WNC}$ as

$$\hat{\mathbf{a}}_{WNC} = \frac{(\mathbf{R} - \mathbf{d}\mathbf{d}^H)^{-1}\mathbf{e}}{\mathbf{e}^H(\mathbf{R} - \mathbf{d}\mathbf{d}^H)^{-1}\mathbf{e}} \tag{3.24}$$

where we require

$$|\,\hat{\mathbf{a}}_{WNC}|^2 = \delta^2. \tag{3.25}$$

Then $\mathbf{R} - \mathbf{d}\mathbf{d}^H$ can be inverted *analytically* via the matrix inversion lemma. Note that the constraint $\hat{\mathbf{a}}_{WNC}^H\,\mathbf{e} = 1$ is still satisfied.

As noted, ideally we would like to simply remove the signal component from R and thus get the nonmismatch weight vector of equation (A.5). The rank-one matrix in this ideal case would be

$$\mathbf{d}\mathbf{d}^H = \sigma_s^2\,\mathbf{s}\mathbf{s}^H\,. \tag{3.26}$$

Obviously we will not know s so we propose the following form of the matrix:

$$\mathbf{d}\mathbf{d}^H = \alpha^2\mathbf{R}\mathbf{e}\mathbf{e}^H\mathbf{R}\,. \tag{3.27}$$

Expanding this equation and using equation (3.1) we get

$$dd^H = \alpha^2(\sigma_n^4 ee^H + \sigma_s^4 |\, e^H s\,|^2 ss^H + \sum_{i=1}^{N} \sigma_{ti}^4 |\, e^H t\,|^2\, t_i t_i^H + K) \tag{3.28}$$

where α^2 is a scalar, $Q = \sum_{i=1}^{N} \sigma_{ti}^2\, t_i t_i^H$ and K is a matrix containing the remaining cross terms. First note that we can disregard the ee^H component of dd^H since it does not enter into the calculation of $\hat{a}_{WNC}$ of equation (3.24). This is shown in appendix A (equation A.5). The ss^H component of dd^H is actually the term we wish to subtract from R, and, as in the optimal solution of equation (3.11), we subtract a portion of the correlated component represented by the third term of equation (3.28). The K matrix of equation (3.28) unfortunately might adversely affect the WNC MVDR processor performance since K does not represent a physical component of R. The effect K might have on performance naturally is dependent on the interferer environment.

Now using dd^H of equation (3.27) we get

$$\hat{a}_{WNC} = \frac{\left[R^{-1} - \dfrac{M}{e^H R e - 1/\alpha^2} I\right] e}{e^H \left[R^{-1} - \dfrac{M}{e^H R e - 1/\alpha^2} I\right] e}\,. \tag{3.29}$$

Now if we let $0 < \alpha^2 < 1/e^H R e$ and use

$$\beta = -\frac{M}{e^H R e - 1/\alpha^2} \tag{3.30}$$

we get the WNC weight vector of equation (3.16). In other words, we can interpret the WNC weight vector as an approximation of the optimal weight vector given by equation (3.11). The performance we achieve using $\hat{a}_{WNC}$ versus $\hat{a}$ of equation (3.11) as measured for instance by PIA is highly dependent on the interferer environment. Interestingly, if $|\, e^H t_{\,i}|^2 = 0$ for all i, i.e., the interferers are orthogonal to the steering vector, then it is easy to show that $K = 0$. Moreover since equation (3.28) will not contain the interferer components we will simply be subtracting the signal component from R. In this case, we actually might achieve superior performance with the WNC algorithm. However this orthogonality scenario is highly improbable. In any case, if $|\, e^H t_{\,i}|^2$ is small the effect of K might be mitigated.

Based upon this analysis we conclude that in the simple one signal case where $Q = 0$ we would expect the performances of the WNC and optimal algorithms to be equal for some bound δ^2. This seems reasonable since in either case we equally will subtract a portion of ss^H from R.

3.2.2 WNC MVDR simulations

We now examine the effect of WNC on MVDR performance under conditions of mismatch by reexamining the simulations described in section 2.0 and the beginning of this section. Figure 3.4 contains the MVDR array response and $|\hat{a}_{WNC}|^2$ for the (σ_n^2 = 0 dB, σ_s^2 = 10 dB) with 0.1λ sensor position error with a WNC or normbound δ^2 = -10 dB. We clearly can see how the weight vector has been "sheered" off at -10 dB. Moreover we see the corresponding increase in output power which results in an increase of output power due to the signal. Table 3.1 lists the $|\hat{a}_{WNC}|^2$ and PIA for this case when we steer at the signal. We note the dramatic increase in PIA over the value shown in table 2.2 (b). However it is still less than zero since we have not removed all of the adaptivity from the processor. Note also the broadening of the peak in figure 3.4 as compared to the nonmismatch case shown in figure 2.1. This fact is expected since we actually inhibit adaptive nulling when the signal falls within the mainlobe and $|\hat{a}|^2 > -10$ dB. So while the WNC algorithm can be used to broaden the mainlobe, it also contributes to a decrease in array resolution.

Table 3.1. $|\hat{a}_{WNC}|^2$ and PIA of the MVDR processor when steered at signal with 0.1λ errors in sensor position estimates with normbound or WNC = -10 dB.

Signal and noise powers	$\|a_{WNC}\|^2$	PIA
σ_n^2 = 0 dB, σ_s^2 = 10 dB	-10.00 dB	-5.14 dB

Figure 3.5 shows the PIA and $|\hat{a}_{WNC}|^2$ for various β when we steer at the signal. As we expect, PIA$\rightarrow$0 dB as β increases. Note the similarities between figure 3.5 and figure 3.1. So the performance of the WNC algorithm is shown here to equal the performance of the optimal technique for this one-signal case.

Next we reexamine the interferer simulations described in the beginning of this section to evaluate the effect an interferer has on the performance of the WNC MVDR algorithm. Figure 3.6 shows the PIA and $|\hat{a}_{WNC}|^2$ versus β when the 10 dB interferer falls on a null. Since the K matrix of equation (3.28) is small in this case, we certainly would expect figure 3.6 to resemble figure 3.2 which was obtained by adding synthetic white noise to R. Conversely, figure 3.7 results from the simulation that produced figure 3.3. Here the interferer falls on a sidelobe. We clearly see the difference between the PIA of the WNC algorithm and that of the optimal synthetic white noise algorithm. Figure 3.7 (a) lacks the hump of figure 3.3 (a). In fact the WNC PIA does not appreciably

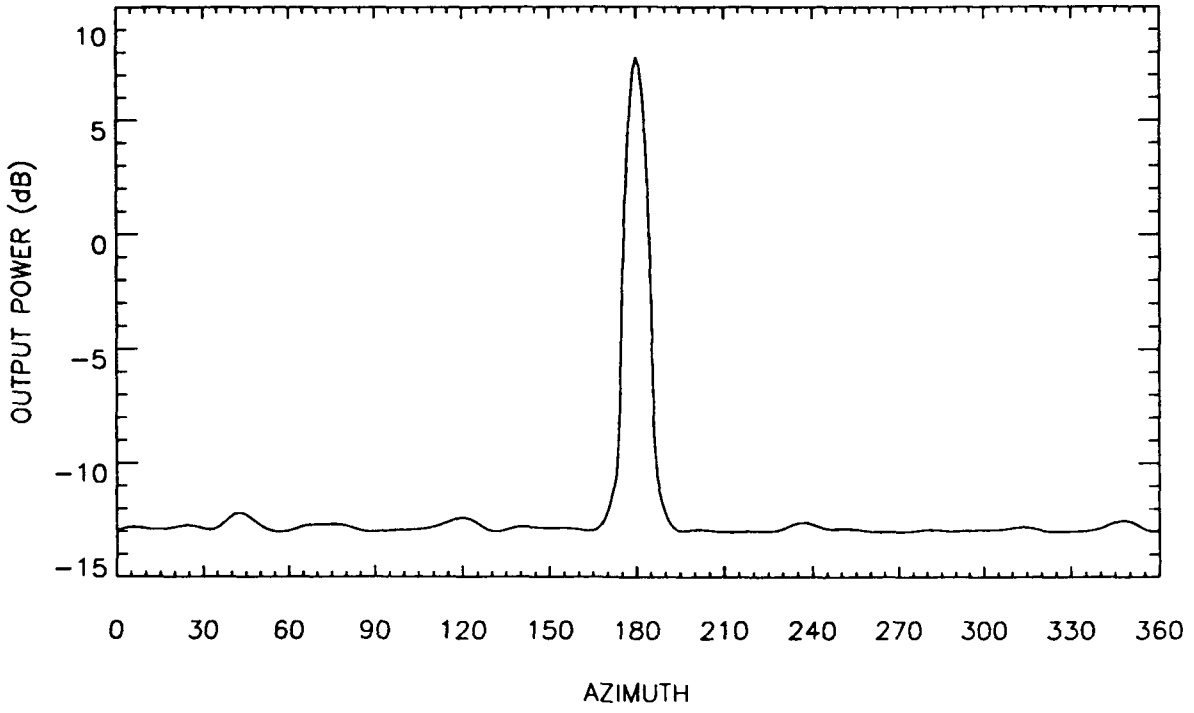

(a)

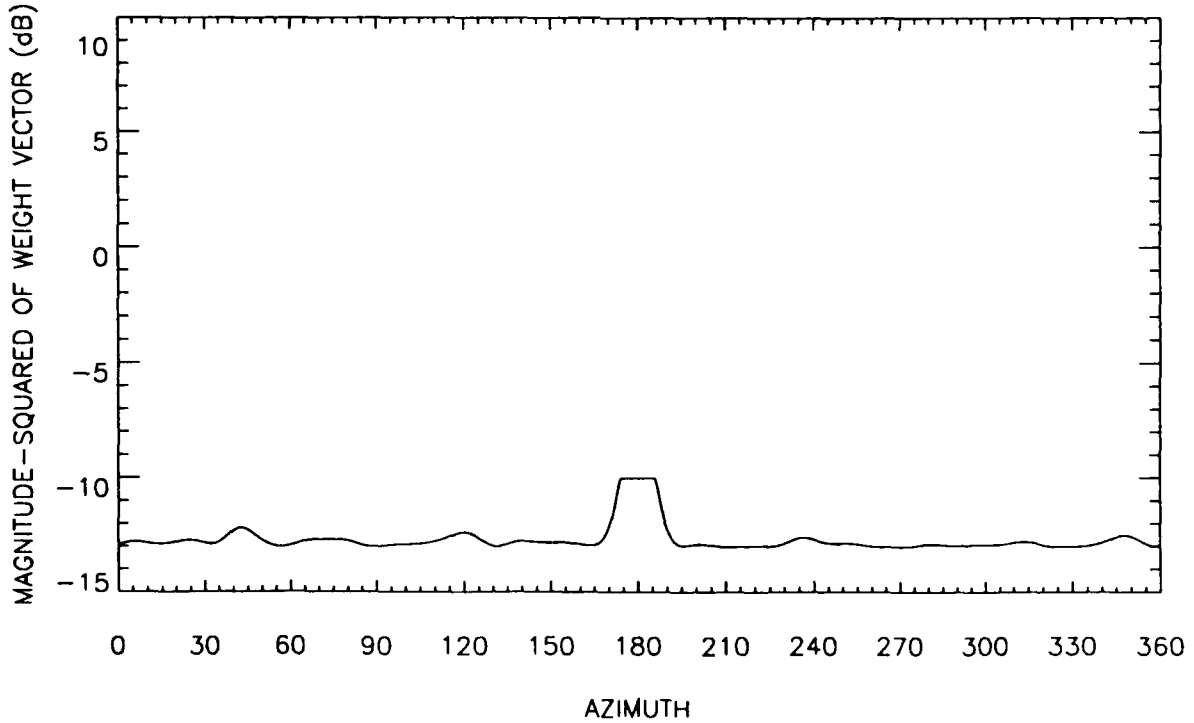

(b)

Figure 3.4. WNC MVDR processor results for signal power $\sigma_s^2 = 10$ dB and noise power $\sigma_n^2 = 0$ dB with 0.1λ sensor position error and δ^2= -10 dB: (a) output power, (b) corresponding magnitude squared of the weight vector $|\hat{a}_{WNC}|^2$.

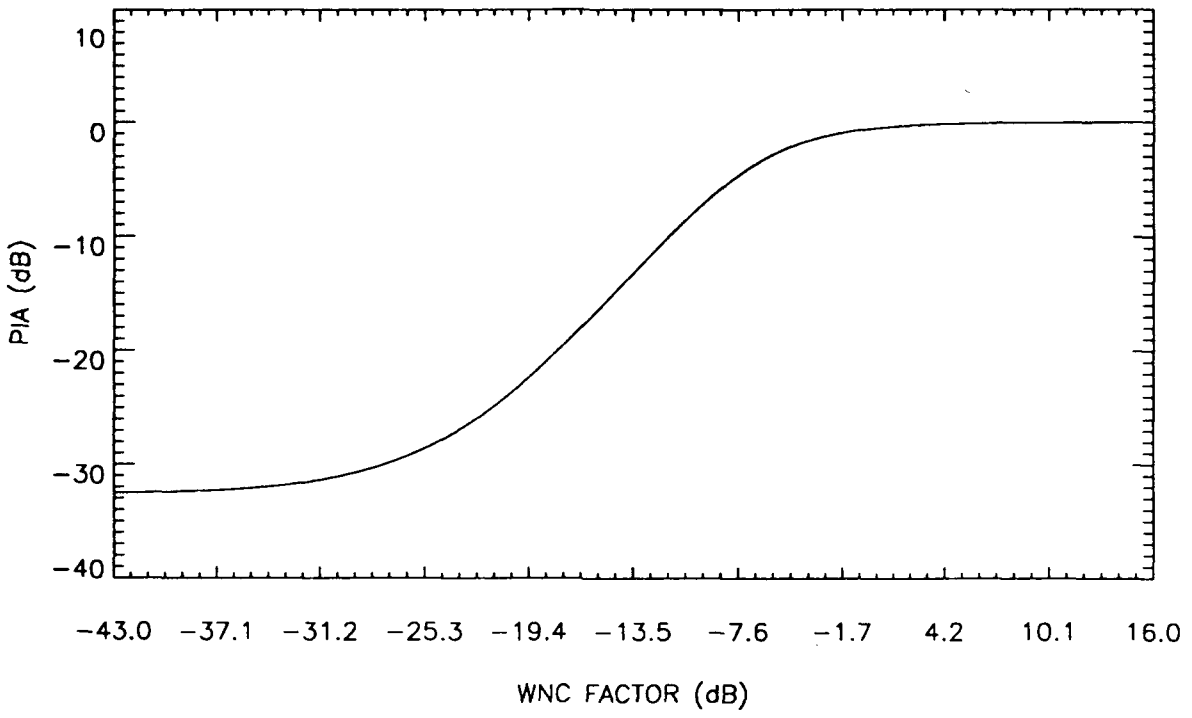

(a)

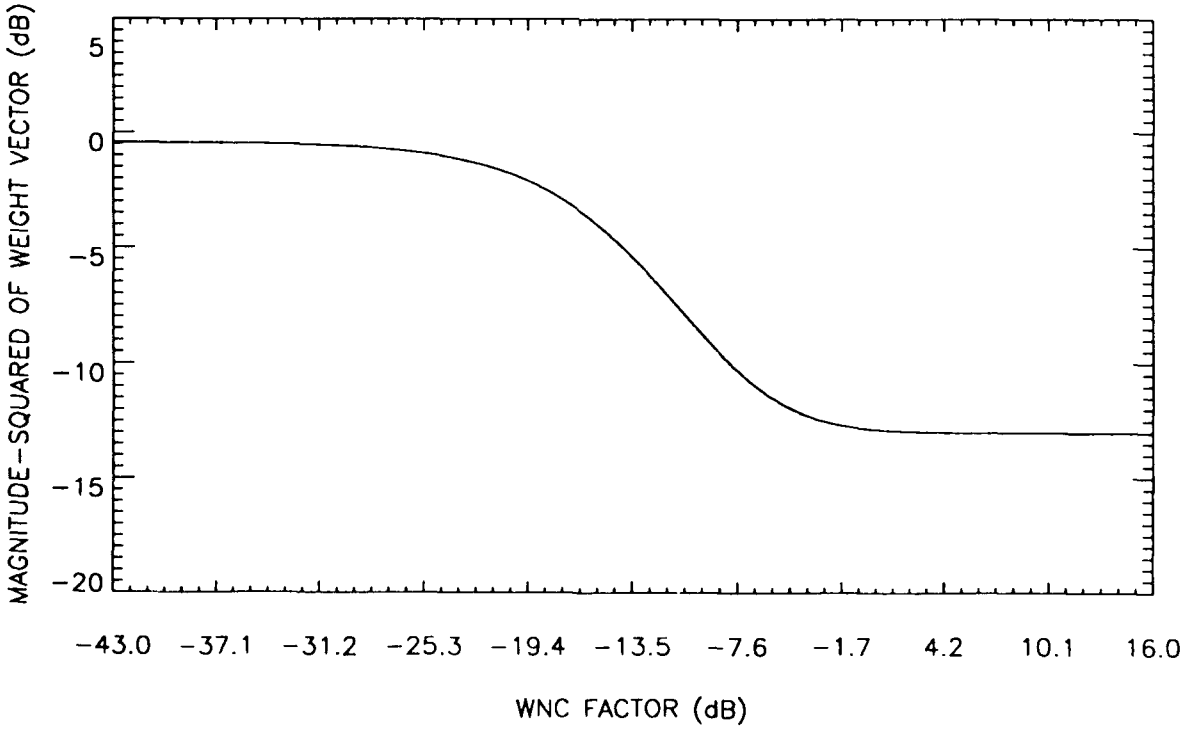

(b)

Figure 3.5. WNC MVDR processor results for signal power $\sigma_s^2 = 10$ dB and noise power $\sigma_n^2 = 0$ dB: (a) PIA vs. β, (b) corresponding magnitude squared of the weight vector $|\hat{a}_{WNC}|^2$.

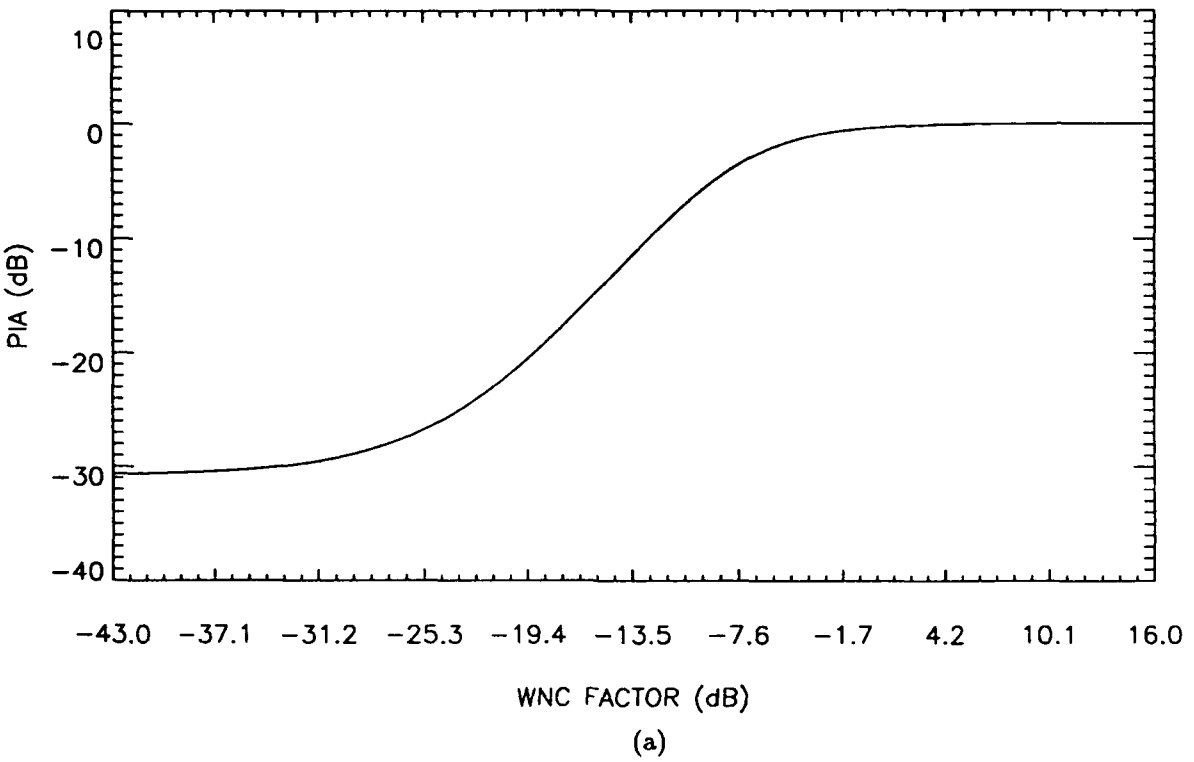

(a)

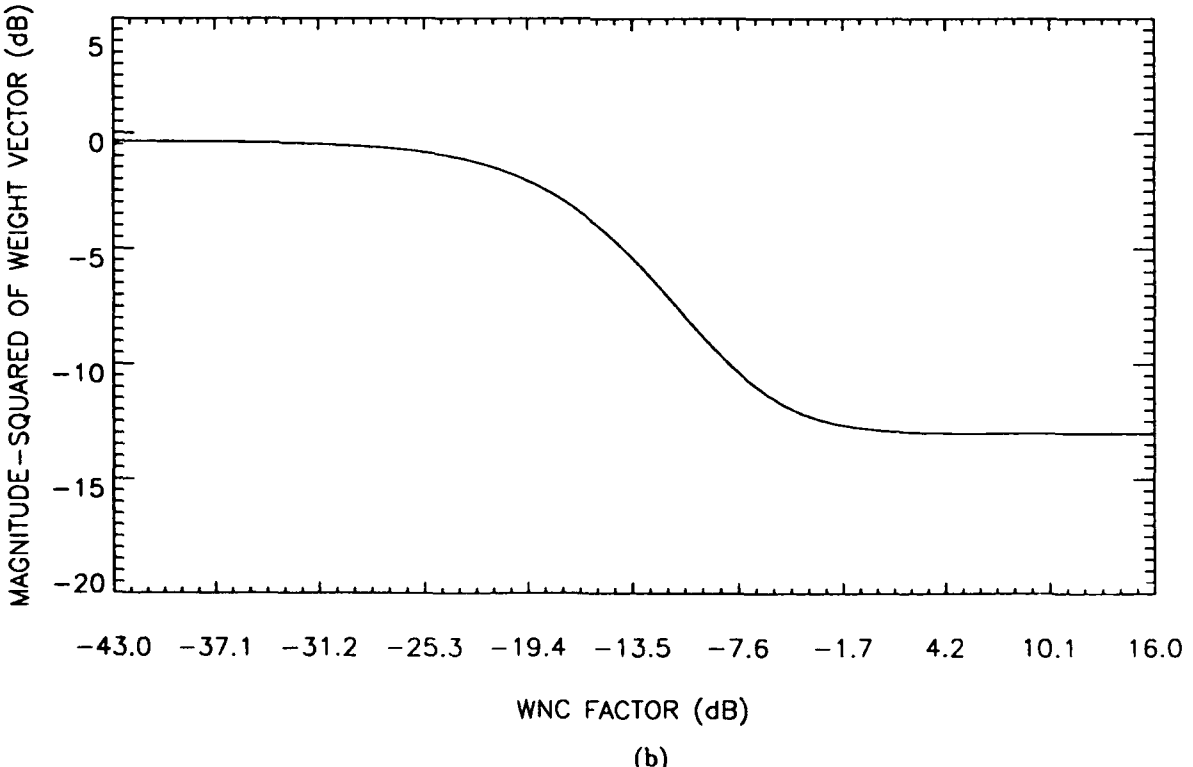

(b)

Figure 3.6. WNC MVDR processor results for signal power $\sigma_s^2 = 10$ dB and noise power $\sigma_n^2 = 0$ dB with 10 dB interferer falling on null: (a) PIA vs. β, (b) corresponding magnitude squared of the weight vector $|\hat{a}_{WNC}|^2$.

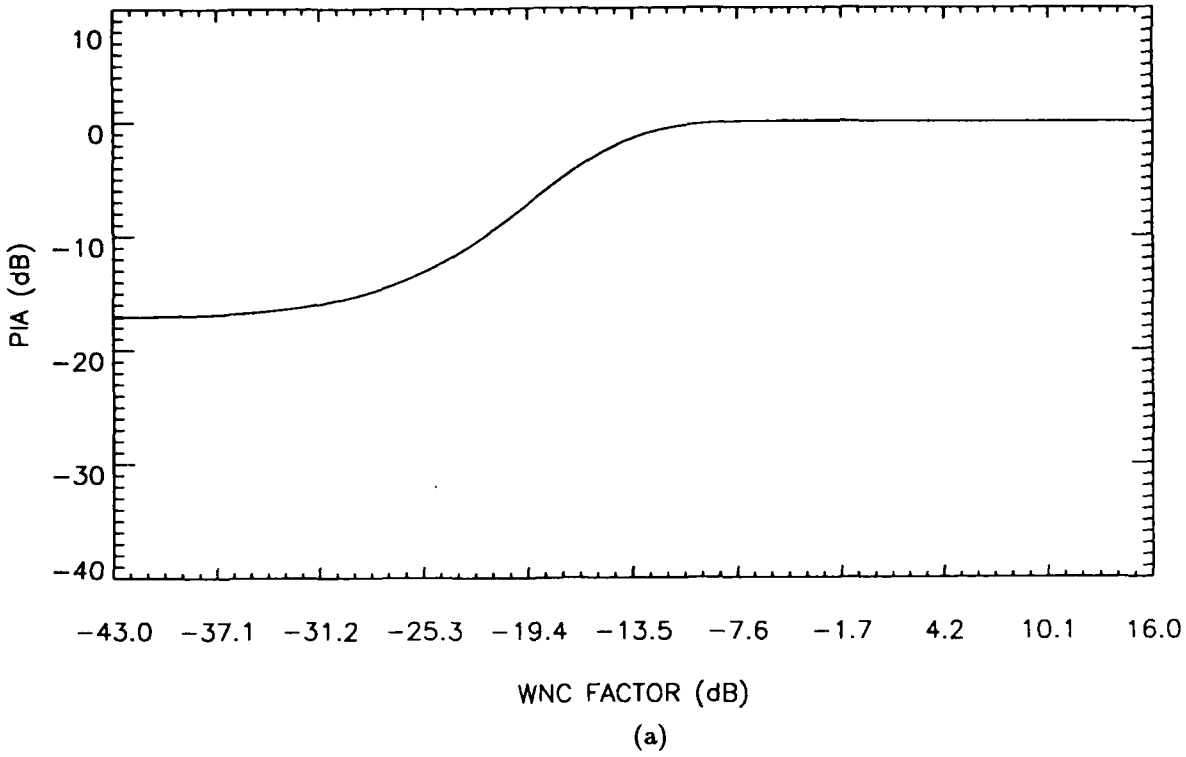

(a)

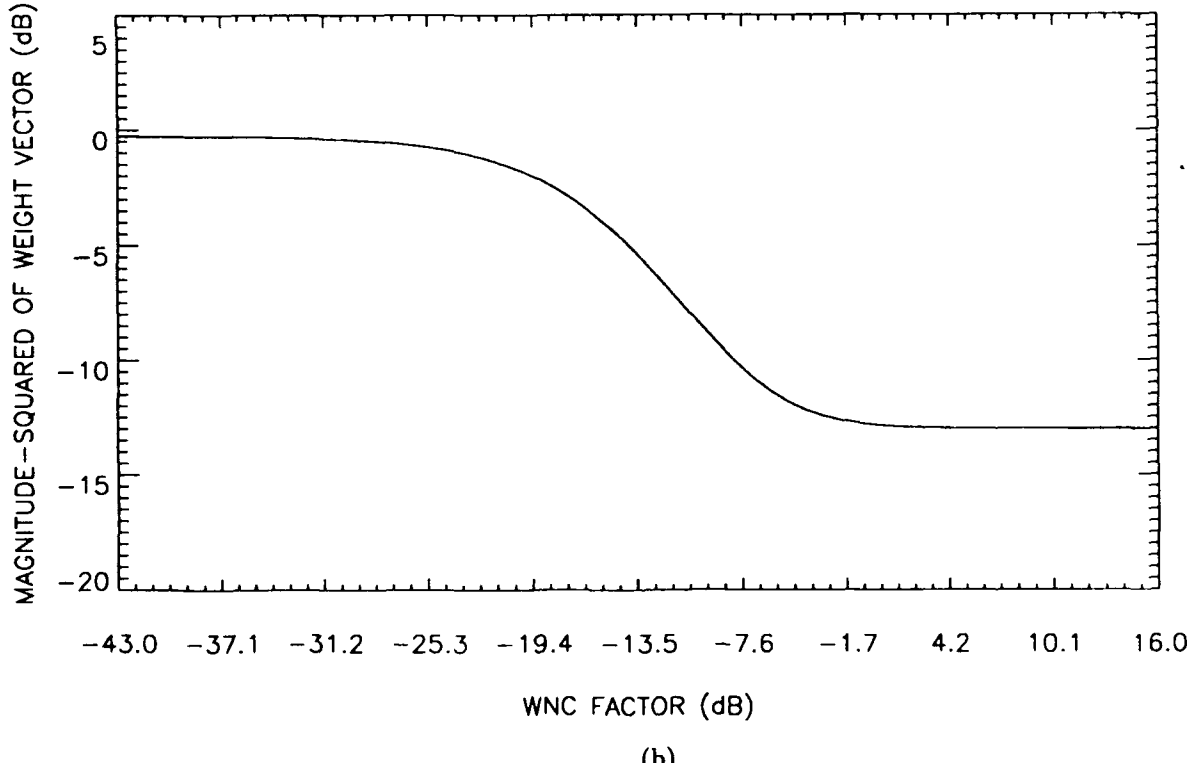

(b)

Figure 3.7. WNC MVDR processor results for signal power $\sigma_s^2 = 10$ dB and noise power $\sigma_n^2 = 0$ dB with 10 dB interferer falling on sidelobe: (a) PIA vs. β, (b) corresponding magnitude squared of the weight vector $|\hat{a}_{WNC}|^2$.

exceed 0 dB. Obviously the K matrix in this case adversely affects WNC MVDR performance.

3.2.3 Possible further work

Possible extensions to this work might involve determining a better rank-one matrix dd^H that will not result in severe cross terms in K. Possibly we could use a sum of rank-one matrices, i.e., $d_1 d_1^H + \ldots + d_p d_p^H$, in order to reduce the effects of K.

3.3 Eigenanalysis Approach to Mismatch

Further insight into mismatch can be gained by analyzing the MVDR processor via the eigen decomposition of R as in equation (3.12). The MVDR weight vector is then

$$a = \frac{\left[\sum_{i=1}^{M} \frac{1}{\lambda_i} v_i v_i^H\right] e}{e^H \left[\sum_{i=1}^{M} \frac{1}{\lambda_i} v_i v_i^H\right] e}. \tag{3.31}$$

It is well known (Johnson, 1982) that if

$$R = \sigma_n^2 I + \sigma_s^2 s s^H + \sum_{i=1}^{k-1} \sigma_{ti}^2 \, t_i t_i^H \tag{3.32}$$

then the eigenvectors associated with the k largest eigenvalues span the subspace containing the signal vectors and the remaining M-k eigenvectors span the subspace which is orthogonal to the signal subspace. Now if we steer towards s (e = s),

$$a = \frac{\sum_{i=1}^{k} \frac{v_i^H e}{\lambda_i} v_i}{\sum_{i=1}^{k} \frac{|\, v_i^H e \,|^2}{\lambda_i}}. \tag{3.33}$$

However, under conditions of mismatch a will be as in equation (3.31) above. In this case we might view

the terms $\sum_{i=k+1}^{M} \frac{v_i^H e}{\lambda_i} v_i$ and $\sum_{i=k+1}^{M} \frac{|\, v_i^H e \,|^2}{\lambda_i}$ in a as contributing to a certain amount of distortion in

the weight vector.

Intuitively we argue that under conditions of mismatch we simply can disregard those M - k eigenvectors in our calculation of the MVDR weight vector and force a to have the form of equation (3.33). Since we usually do not know k (the number of spatially correlated components in R) we propose using the magnitude squared of the weight vector as a gauge to determine the number of

eigenvectors we can eliminate. That is we compute **a** as in equation (3.33) with the largest k such that $|\mathbf{a}|^2 < \delta^2$.

3.3.1 *Simulation*

To determine whether we obtain any performance improvement under mismatch conditions with this method, we examine the previous simulation involving the 10 dB interferer falling on a sidelobe when we steer at the signal with $\sigma_n^2 = 0$ dB and $\sigma_s^2 = 10$ dB. Figure 3.8 is a plot of PIA and $|\mathbf{a}|^2$ versus k. Note for k=2, $|\mathbf{a}|^2 <$ -12 dB. For this value of k we gain considerably in PIA over the WNC results of figure 3.7 and the synthetic white noise results of figure 3.3. In fact, the PIA at k=2 is merely 1 dB less than the PIA of table 2.4 (a) that we obtain with no mismatch. Also note the dramatic rise of $|\mathbf{a}|^2$ at k=3 and the associated dip in PIA resulting from mismatch. For comparison purposes we have included the corresponding plots for the nonmismatch case in figure 3.9.

3.4 Possible Improvements to MVDR Nulling

In this section we briefly propose an approach that might lead to improved MVDR nulling performance. As we have seen, computing the weight vector $\hat{\mathbf{a}}$ with the addition of synthetic white noise to the CSDM R leads to decreased emphasis on MVDR adaptive nulling. Since the level of white noise power in R has such a significant impact on MVDR performance, one might argue that subtracting a certain amount of white noise from R would lead to *improvement* in PIA under nonmismatch conditions. That is we can compute the weight vector as

$$\hat{\mathbf{a}} = \frac{(\mathbf{R} - \mu^2\mathbf{I})^{-1}\mathbf{e}}{\mathbf{e}^H(\mathbf{R} - \mu^2\mathbf{I})^{-1}\mathbf{e}} . \tag{3.34}$$

Then,

$$\hat{P}_{MVDR} = \hat{\mathbf{a}}^H(\mathbf{R} - \mu^2\mathbf{I})\hat{\mathbf{a}} = \hat{\mathbf{a}}^H\mathbf{R}\hat{\mathbf{a}} - \mu^2|\hat{\mathbf{a}}|^2 \tag{3.35}$$

where now we also subtract the white noise term $\mu^2\mathbf{I}$ from R in our calculation of $\hat{P}_{MVDR}$. Then

$$\hat{P}_{MVDR} = \frac{1}{\mathbf{e}^H(\mathbf{R} - \mu^2\mathbf{I})^{-1}\mathbf{e}} . \tag{3.36}$$

The obvious difficulty involves choosing the "best" μ^2. Certainly $(\mathbf{R} - \mu^2\mathbf{I})$ must be full rank and physically meaningful. That is we would not want to subtract more white noise than what is contained in R. Previous similar work in the field of spectral estimation (Pisarenko, 1973) involved subtracting the largest quantity μ^2 from the diagonal while still preserving the nonnegative definite property of the matrix (Johnson, 1982).

In section 2.0 and in appendix B we presented how adaptive nulling and the magnitude squared of the weight vector are related to white noise in R. Referring to equations (B.4) and (B.14) for the one interferer case we see that as white noise power becomes very small, the null of the MVDR

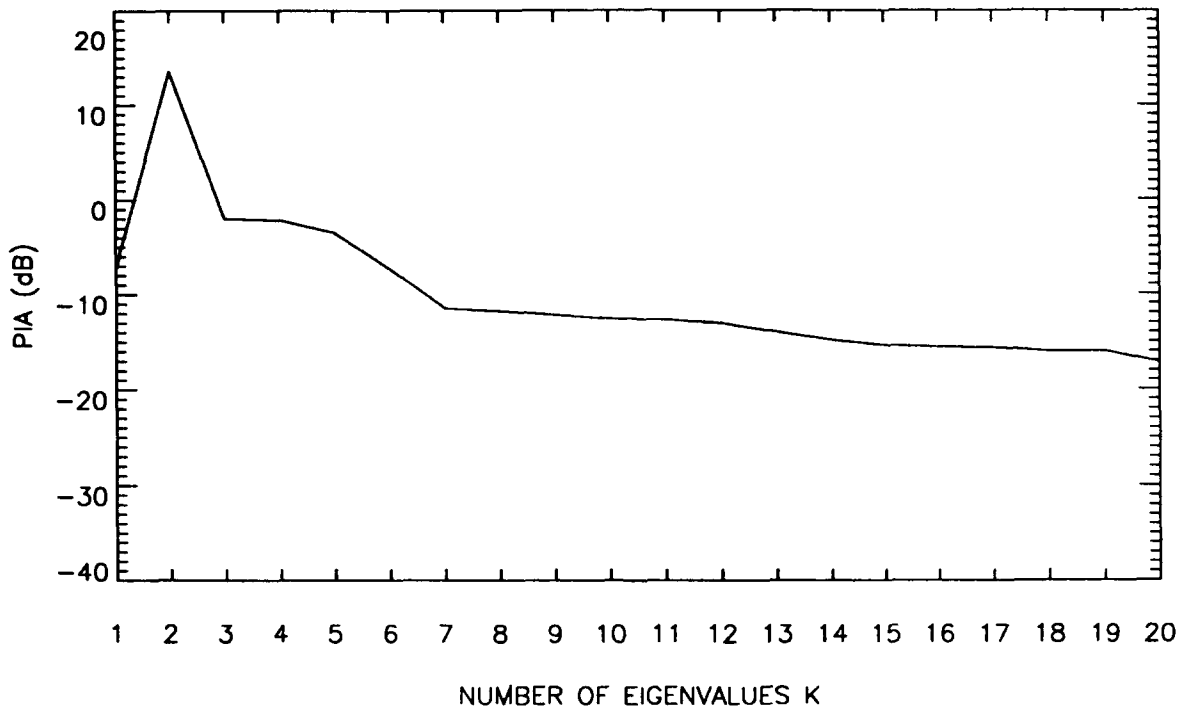

(a)

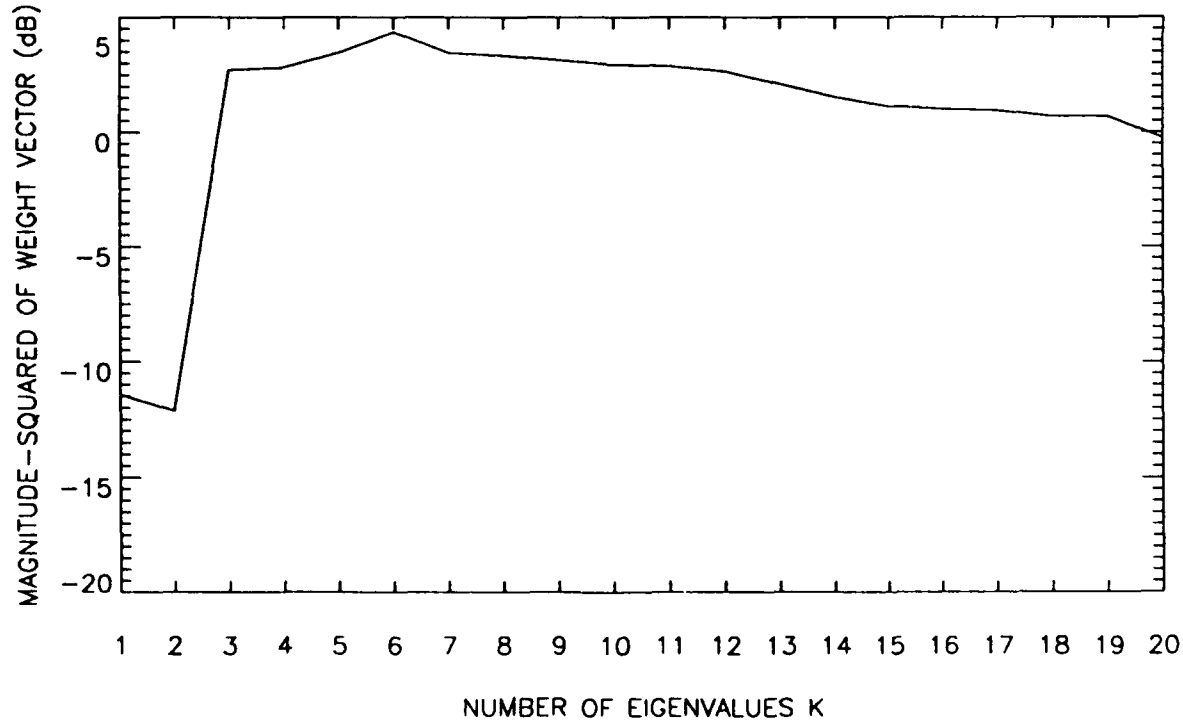

(b)

Figure 3.8. Eigenvector-based robust MVDR processor results for signal power $\sigma_s^2 = 10$ dB and noise power $\sigma_n^2 = 0$ dB with 10 dB interferer falling on sidelobe: (a) PIA vs. k, (b) corresponding magnitude squared of the weight vector $| \mathbf{a} |^2$.

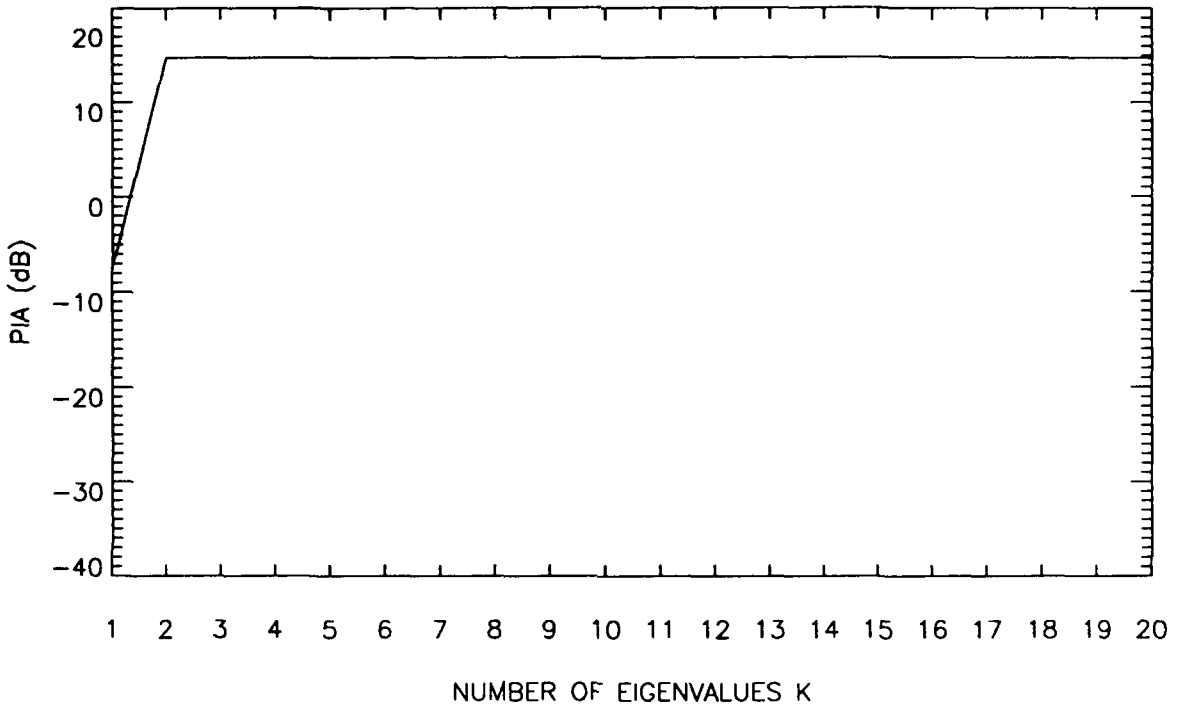

(a)

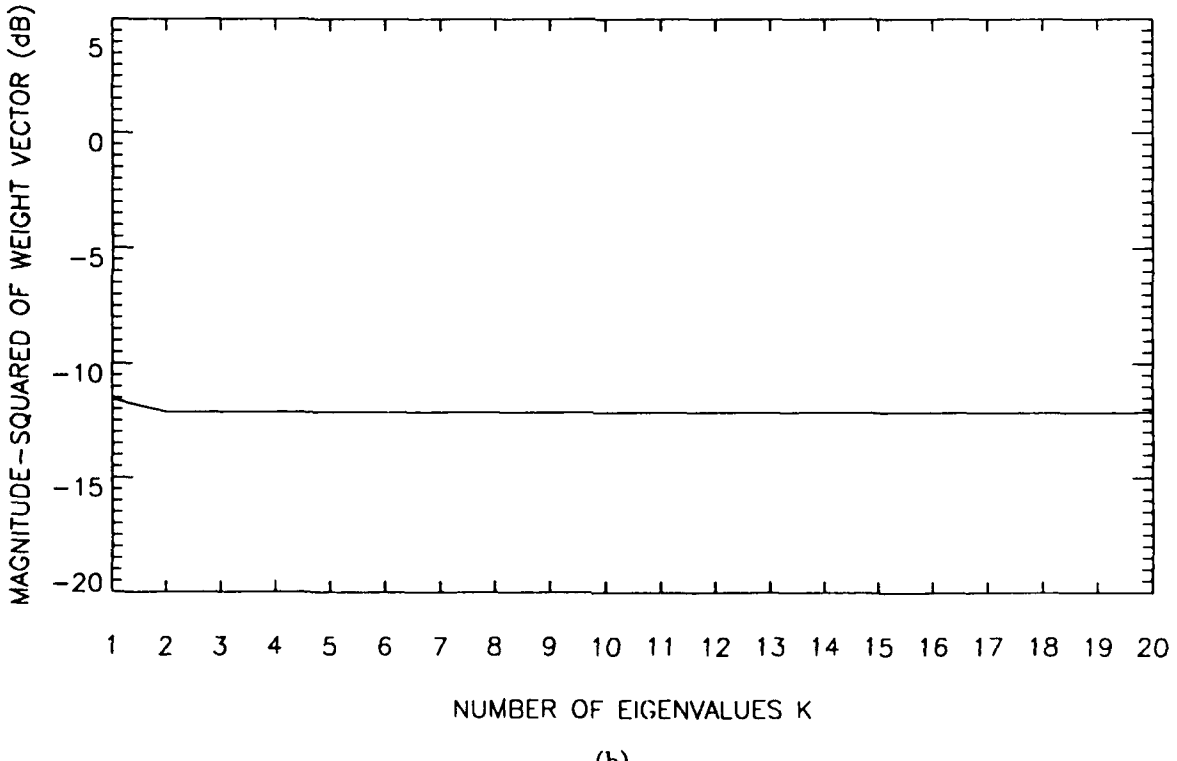

(b)

Figure 3.9. Eigenvector-based MVDR processor results with no mismatch for signal power $\sigma_s^2 = 10$ dB and noise power $\sigma_n^2 = 0$ dB with 10 dB interferer falling on sidelobe: (a) PIA vs. k, (b) corresponding magnitude squared of the weight vector $| \mathbf{a} |^2$.

beampattern at t becomes very deep while $|\ \mathbf{a}\ |^2$ increases. Thus we argue that we actually want to *increase* $|\ \mathbf{a}\ |^2$ to improve nulling performance. An MVDR-based algorithm that enhances nulling performance would then increase the magnitude squared of the weight vector by subtracting an appropriate μ^2 from R while maintaining a sufficient bound on $|\ \mathbf{a}\ |^2$ to prevent unwanted signal nulling. However, as in the optimal robustness technique of equation (3.11), it is difficult to solve for μ^2 in equation (3.34) such that $|\ \hat{\mathbf{a}}\ |^2$ equals some lower bound.

One approach would be to modify the robustness technique of section 3.1.2 and Hudson (1981) to subtract a scalar factor from R rather than to add one. That is we define the output power as

$$\hat{P}_{MVDR} = \frac{1}{\sum_{i=1}^{M} \frac{|\ e^H v_i\ |^2}{\lambda_i - \mu^2}} \tag{3.37}$$

where we find μ^2 such that

$$|\ \hat{\mathbf{a}}\ |^2 = \frac{\sum_{i=1}^{M} \left[\frac{1}{\lambda_i - \mu^2}\right]^2 |\ e^H v_i\ |^2}{\left[\sum_{i=1}^{M} \frac{|\ e^H v_i\ |^2}{\lambda_i - \mu^2}\right]^2} = \eta^2 \tag{3.38}$$

where η^2 is the *minimum* bound constraint on $|\ \mathbf{a}\ |^2$.

4.0 Simulations

In this section we present MVDR processor simulation results from a 100 element horizontal random array of diameter 72λ at 30 Hz or 3566 m in noise environments consisting of white noise with multiple interferers. We attempt to detect and process four signals of various powers and to demonstrate the effect of interferers and mismatch on MVDR performance. We also show how the WNC MVDR algorithm improves performance under conditions of mismatch.

We will process the four signals of interest described in table 4.1. All spectral energy is assumed narrowband at 30 Hz.

Table 4.1. Power and bearing of the four signals of interest.

Signal powers	Bearing
0 dB	180° Az. 0° De.
-5 dB	280° Az. 0° De.
-10 dB	300° Az. 0° De.
-15 dB	220° Az. 0° De.

4.1 20 Interferers

The first environment consists of white noise power of 0 dB with 20 0 dB interferers impinging on the array from 2° to 40° azimuth, with 2° spacings and 0° declination angle. Figure 4.1 displays the MVDR output power and magnitude squared of the weight vector $|\ \mathbf{a}\ |^2$ when we steer from 0° to 359° in azimuth at 1° intervals and 0° declination angle. We also include the PIA obtained with the adaptive processor for each signal of interest. Note that since in this simulation the array beamwidth is less than 1° for all directions of look figure 4.1 (b) lacks the characteristic peaks of figure 2.1 (b) for steering directions close to those of the signals. Naturally if we were to azimuthally sample at a higher rate we would also see these peaks in $|\ \mathbf{a}\ |^2$.

Next we include the sensor position error discussed in section 1.0 in our estimate of the array geometry. Figure 4.2 (a) shows the characteristic drop in MVDR output power and the corresponding increase in $|\ \mathbf{a}\ |^2$ in the direction of the stronger signals. We note the illuminating drop in PIA for the three strongest signals. However the PIA of the weakest signal at 220° az has dropped only slightly.

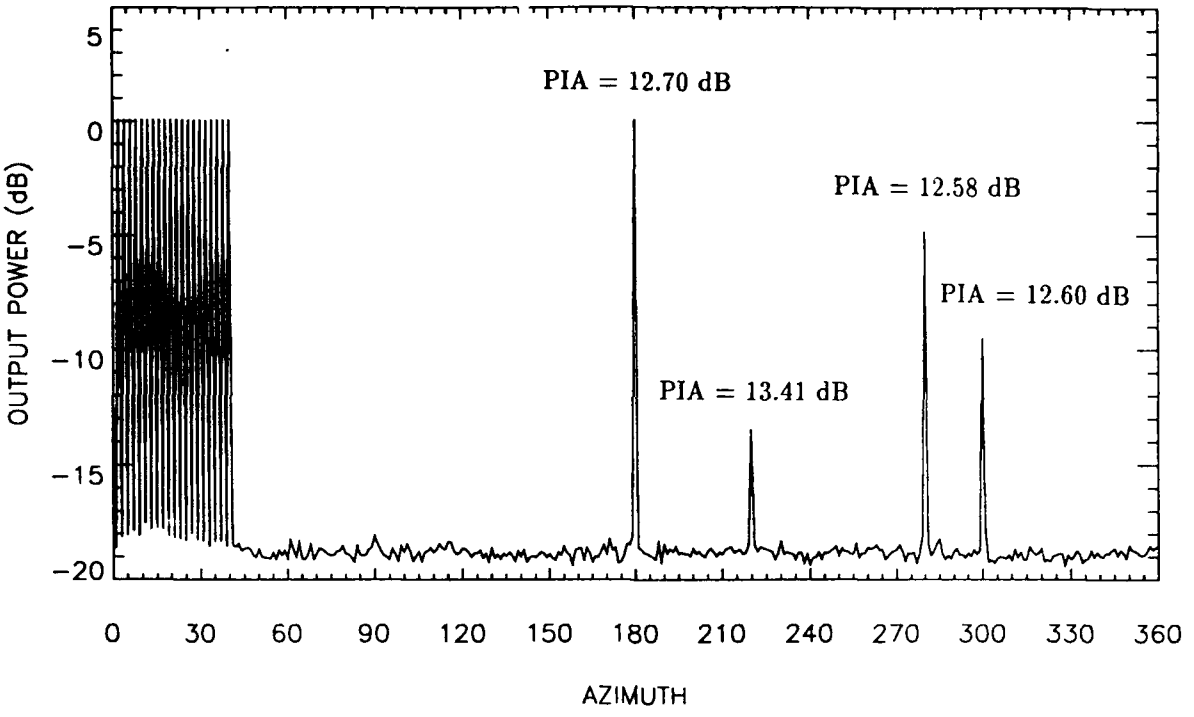

(a)

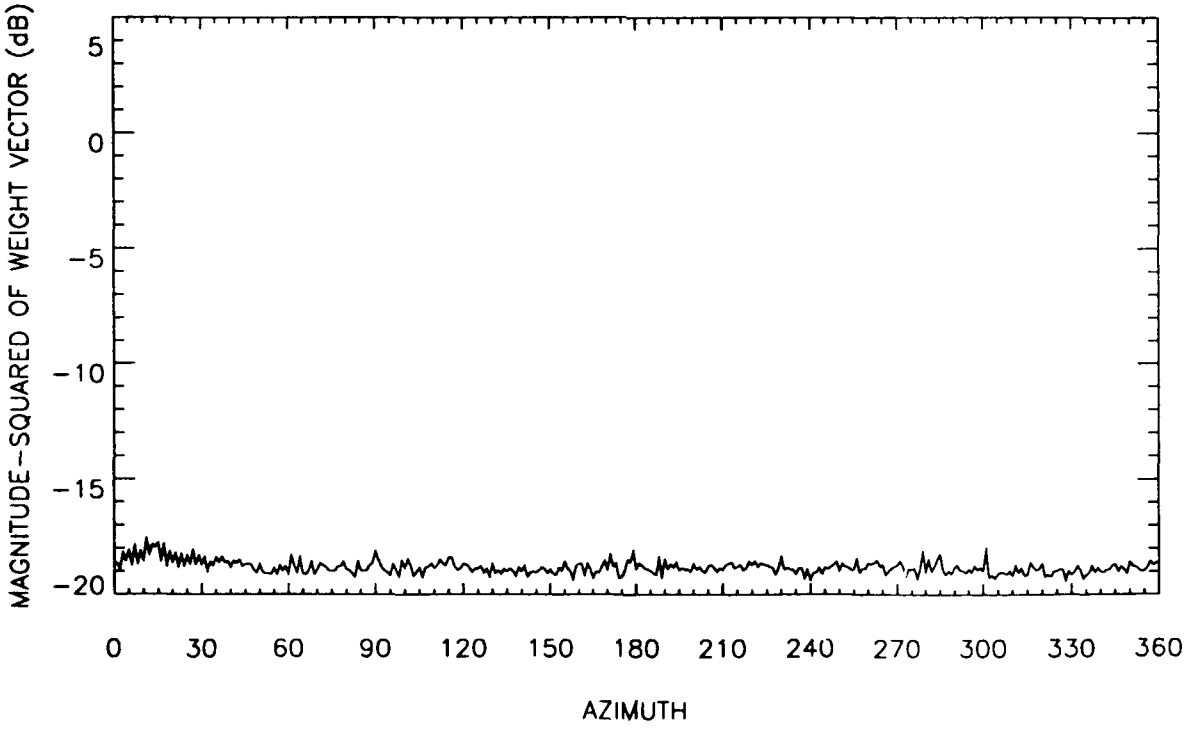

(b)

Figure 4.1. MVDR processor results for the 20 interferer environment: (a) output power with PIA values for the signals of interest, (b) corresponding magnitude squared of the weight vector $|\mathbf{a}|^2$.

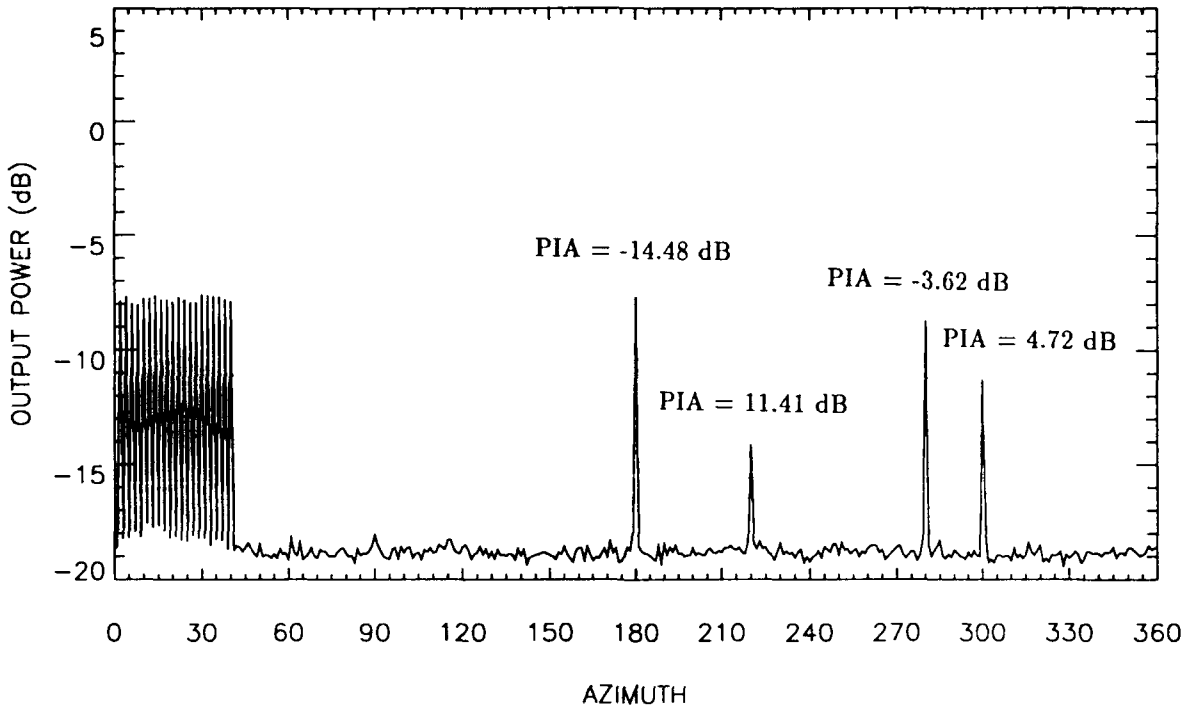

(a)

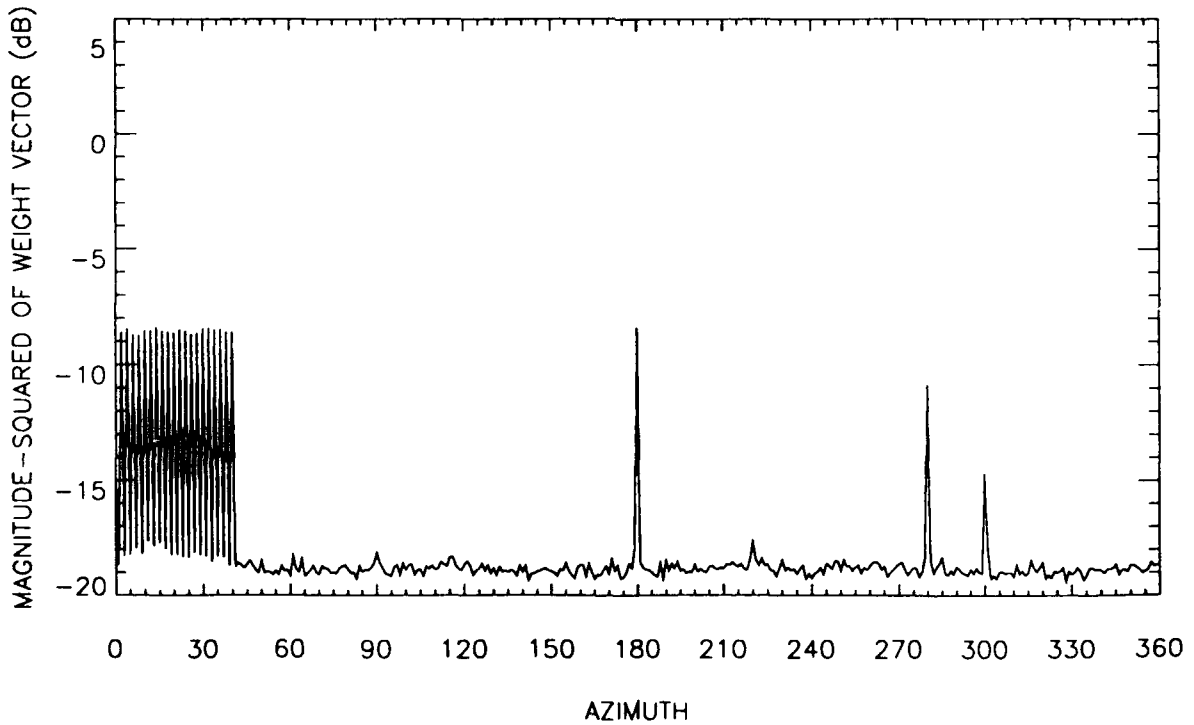

(b)

Figure 4.2. MVDR processor results for the 20 interferer environment with 0.1λ sensor position error: (a) output power with PIA values for the signals of interest, (b) corresponding magnitude squared of the weight vector $|\mathbf{a}|^2$.

This fact is supported by the slight increase in $|\mathbf{a}|^2$ at 220° az over the corresponding value of figure 4.1 (a). Thus we conclude the MVDR processor is not sensitive to mismatch in this noise environment when steered at the -15 dB signal.

We now apply a WNC to the MVDR algorithm of -18 dB. We choose this value essentially because it is approximately the average $|\mathbf{a}|^2$ of the nonmismatch case of figure 4.1 (b). Figure 4.3 represents the results. We clearly see the increase in output power for the three strongest signal directions. However note that while the PIA has increased for the two strongest signals over the values shown in figure 4.2 (a), the PIA has actually dropped for the -10 dB and -15 dB signals. Thus while we are inhibiting unwanted signal nulling in these directions we are doing so at the expense of interferer nulling.

As stated in the previous section, it is difficult to determine the optimal WNC to apply to the MVDR processor since the value of the WNC that optimizes PIA is dependent on the signal power and the noise environment (white noise and interferer powers *and* the spatial distribution of the interferers.) In fact, if the 0 dB signal were originating from a direction other than 180° azimuth we would not expect the WNC of -18 dB to produce a PIA of 0.00 dB. Thus, the optimal (in the PIA sense) WNC that we apply to the MVDR processor must necessarily be unique for each direction of look. In order to demonstrate the PIA values we obtain for various WNC, we plot PIA versus WNC for each of these four signals in figure 4.4. The WNC values that optimize PIA for each signal also are marked. We see that the PIA values for the mismatch case of figure 4.2 are represented by the flat portions of the plots and occur when WNC $> |\mathbf{a}|^2$, since we do not institute the constraint if this condition occurs. Coincidentally, the optimum WNC for the -5 dB and -10 dB signals are approximately equal for this simulation. We also see that a WNC for the -15 dB signal is really not required. We might conclude that a WNC of -15.5 dB for all directions of look might represent the best choice for this signal and noise environment.

4.2 40 Interferers

The next noise environment consists of 40 dB interferers arriving from 2° to 80° azimuth with 2° spacings and 0° declination angle. Figure 4.5 displays the MVDR output power and $|\mathbf{a}|^2$. Comparison with figure 4.1 (a) reveals that the 20 additional interferers result in an increase in PIA for the four steering directions due to the adaptive nulling of the MVDR processor. Figure 4.6 represents the MVDR output powers and $|\mathbf{a}|^2$ under the condition of mismatch caused by errors in sensor position estimates. Comparison with figure 4.2 indicates that mismatch causes less severe unwanted signal nulling in this case as indicated by the PIA values. This agrees with the results of section 2.0 which demonstrated that a strong interferer environment forces the MVDR processor to place a great deal of emphasis on minimizing $|\mathbf{a}|^2$, resulting in less pronounced unwanted signal nulling. Figure 4.7 is the result of placing a WNC of -16.5 dB on the MVDR processor. Figure 4.8 plots PIA versus WNC for this environment. As expected the plots have moved upward from those of figure 4.4. The most

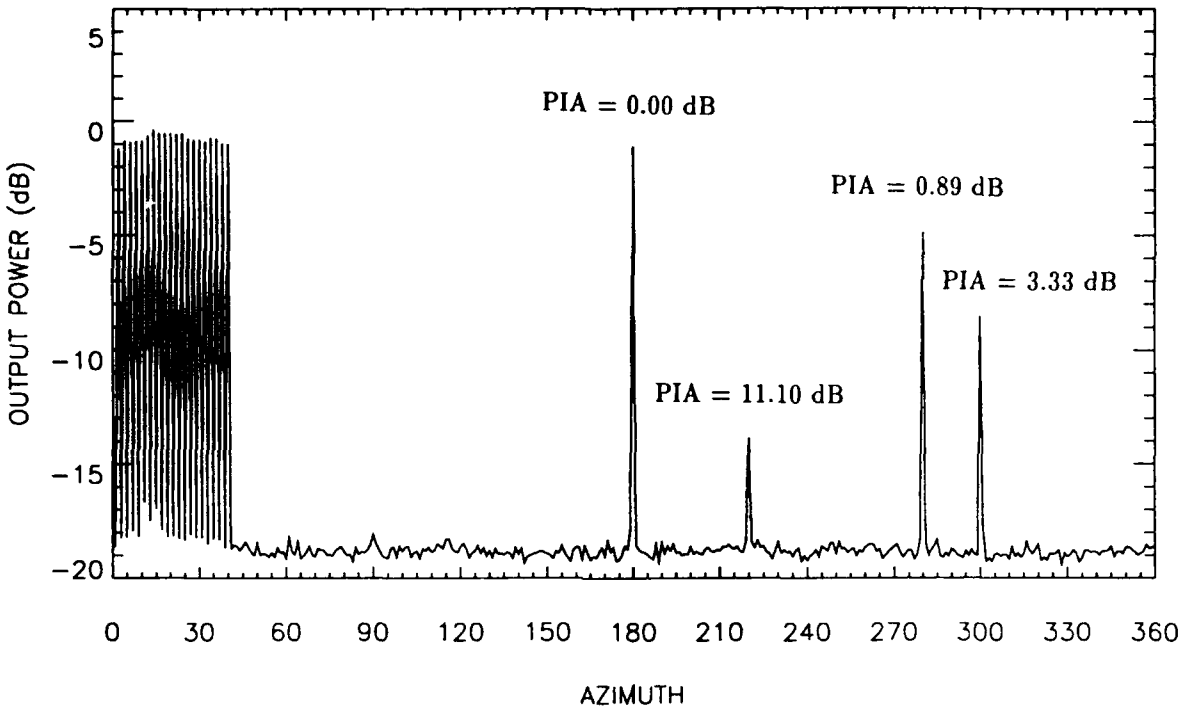

(a)

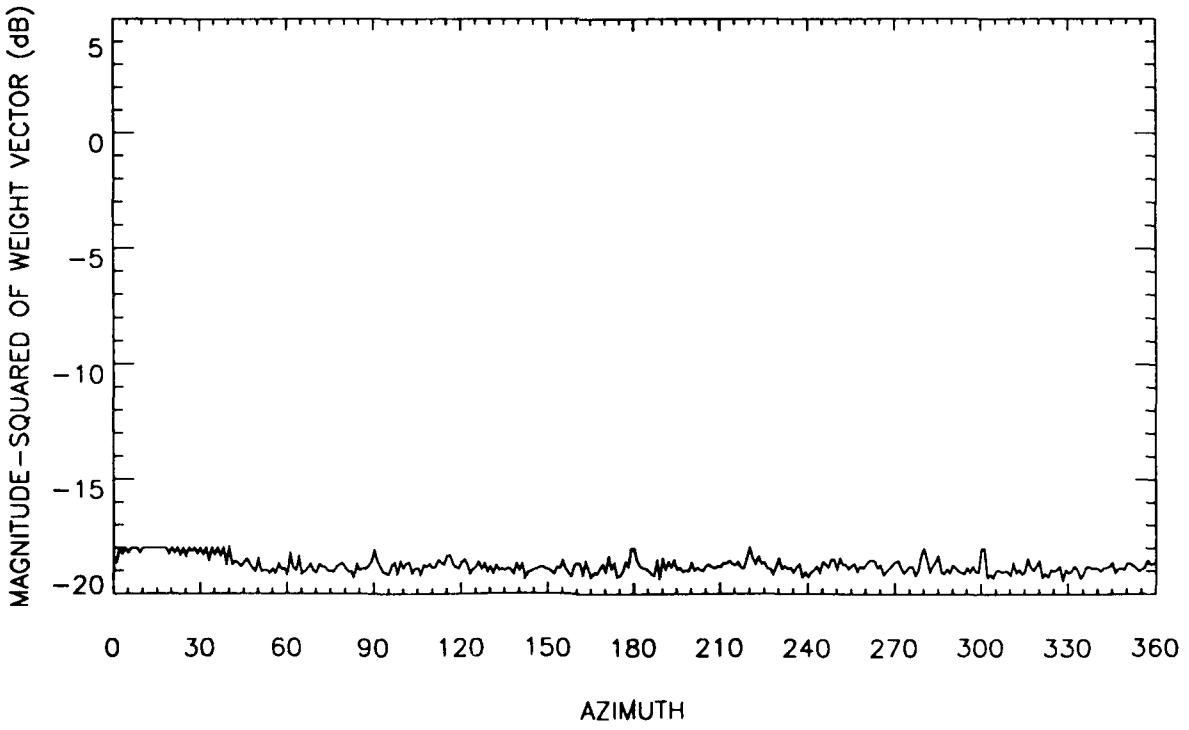

(b)

Figure 4.3. MVDR processor results for the 20 interferer environment with 0.1λ sensor position error and WNC = -18.0 dB: (a) output power with PIA values for the signals of interest, (b) corresponding magnitude squared of the constrained weight vector $| \hat{a}_{WNC} |^2$.

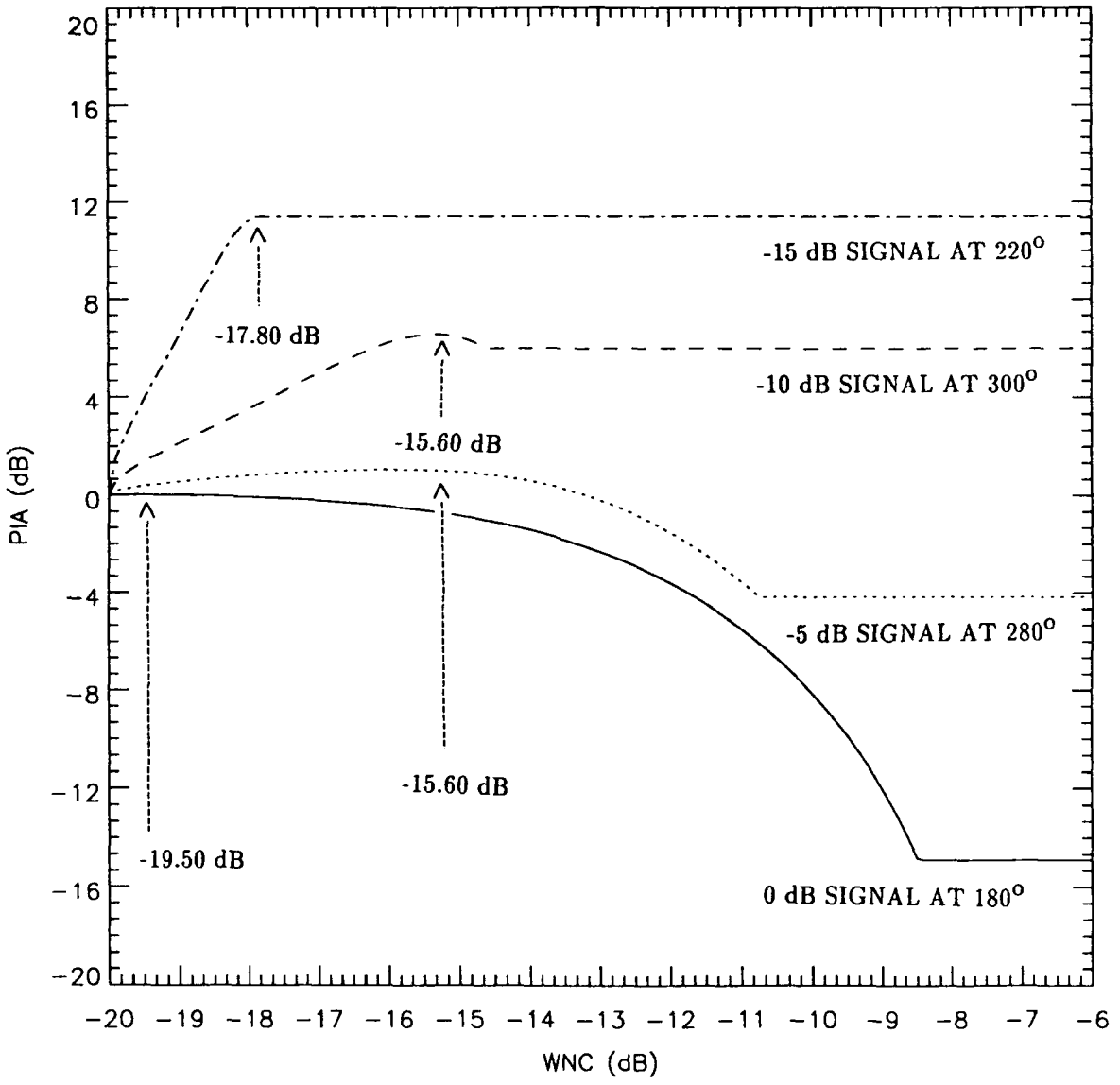

Figure 4.4. PIA versus WNC for the four signals of interest in the 20 interferer environment.

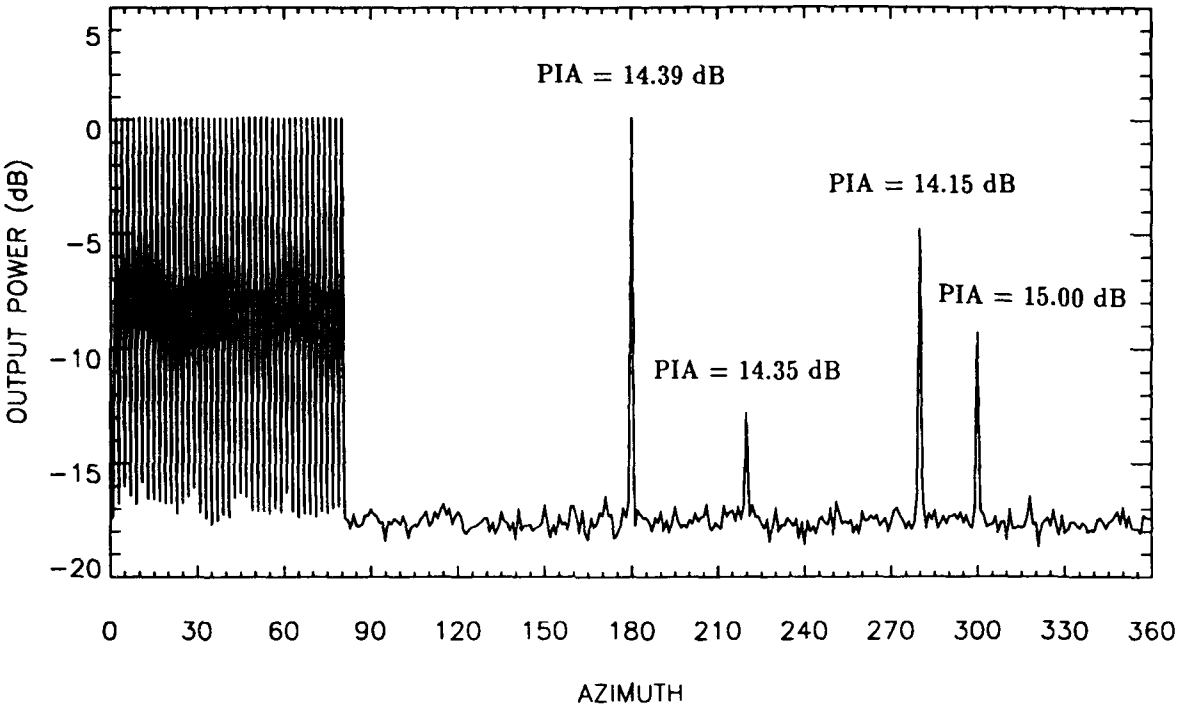

(a)

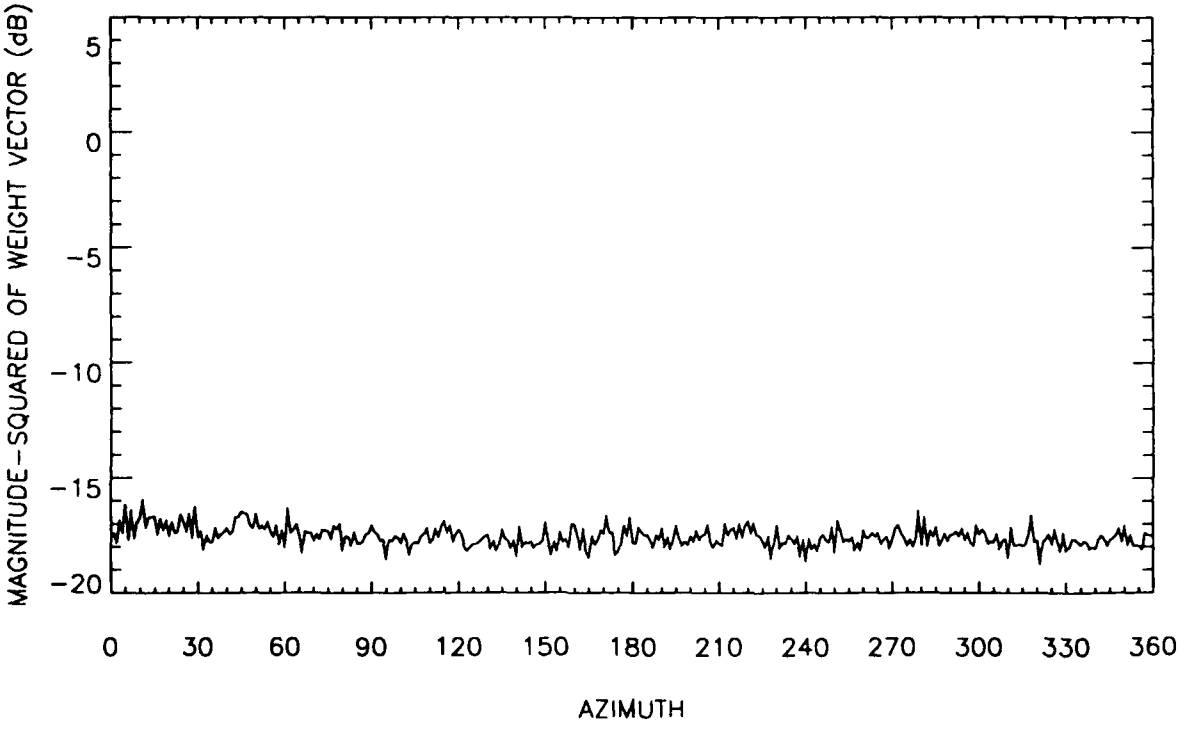

(b)

Figure 4.5. MVDR processor results for the 40 interferer environment: (a) output power with PIA values for the signals of interest, (b) corresponding magnitude squared of the weight vector $| \mathbf{a} |^2$.

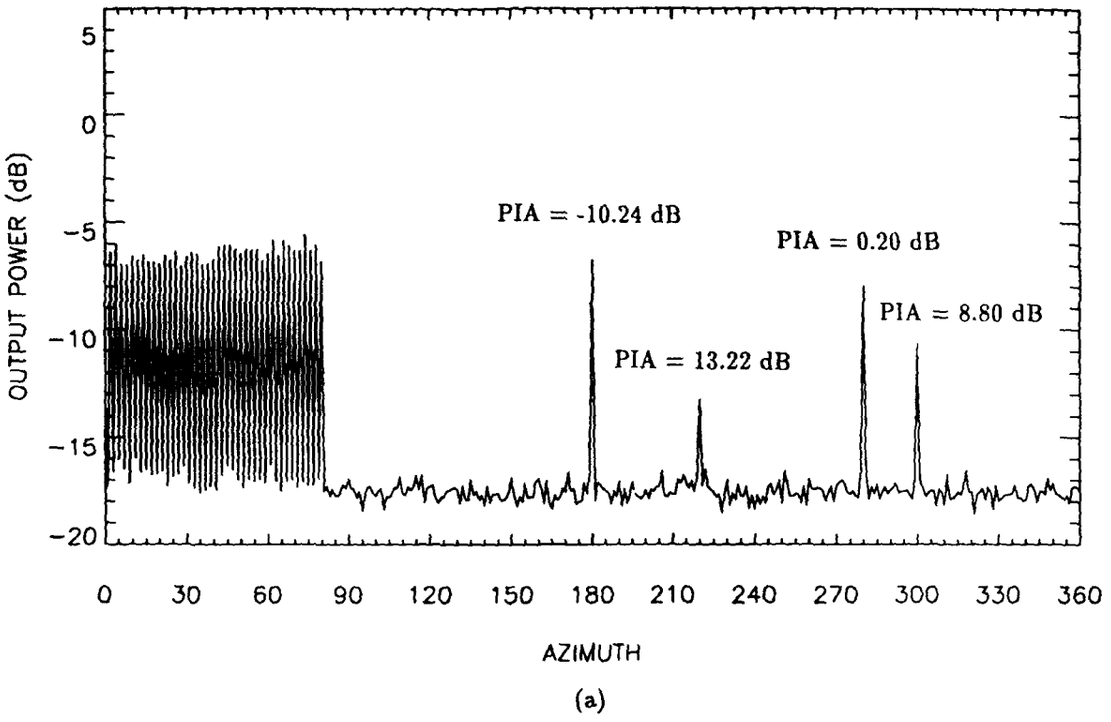

(a)

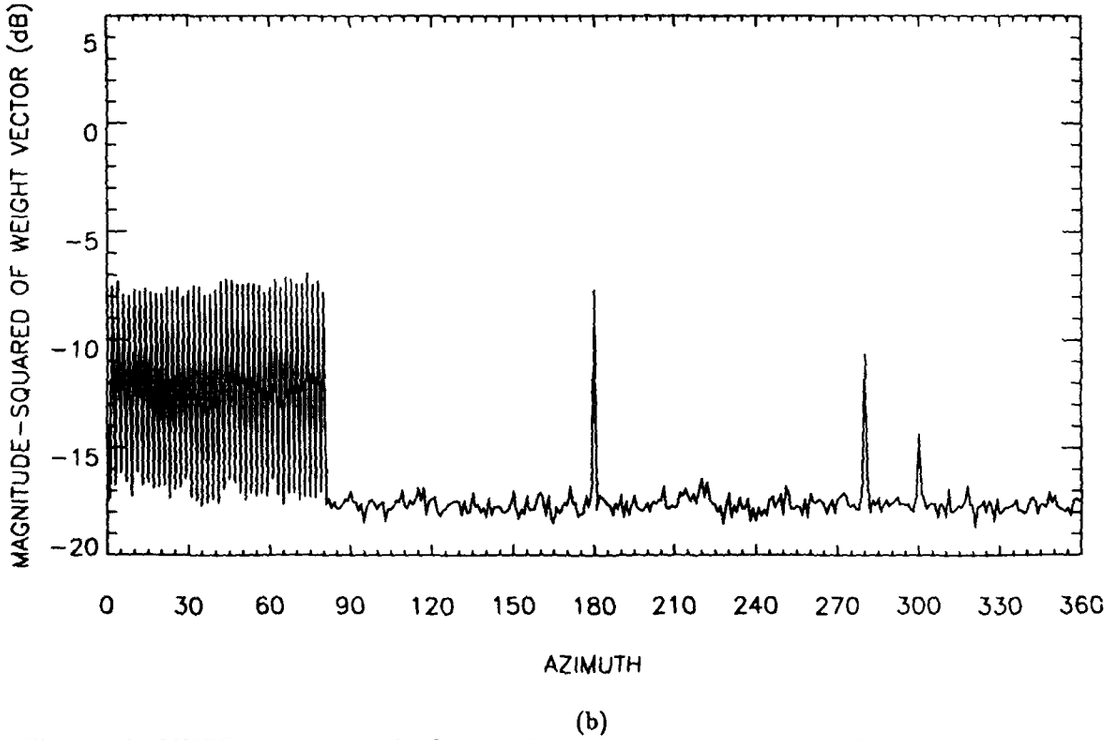

(b)

Figure 4.6. MVDR processor results for the 40 interferer environment with 0.1λ sensor position error: (a) output power with PIA values for the signals of interest, (b) corresponding magnitude squared of the weight vector $| a |^2$.

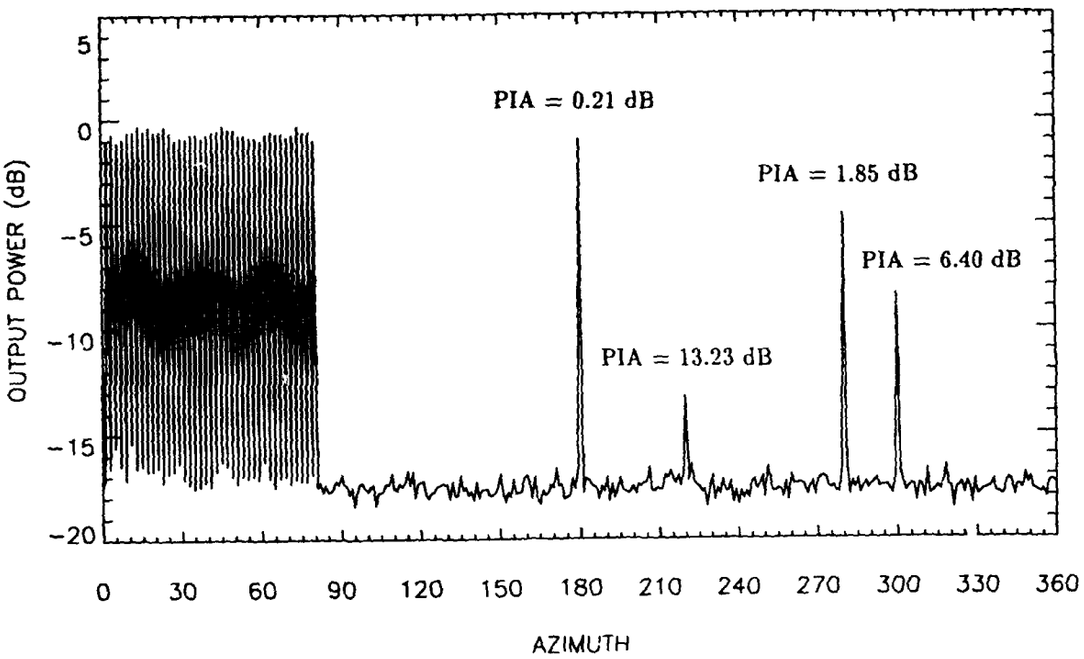

(a)

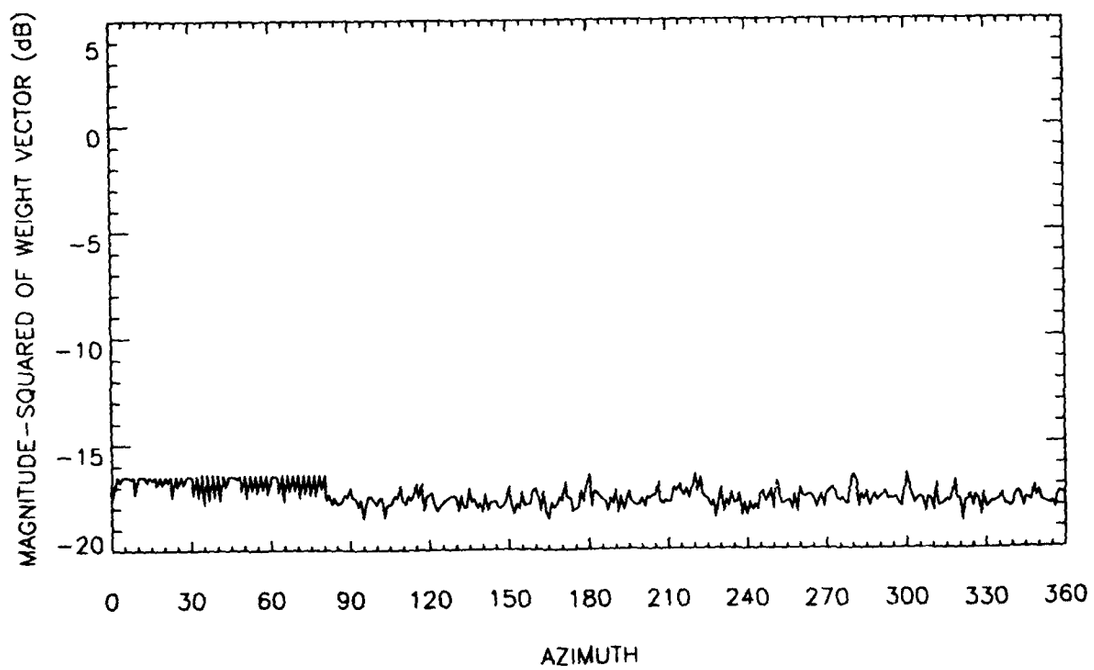

(b)

Figure 4.7. MVDR processor results for the 40 interferer environment with 0.1λ sensor position error and WNC = -16.5 dB: (a) output power with PIA values for the signals of interest, (b) corresponding magnitude squared of the constrained weight vector $| \hat{a}_{WNC} |^2$.

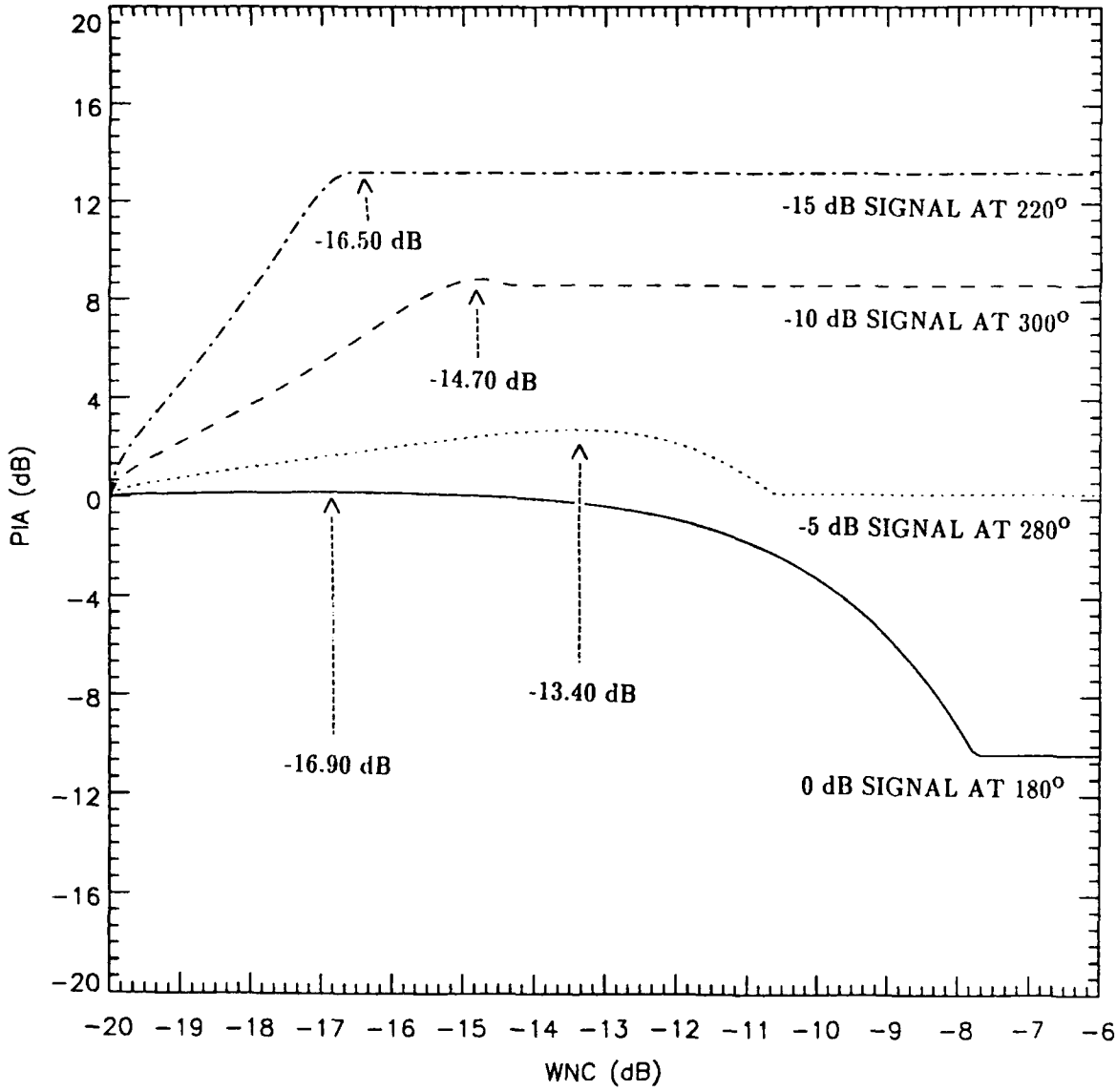

Figure 4.8. PIA versus WNC for the four signals of interest in the 40 interferer environment.

pronounced movement comes from the 0 dB signal since it was the most sensitive to mismatch in the 20 interferer case.

4.3 60 Interferers

The final noise environment consists of 60 0 dB interferers arriving from 2^{o} to 120^{o} azimuth. Figure 4.9 is the resulting MVDR output power and $|\ a\ |^2$. We see that the additional 20 interferers do not cause an increase in PIA over those shown in figure 4.5 (a) for the 40 interferer case. In fact the PIA's for the 0 dB, -5 dB and -15 dB signals actually have decreased since the great number of interferers is adversely affecting adaptive nulling (Mohnkern, 1989), and as a result causing increased emphasis on $|\ a\ |^2$ minimization. Figure 4.10 results from the mismatch conditions. Note that here the large number of interferers causes the MVDR processor to be less sensitive to mismatch than in the 40 interferer environment of figure 4.6. Figure 4.11 is the result of adding a WNC of -16.00 dB. Finally figure 4.12 displays PIA versus WNC. We note that indeed the plots have moved upward from those of figure 4.8 indicating less MVDR sensitivity to mismatch in this environment.

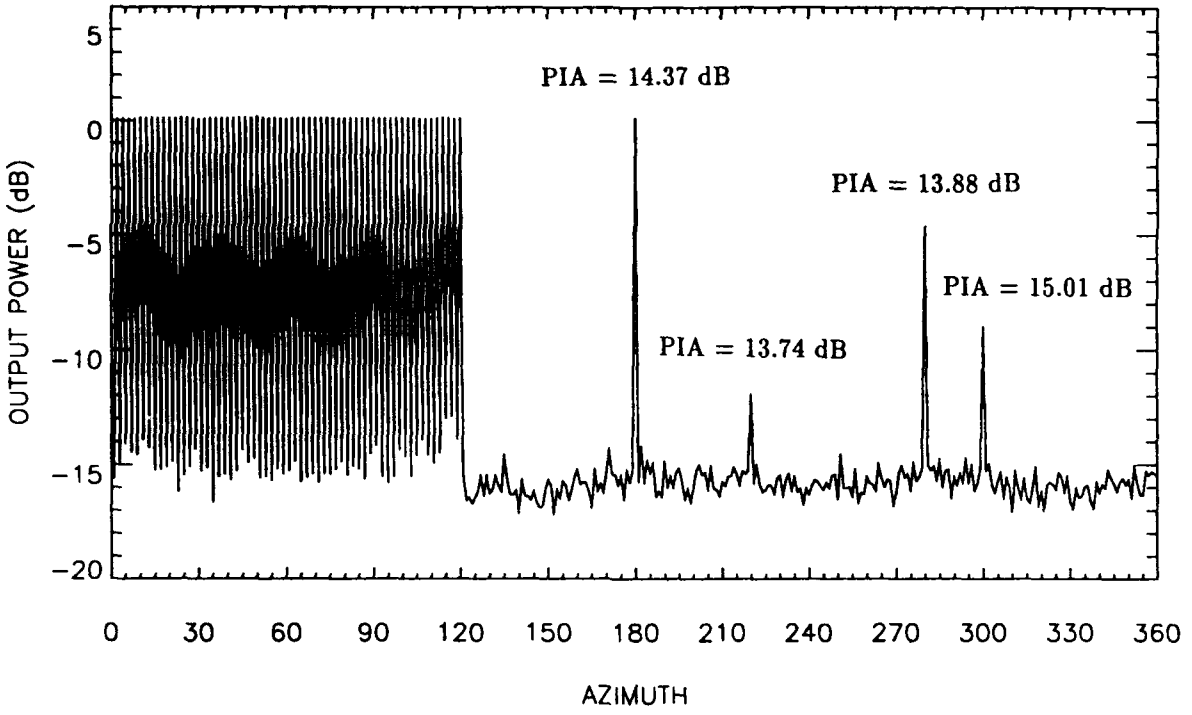

(a)

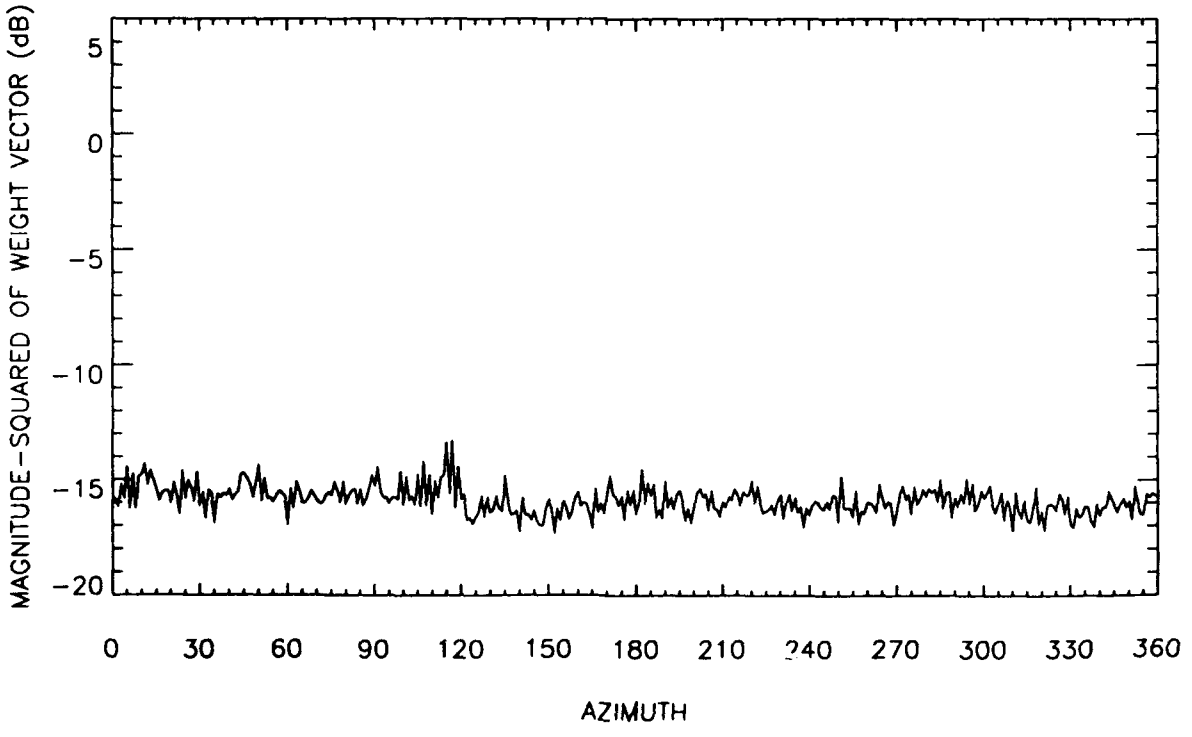

(b)

Figure 4.9. MVDR processor results for the 60 interferer environment: (a) output power with PIA values for the signals of interest, (b) corresponding magnitude squared of the weight vector $|\mathbf{a}|^2$.

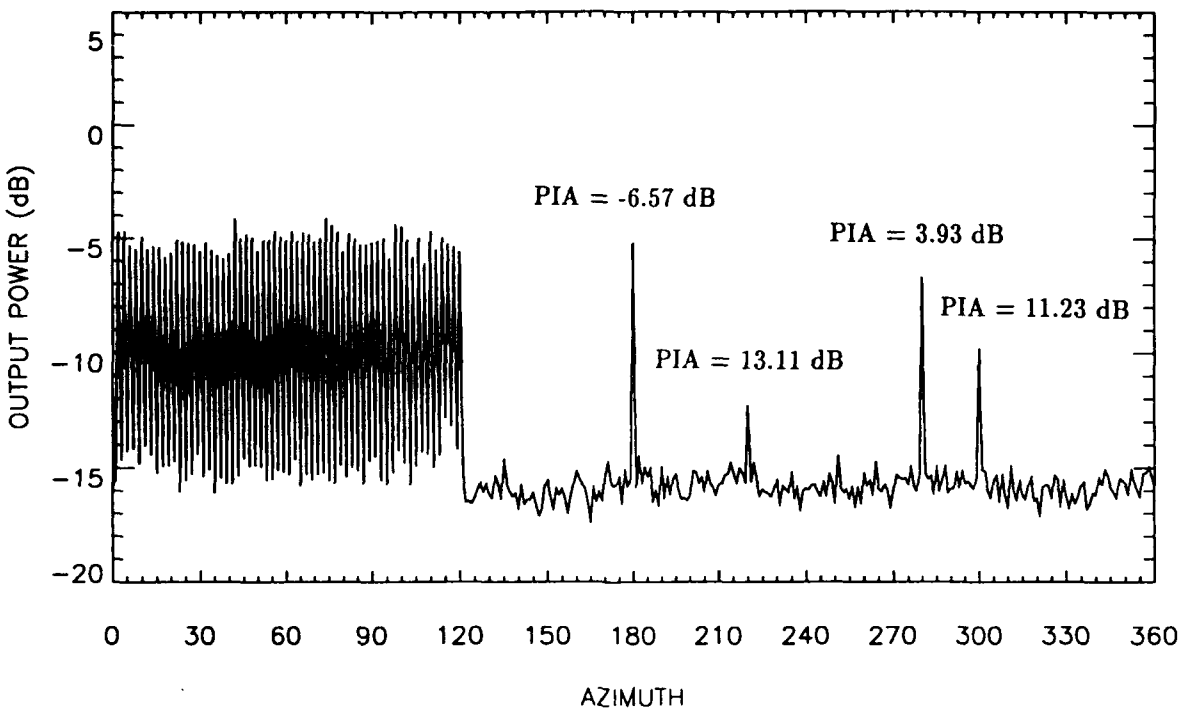

(a)

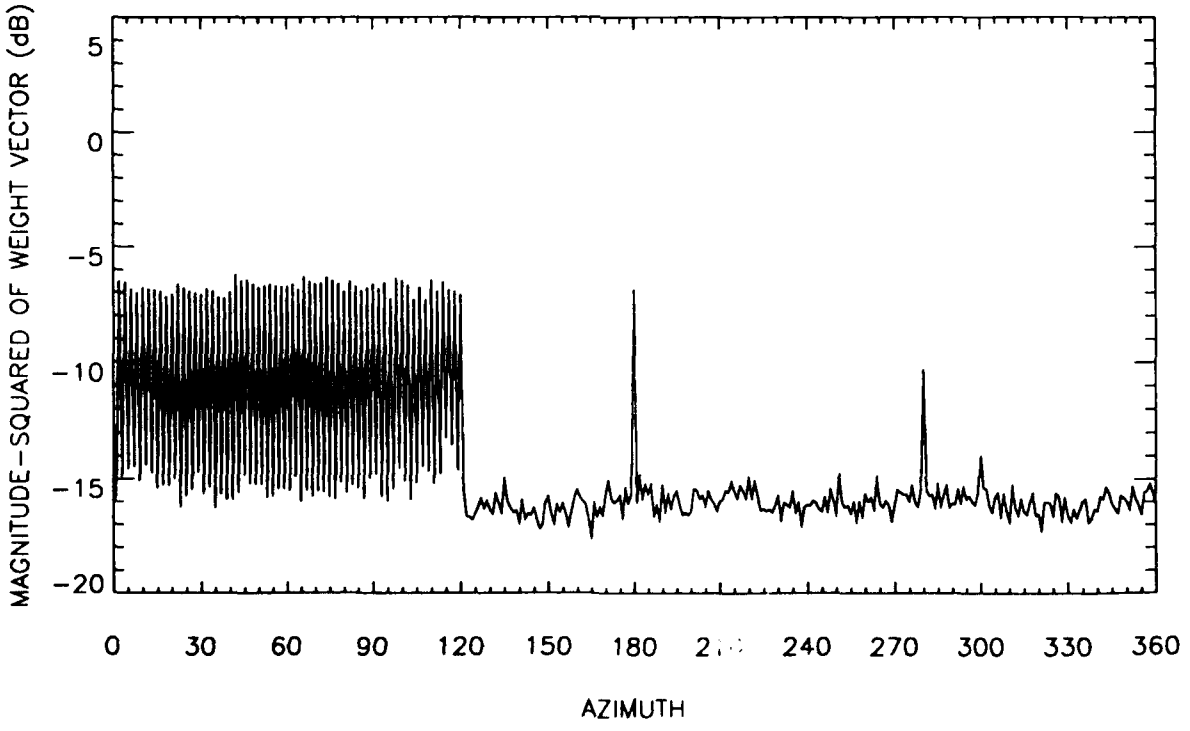

(b)

Figure 4.10. MVDR processor results for the 60 interferer environment with 0.1λ sensor position error: (a) output power with PIA values for the signals of interest, (b) corresponding magnitude squared of the weight vector $|\mathbf{a}|^2$.

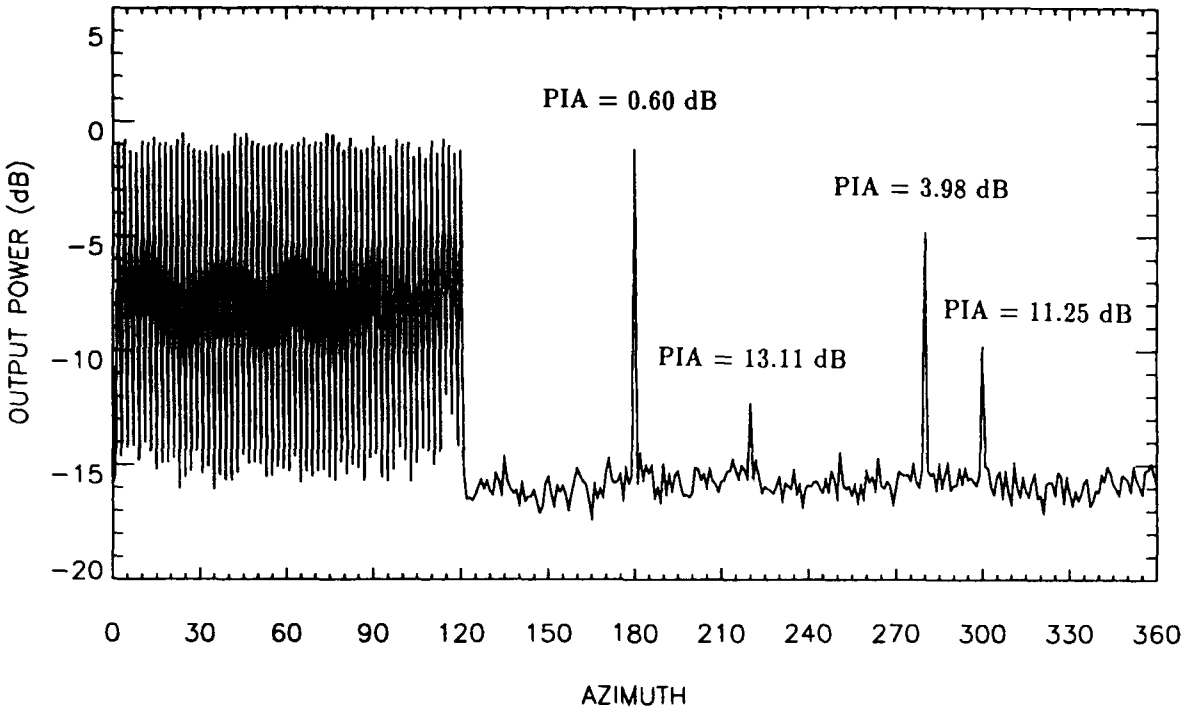

(a)

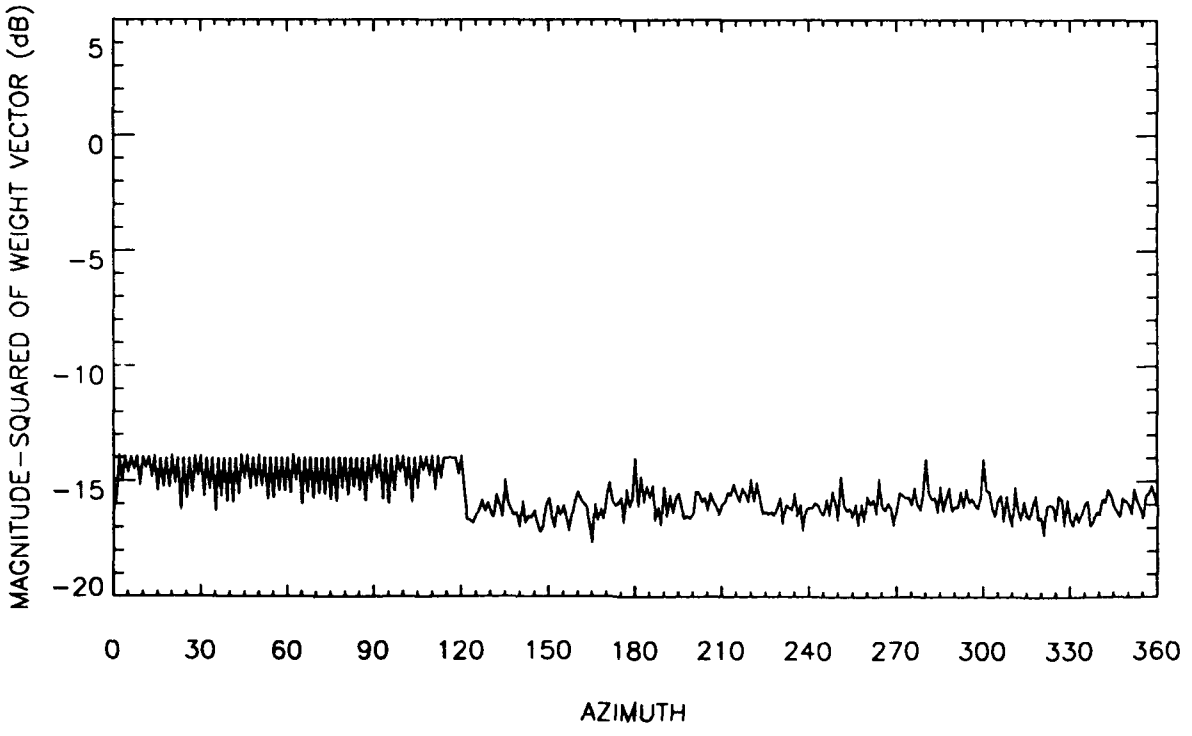

(b)

Figure 4.11. MVDR processor results for the 60 interferer environment with 0.1λ sensor position error and WNC = -14.0 dB: (a) output power with PIA values for the signals of interest, (b) corresponding magnitude squared of the constrained weight vector $| \hat{a}_{WNC} |^2$.

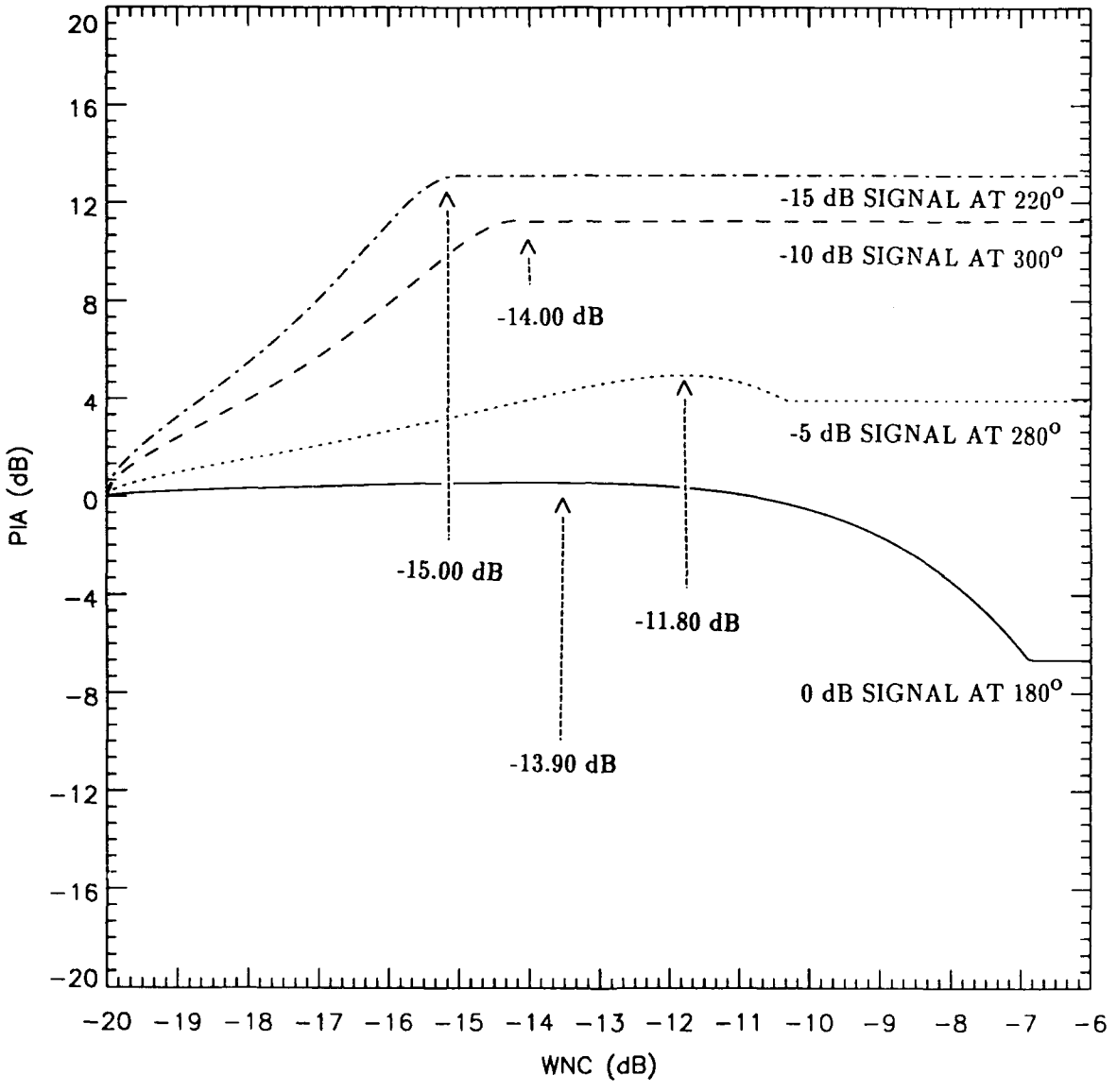

Figure 4.12. PIA versus WNC for the four signals of interest in the 60 interferer environment.

Appendix A

In this appendix we compute the MVDR weight vector for the case where we steer *towards* the signal of interest.

Let the cross spectral density matrix R be given by

$$R = \sigma_n^2 I + \sigma_s^2 s s^H + Q \ . \tag{A.1}$$

We can analytically invert R via the matrix inversion lemma (Johnson, 1982, Hudson, 1981, and Steinhardt and Van Veen, 1989) as

$$R^{-1} = W^{-1} - \frac{W^{-1} s s^H W^{-1}}{s^H W^{-1} s + \frac{1}{\sigma_s^2}} \tag{A.2}$$

where

$$W = \sigma_n^2 I + Q \ . \tag{A.3}$$

Then the MVDR weight vector a will be

$$a = \frac{W^{-1}e - \frac{s^H W^{-1} e}{s^H W^{-1} s + \frac{1}{\sigma_s^2}} W^{-1} s}{e^H W^{-1} e - \frac{e^H W^{-1} s s^H W^{-1} s}{s^H W^{-1} s + \frac{1}{\sigma_s^2}}} \ . \tag{A.4}$$

Now if we steer at the signal s, i.e., the steering vector e is equal to the signal vector s,

$$a = \frac{W^{-1} e}{e^H W^{-1} e} \ . \tag{A.5}$$

So in this case the matrix inverse term in the MVDR weight vector equation (A.5) is not a function of s (or e).

Appendix B

In this appendix we determine the effect of the noise environment on MVDR nulling and the magnitude squared of the MVDR weight vector.

First we show that

$$| a^H t |^2 = \frac{\left[\frac{\alpha^2}{M + \alpha^2}\right]^2 | e^H t |^2}{\left[M - \frac{| e^H t |^2}{M + \alpha^2}\right]^2} \tag{B.1}$$

is an increasing function of α^2 for $0 < \alpha^2 < \infty$ and $0 \leq | e^H t |^2 < M^2$. Taking the derivative of $| a^H t |^2$ with respect to α^2 we get

$$\frac{d| a^H t |^2}{d\alpha^2} = \frac{2\left[\frac{| e^H t |^2 \alpha^2}{(M + \alpha^2)^3}\right]\left[M^2 - | e^H t |^2\right]}{\left[M - \frac{| e^H t |^2}{M + \alpha^2}\right]^3} . \tag{B.2}$$

Now, using the fact that $| e^H t |^2 < M^2$ we get

$$\frac{d| a^H t |^2}{d\alpha^2} > 0 \tag{B.3}$$

for $0 < \alpha^2 < \infty$ and $0 \leq | e^H t | < M^2$ with

$$| a^H t |^2_{MIN} \rightarrow 0 \quad \text{for } \alpha^2 \rightarrow 0 \tag{B.4}$$

and

$$| a^H t |^2_{MAX} \rightarrow \frac{| e^H t |^2}{M^2} \quad \text{as } \alpha^2 \rightarrow \infty . \tag{B.5}$$

Next we show that $| a^H t |^2$ is an increasing function of $| e^H t |^2$ for $0 \leq | e^H t |^2 < M^2$

and $0 < \alpha^2 < \infty$. Taking the derivative of $| a^{Ht} |^2$ with respect to $| e^{Ht} |^2$ we get

$$\frac{d| a^{Ht} |^2}{d| e^{Ht} |^2} = \frac{\frac{\alpha^2}{M + \alpha^2}\left[M + \frac{| e^{Ht} |^2}{M + \alpha^2}\right]}{\left[M - \frac{| e^{Ht} |^2}{M + \alpha^2}\right]^3} \quad . \tag{B.6}$$

Since $| e^{Ht} |^2 < M^2$ we get

$$\frac{d| a^{Ht} |^2}{d| e^{Ht} |^2} > 0 \tag{B.7}$$

for $0 < \alpha^2 < \infty$ and $0 \leq | e^{Ht} | < M^2$ with

$$| a^{Ht} |^2_{MIN} = 0 \quad \text{for } | e^{Ht} |^2 = 0 \tag{B.8}$$

and

$$| a^{Ht} |^2_{MAX} \rightarrow M^2 \text{ as } | e^{Ht} |^2 \rightarrow \infty \, . \tag{B.9}$$

Now we show that

$$| a |^2 = \frac{M + \frac{1}{M + \alpha^2}\left[\frac{M}{M + \alpha^2} - 2\right] | e^{Ht} |^2}{\left[M - \frac{| e^{Ht} |^2}{M + \alpha^2}\right]^2} \tag{B.10}$$

is a decreasing function of α^2 for $0 < \alpha^2 < \infty$ and $0 \leq | e^{Ht} |^2 < M^2$. Taking the derivative of $| a |^2$ with respect to α^2 we get

$$\frac{d| a |^2}{d\alpha^2} = \frac{2\left[\frac{| e^{Ht} |^2}{(M + \alpha^2)^3}\right]\left[| e^{Ht} |^2 - M^2\right]}{\left[M - \frac{| e^{Ht} |^2}{M + \alpha^2}\right]^3} \quad . \tag{B.11}$$

Now, using the fact that $| e^H t |^2 < M^2$ we get

$$\frac{d| a |^2}{d\alpha^2} < 0 \tag{B.12}$$

for $0 < \alpha^2 < \infty$ and $0 \leq | e^H t | < M^2$ with

$$| a |^2_{MIN} \rightarrow \frac{1}{M} \quad \text{as } \alpha^2 \rightarrow \infty \tag{B.13}$$

and

$$| a |^2_{MAX} \rightarrow \frac{1}{M - \frac{| e^H t |^2}{M}} \quad \text{for } \alpha^2 \rightarrow 0 . \tag{B.14}$$

Finally we look at the behavior of $| a |^2$ with respect to $| e^H t |^2$. Taking the derivative of $| a |^2$ with respect to $| e^H t |^2$ we get

$$\frac{d| a |^2}{d| e^H t |^2} = \frac{M^2(M + \alpha^2) - (M + 2\alpha^2) | e^H t |^2}{\left[M(M + \alpha^2) - | e^H t |^2\right]^3} . \tag{B.15}$$

We see that for

$$| e^H t |^2 = \frac{M^2(M + \alpha^2)}{M + 2\alpha^2} \tag{B.16}$$

$| a |^2$ is maximized where

$$| a |^2_{MAX} = \frac{(M + 2\alpha^2)^2}{4M\alpha^2(M + \alpha^2)} . \tag{B.17}$$

Note that for small α^2, $| a |^2$ is maximum for $| e^H t |^2 \approx M^2$.

Appendix C

In this appendix we show that the WNC weight vector of (Cox, Zeskind, and Owen, 1987) can be computed in an alternate form.

The form of the WNC weight vector $\hat{a}_{WNC}$ given in (Cox, Zeskind, and Owen, 1987) for the single boresight constraint is comprised of two orthogonal components as

$$\hat{a}_{WNC} = \sqrt{\frac{\delta^2 - \frac{1}{M}}{|a|^2 - \frac{1}{M}}}\left[a - \frac{e}{M}\right] + \frac{e}{M}, \tag{C.1}$$

where, using the notation of [13],

$$\frac{e}{M} = w_c, \tag{C.2}$$

$$a - \frac{e}{M} = v \tag{C.3}$$

and

$$\sqrt{\frac{\delta^2 - \frac{1}{M}}{|a|^2 - \frac{1}{M}}} = \frac{b}{|v|}. \tag{C.4}$$

Also,

$$a = \frac{R^{-1} e}{e^H R^{-1} e}. \tag{C.5}$$

Note, our δ^2 is the inverse of the norm bound term given in (Cox, Zeskind, and Owen, 1987).

Now, since

$$a - \frac{e}{M} = \frac{M R^{-1} e - (e^H R^{-1} e) e}{M e^H R^{-1} e} \tag{C.6}$$

and using (C.1), we have

$$\hat{a}_{WNC} = \frac{M R^{-1} e - (e^H R^{-1} e) e}{M e^H R^{-1} e \sqrt{\frac{|a|^2 - \frac{1}{M}}{\delta^2 - \frac{1}{M}}}} + \frac{e}{M} \tag{C.7}$$

or

$$\hat{a}_{WNC} = \frac{M R^{-1} e - (e^H R^{-1} e) e}{M \left[e^H R^{-1} e + e^H R^{-1} e \left[\sqrt{\frac{|a|^2 - \frac{1}{M}}{\delta^2 - \frac{1}{M}}} - 1 \right] \right]} + \frac{e}{M} . \tag{C.8}$$

Now, by setting

$$\beta = \frac{e^H R^{-1} e}{M} \left[\sqrt{\frac{\delta^2 - \frac{1}{M}}{|a|^2 - \frac{1}{M}}} - 1 \right] \tag{C.9}$$

we get

$$\hat{a}_{WNC} = \frac{M R^{-1} e - (e^H R^{-1} e) e}{M \left[e^H R^{-1} e + M\beta \right]} + \frac{e}{M} , \tag{C.10}$$

or

$$\hat{a}_{WNC} = \frac{M R^{-1} e + (M\beta - e^H R^{-1} e - M\beta) e}{M \left[e^H R^{-1} e + M\beta \right]} + \frac{e}{M} . \tag{C.11}$$

Then

$$\hat{a}_{WNC} = \frac{M\,(R^{-1}\,e + \beta e) - (e^{H}\,R^{-1}\,e + M\beta)\,e}{M\left[e^{H}\,R^{-1}\,e + M\beta\right]} + \frac{e}{M}\,, \tag{C.12}$$

or finally

$$\hat{a}_{WNC} = \frac{(R^{-1} + \beta I)\,e}{e^{H}(R^{-1} + \beta I)\,e}\,. \tag{C.13}$$

where β is given by (C.9).

References

Cox, H. 1973. "Resolving Power and Sensitivity to Mismatch of Optimum Array Processors," *J. Acoust. Soc. Amer.*, vol. 54, no. 3, pp. 771-785.

Cox, H., R. M. Zeskind, and M. M. Owen. 1987. "Robust Adaptive Beamforming," *IEEE Trans, Acoust. Speech, Signal Processing*, vol. ASSP-35, no. 10, pp. 1365-1376, Oct.

Hudson, J. E. 1981. *Adaptive Array Principles*, The Institution of Electrical Engineers, London, NY.

Jablon, N. K. 1986. "Steady State Analysis of the Generalized Sidelobe Canceller by Adaptive Noise Cancelling Techniques," *IEEE Trans. Antennas Propagat.*, vol. AP-34, no. 3, pp. 330-337, Mar.

Johnson, D. H. 1982. "The Application of Spectral Estimation Methods to Bearing Estimation Problems," *Proceedings of the IEEE*, vol. 70, no. 9, pp. 1018-1028, Sep.

Kahaner, D. K., C. Moler, and S. Nash. 1989. *Numerical Methods and Software*, Prentice-Hall, Englewood Cliffs, NJ, pp. 239-248.

Lapic, S. K., J.C. Lockwood, and D.F. Gingras. 1988. "Effect of the Conventional Beampattern on Adaptive Beamformer Performance." NOSC TD 1307 (Dec). Naval Ocean Systems Center, San Diego, CA.

Mohnkern, G. L. 1989. "Effects of Errors and Limitations on Interference Suppression: Preliminary Report for High-Gain Initiative." NOSC TD 1478 (Feb). Naval Ocean Systems Center, San Diego, CA.

Owsley, N., in S. Haykin (ed.). 1985. *Array Signal Processing*, Prentice-Hall, Englewood Cliffs, NJ, chap. 3.

Pisarenko, V. F. 1973. "The Retrieval of Harmonics From a Covariance Function," *Geophys. J.R. Astr. Soc.*, vol. 33, pp. 347-366.

Steinhardt, A. O., and B.D. Van Veen. 1989. "Adaptive Beamforming," *International Journal of Adaptive Control and Signal Processing*, vol. 3.

REPORT DOCUMENTATION PAGE

Form Approved
OMB No. 0704-0188

1. AGENCY USE ONLY *(Leave blank)*	2. REPORT DATE	3. REPORT TYPE AND DATES COVERED
	November 1990	Final

4. TITLE AND SUBTITLE

CHARACTERIZING AND IMPROVING THE PERFORMANCE OF THE MVDR PROCESSOR

5. FUNDING NUMBERS

PE: 0602314N
WU: DN307489

6. AUTHOR(S)

M. Reuter

7. PERFORMING ORGANIZATION NAME(S) AND ADDRESS(ES)

Naval Ocean Systems Center
San Diego, CA 92152-5000

8. PERFORMING ORGANIZATION REPORT NUMBER

NOSC TD 1983

9. SPONSORING/MONITORING AGENCY NAME(S) AND ADDRESS(ES)

Office of Naval Technology
Arlington, VA 22217

10. SPONSORING/MONITORING AGENCY REPORT NUMBER

11. SUPPLEMENTARY NOTES

12a. DISTRIBUTION/AVAILABILITY STATEMENT

Approved for public release; distribution is unlimited.

12b. DISTRIBUTION CODE

13. ABSTRACT *(Maximum 200 words)*

In this document we demonstrate the utility of the magnitude squared of the minimum variance distortionless response (MVDR) weight vector and the performance improvement due to adaptivity (PIA) in characterizing MVDR performance. We use these parameters to determine how and under what conditions MVDR performance is degraded due to various environmental conditions. We also use these parameters as a basis for improving MVDR performance.

We will confine ourselves to the plane-wave signal model in this document to concentrate on the issues of adaptive array processing and to separate the analysis from the more general matched-field problem. Thus, the simulations presented here will involve only sparse, horizontal random arrays.

In section 1.0 we introduce basic array processing principles. In section 2.0 we describe these useful parameters and show under what conditions MVDR performance is enhanced or degraded. In section 3.0 we present and analyze approaches to improving MVDR performance that are based upon synthetic alterations of the environment. Finally in section 4.0 we present MVDR processor simulation results that demonstrate the effect various environmental conditions have on performance and how the white noise constraint (WNC) "robust" MVDR algorithm can improve MVDR performance under conditions of mismatch.

14. SUBJECT TERMS

minimum variance distortionless response (MVDR)
white noise constraint (WNC)

15. NUMBER OF PAGES

78

16. PRICE CODE

17. SECURITY CLASSIFICATION OF REPORT	18. SECURITY CLASSIFICATION OF THIS PAGE	19. SECURITY CLASSIFICATION OF ABSTRACT	20. LIMITATION OF ABSTRACT
UNCLASSIFIED	UNCLASSIFIED	UNCLASSIFIED	SAME AS REPORT

INITIAL DISTRIBUTION

Code 0012	Patent Counsel	(1)
Code 0144	R. November	(1)
Code 702	R. Hearn	(1)
Code 705	N. Booth	(1)
Code 7304	G. Mohnkern	(1)
Code 733	D. Barbour	(1)
Code 733	M. Reuter	(3)
Code 961	Archive/Stock	(6)
Code 964B	Library	(3)

Defense Technical Information Center
Alexandria, VA 22304-6145 (4)

NOSC Liaison Office
Washington, DC 20363-5100 (1)

Center for Naval Analyses
Alexandria, VA 22302-0268 (1)